

**DEVELOPMENT OF BOVINE CARTILAGE EXTRACELLULAR
MATRIX AS A POTENTIAL SCAFFOLD FOR CHONDROGENIC
INDUCTION OF HUMAN DERMAL FIBROBLASTS**

ALI MORADI

**FACULTY OF ENGINEERING
UNIVERSITY OF MALAYA
KUALA LUMPUR**

2015

DEVELOPMENT OF BOVINE CARTILAGE EXTRACELLULAR
MATRIX AS A POTENTIAL SCAFFOLD FOR CHONDROGENIC
INDUCTION OF HUMAN DERMAL FIBROBLASTS

ALI MORADI

THESIS SUBMITTED IN FULFILLMENT OF THE
REQUIREMENTS FOR THE DEGREE OF DOCTOR OF PHILOSOPHY

FACULTY OF ENGINEERING
UNIVERSITY OF MALAYA
KUALA LUMPUR

2015

UNIVERSITY OF MALAYA
ORIGINAL LITERARY WORK DECLARATION

Name of Candidate: Ali Moradi (Passport No: H95660248)

Matric No: KHA100055

Name of Degree: Doctor of Philosophy

Title of Thesis: The development of bovine cartilage extracellular matrix
as a potential scaffold for chondrogenic induction of human dermal fibroblasts

Field of Study: Tissue Engineering

I do solemnly and sincerely declare that:

- (1) I am the sole author/writer of this Work;
- (2) This Work is original;
- (3) Any use of any work in which copyright exists was done by way of fair dealing and for permitted purposes and any excerpt or extract from, or reference to or reproduction of any copyright work has been disclosed expressly and sufficiently and the title of the Work and its authorship have been acknowledged in this Work;
- (4) I do not have any actual knowledge nor do I ought reasonably to know that the making of this work constitutes an infringement of any copyright work;
- (5) I hereby assign all and every rights in the copyright to this Work to the University of Malaya (“UM”), who henceforth shall be owner of the copyright in this Work and that any reproduction or use in any form or by any means whatsoever is prohibited without the written consent of UM having been first had and obtained;
- (6) I am fully aware that if in the course of making this Work I have infringed any copyright whether intentionally or otherwise, I may be subject to legal action or any other action as may be determined by UM.

Candidate’s Signature

Date:

Subscribed and solemnly declared before,

Witness’s Signature

Date:

Name:

Designation:

ABSTRACT

Tissue engineering aims to find an ultimate solution for cartilage regeneration. Current strategies for cartilage repair using chondrocytes are limited by the usability of cell sources as observed in several contemporary techniques such as autologous cell implantations. Cartilage tissue engineering strategies involving scaffold fabrication are common. However, only few studies have described the use of scaffolds as a promoter for chondrogenic differentiation. Cartilage extracellular matrix derived scaffolds contain many bioactive factors that have chondrogenic potential of which if appropriately managed, may provide the key to successful cartilage repair outcomes. The present thesis describes a potential biomaterial derived from bovine articular cartilage that possesses chondrogenic properties, thereby being expected to promote cartilage regeneration.

Bovine articular cartilage matrix derived (CMD) porous scaffolds were fabricated at three different concentrations (5%, 15% and 30%), through the use of freeze-drying method or, physically treated for cross-linking enhancement using either ultra-violet (UV) light or, dehydrothermal (DHT) treatment or a combination of both methods. The scaffolds were characterized using morphology, FESEM, FTIR, TGA, DSC, and porosimetry. UV and UVDHT treated 15% CMD scaffolds were found to be the best scaffold possessing the best possible physical properties. Human dermal fibroblast cells (HDF) isolated from redundant skin obtained through cosmoplastic surgery were used as cells for the in vitro analysis. HDF cells were cultured on UV and UVDHT treated 15% CMD scaffolds for 42 days. Resazurin reduction test and DNA quantification showed an increasing cell proliferation during the first 3 weeks. GAGs production and the up-regulation of SOX9, COMP, COL2A1, and ACAN genes were seen throughout 6 weeks of cell-scaffold culture. The increase or decrease in HDF cell proliferation,

GAGs production and gene expression appeared correlated with the scaffold shrinkage and contraction patterns.

In conclusion, bovine articular CMD porous scaffolds have the potential to induce chondrogenic differentiation in human dermal fibroblasts. Whilst the present thesis did not demonstrate the precise underlying mechanisms by which chondroinduction is achieved from these CMD scaffolds, it is proposed that future studies are conducted to investigate the involved pathways to better demonstrate the chondrogenic properties of this material.

ABSTRAK

Kejuruteraan tisu bertujuan untuk mencari penyelesaian muktamad untuk pertumbuhan semula rawan. Strategi semasa untuk membaiki tulang rawan menggunakan kondrosit adalah terhad dengan kebolegunaan sumber sel seperti yang berlaku di beberapa teknik kontemporari seperti implantations sel autologous. Strategi kejuruteraan tisu tulang rawan yang melibatkan fabrikasi perancah adalah biasa. Walau bagaimanapun, hanya beberapa kajian telah menggambarkan penggunaan perancah sebagai penganjur bagi pembezaan chondrogenic. Perancah matriks extracellular tulang rawan mengandungi banyak faktor bioaktif yang mempunyai potensi chondrogenic jika diurus dengan baik, boleh menyediakan kunci kepada hasil membaiki rawan berjaya. Tesis ini menerangkan biobahan potensi berasal dari tulang rawan artikular lembu yang mempunyai ciri-ciri chondrogenic, yang dijangka menggalakkan pertumbuhan semula rawan. Perancah berliang matriks tulang rawan artikular lembu (CMD) yang diperolehi telah direka di tiga kepekatan yang berbeza (5%, 15% dan 30%), dengan menggunakan kaedah beku-pengeringan atau, fizikal dirawat untuk peningkatan hubungan silang sama ada menggunakan ultra-ungu (UV) atau, dehydrothermal (DHT) rawatan atau gabungan kedua-dua kaedah. Perancah telah dicirikan menggunakan morfologi, FESEM, FTIR, TGA, DSC, dan porosimetri. Perancah CMD yang dirawat dengan 15% UV dan UVDHT merupakan perancah terbaik yang mempunyai kemungkinan sifat-sifat fizikal. Sel-sel kulit fibroblast manusia (HDF) diasingkan daripada kulit berlebihan yang diperolehi melalui pembedahan cosmoplastic telah digunakan sebagai sel-sel dalam vitro analisis. Sel HDF dikulturkan di atas perancah CMD dirawat dengan 15% UV dan UVDHT untuk 42 hari. Pengurangan dalam ujian Resazurin dan kuantifikasi DNA menunjukkan percambahan sel yang semakin meningkat dalam tempoh 3 minggu pertama. Penghasilan GAGs dan kitaran atasan bagi gen SOX9, COMP, COL2A1, dan ACAN diperhatikan sepanjang 6 minggu kultur sel-perancah. Peningkatan atau

pengurangan dalam percambahan sel HDF, penghasilan GAGs dan ekspresi gen yang muncul dikaitkan dengan pengecutan perancah dan corak pengecutan.

Kesimpulannya, perancah berliang artikular lembu CMD mempunyai potensi untuk mendorong pembezaan chondrogenic dalam fibroblas kulit manusia. Manakala tesis ini tidak menunjukkan mekanisme yang tepat tentang chondroinduction yang dicapai daripada ini perancah CMD, adalah dicadangkan bahawa kajian masa depan perlu dijalankan untuk menyiasat laluan yang terlibat supaya lebih sifat chondrogenic bahan ini dapat ditunjukkan.

ACKNOWLEDGEMENT

Foremost, I would like to express my sincere gratitude to my advisors namely Prof. Dr. Belinda Murphy and Prof. Dr. Tunku Kamarul Zaman for the continuous support of my Ph.D study and research, for their patience, motivation, enthusiasm, and immense knowledge. Their guidance helped me in all the time of research and writing of this thesis. I could not have imagined having better advisors and mentors for my Ph.D study. Besides my advisor, I would like to thank Dr. Sumit Pramanik, for his encouragement, insightful comments, and hard questions.

I thank my fellow lab-mates in Tissue Engineering Lab, Faculty of Engineering, and Tissue Engineering Group (TEG), National Orthopaedic Centre for Research and Learning (NOCERAL), Faculty of Medicine, University of Malaya: Dr. Havva Dashtdar, Dr. Hussin Rothan Alwan, Eng. Haris Bin Akram, Eng. Iklil Radzi, Dr. Forough Ataollahi, Eng. Adel Dalilottojari, Eng. K. Sayar, Dr. Yasir Muhammad Al-Saffar, Eng. Eraj Homayoun Mirza, Eng. Poon Chi Tat, and Liyana Binti Abu, for the stimulating discussions, for the sleepless nights we were working together before deadlines, and for all the fun we have had in the last four years.

Last but not the least I would like to thank my family: my mother, my wife Rose, my sons Homayoun and Hooman and my brothers and sisters for supporting me spiritually throughout my life.

TABLE OF CONTENTS

ABSTRACT	iii
ABSTRAK	v
ACKNOWLEDGEMENT	vii
TABLE OF CONTENTS.....	viii
LIST OF FIGURES	xii
LIST OF TABLES	xx
LIST OF SYMBOLS AND ABBREVIATIONS	xxi
CHAPTER 1: INTRODUCTION	1
1.1 Introduction	1
1.2 Problem statement	3
1.3 Objectives	4
1.4 Thesis layout.....	4
CHAPTER 2: LITERATURE REVIEW	5
2.1 Introduction	5
2.2 Biochemical Composition of Articular Cartilage.....	6
2.2.1 Water	7
2.2.2 Collagens.....	8
2.2.3 Proteoglycans	8
2.3 Rationale of Current Study	8
2.4 Bovine Articular Cartilage: A Potential Source of Cartilage Matrix	10
2.5 Enhancing Mechanical Properties	11
2.5.1 Chemical cross-linking.....	11
2.5.2 Physical cross-linking	12
2.6 Human Skin: A potential source of cells (Fibroblasts)	13
CHAPTER 3: FABRICATION, CHARACTERIZATION AND OPTIMIZATION OF CMD SCAFFOLDS	17
3.1 Introduction	17

3.2	Materials and Methods	19
3.2.1	Cartilage Matrix Derived (CMD) Scaffold Preparation	19
3.2.2	Characterization of CMD Scaffolds.....	21
3.3	Results	24
3.3.1	Bovine Articular Cartilage Water Content.....	24
3.3.2	Macro and Micro Morphologies of the CMD Scaffolds.....	24
3.3.3	Porosity of CMD scaffolds	29
3.3.4	Compressive tests.....	32
3.3.5	Surface Morphology.....	33
3.3.6	Thermogravimetric Analysis (TGA).....	34
3.3.7	Differential Scanning Calorimetry (DSC)	35
3.3.8	FTIR	36
3.4	Discussion	38
CHAPTER 4: DEVELOPMENT OF MICROVOLUMETRIC MODIFICATION OF LIQUID DISPLACEMENT METHOD FOR POROSITY MEASUREMENT		42
4.1	Introduction	42
4.2	Materials and Methods	45
4.2.1	Experimental Set up	45
4.2.2	Validation of Microvolumetric method	49
4.2.3	Statistical Analysis	50
4.3	Results	50
4.4	Conclusion.....	89
CHAPTER 5: ISOLATION, CULTURE AND CHARACTERIZATION OF HUMAN DERMAL FIBROBLASTS		91
5.1	Introduction	91
5.2	Materials and Methods	91
5.2.1	Cell Isolation	91
5.2.2	Cell Harvesting.....	93
5.2.3	Cell Count and Viability (Dye Exclusion Method).....	94

5.2.4	Resazurin Standard Curve for HDFs.....	96
5.2.5	HDF cell doubling time.....	99
5.2.6	Characterization of HDFs	103
5.3	Results	112
5.3.1	HDF Cell Morphology	112
5.3.2	HDF Resazurin Standard Curves	113
5.3.3	DNA standard Curve.....	120
5.3.4	HDF Cell Doubling Time.....	121
5.3.5	Tri-lineage differentiation	121
5.3.6	Immunostaining	123
5.3.7	Gene expression	125
5.4	Discussion	126

CHAPTER 6: CHONDROGENIC EFFECTS OF CMD SCAFFOLDS ON HDFs 128

6.1	Introduction	128
6.2	Materials and Methods	129
6.2.1	Cell Seeding	129
6.2.2	Cell Growth and Viability.....	130
6.2.3	Cell Proliferation.....	130
6.2.4	Cell-scaffold Interaction Studies.....	131
6.2.5	DNA Quantification.....	131
6.2.6	Construct Shrinkage and Contraction	131
6.2.7	GAGs Quantification	133
6.2.8	Gene Expression.....	133
6.2.9	Gene Expression.....	137
6.2.10	FESEM.....	138
6.3	Results	138
6.3.1	Resazurin Reduction	138
6.3.2	Confocal laser scanning microscopy (CLSM).....	139

6.3.3	DNA Quantification	142
6.3.4	FESEM.....	143
6.3.5	Scaffold Shrinkage/Contraction.....	147
6.4	Chondrogenic Differentiation.....	151
6.4.1	GAGs Content.....	151
6.4.2	QPCR	154
6.5	Discussion	160
CHAPTER 7: DISCUSSION AND CONCLUSION		164
REFERENCES.....		167
LIST OF PUBLICATIONS.....		182

LIST OF FIGURES

- Figure 3-1: A) lengthwise incision along the cannon bone down to metacarpophalangeal joint, B&C) Peeling the skin off, D) Opening the joint, E) Shaving the cartilage from bone, F) De-cartilaged bone with shaved cartilage flakes in the container. 19
- Figure 3-2: Fabrication process of CMD scaffolds consists of the following steps: (A&B) mincing and shattering the cartilage flakes, (C) homogenization in PBS-EDTA-PMSF solution, (D) yielding the slurry after several wash/centrifugation steps, and (E&F) dispensing the diluted slurry into the holes of the Teflon mold. 21
- Figure 3-3: Weight measurements of wet and freeze-dried native bovine articular cartilage samples showed the average weight percentage of dry material in bovine articular cartilage to be $30.9 \pm 3.1\%$, which is the maximum solid content of BAC samples..... 24
- Figure 3-4: Photograph of representative non-treated A) 30%, B) 15% and C) 5% CMD scaffolds. The inset image D) depicts the spongy elastic nature of a 15% CMD scaffold.25
- Figure 3-5: Percentage of shrinkage in CMD scaffolds ($n \geq 7$ for each group) with different concentrations and treatment methods. *: $P > 0.05$ 26
- Figure 3-6: FESEM images of CDM scaffolds with different concentration and treatments. The scale bars represent 1 mm. Inset images with the same scale bars are representative of colour thresholding through ImageJ® software used for pore size measurement. 28
- Figure 3-7: Pore sizes of non-treated and treated CMD scaffolds with different concentrations and treatments ($n \geq 50$ for each group), calculated form FESEM images using ImageJ® software. Asterix stands for $P > 0.05$ (non-significant difference)..... 29

Figure 3-8: Percentage of porosity of different scaffolds consisting of varying cartilage matrix concentrations and different treatments ($n \geq 11$ for each group). Porosity measurements have been done through microvolumetric modification of liquid displacement method. *: $P < 0.05$ 30

Figure 3-9: Correlation between shrinkage and porosity among CMD scaffolds with different concentrations and treatments. Markers with small, middle, and big sizes indicate for 5%, 15%, and 30% cartilage matrix concentrations respectively. 31

Figure 3-10: The compressive stress/strain representative curves of untreated and treated 15% and 30% UV treated CMD scaffolds. The inset graph compares the Young's modulus ($n=7$) of differently treated 15% CMD scaffolds. (*: $P > 0.05$). 33

Figure 3-11: FESEM images of fibrous surface morphology of A) Non-treated, B) UV, C) DHT, D) UVDHT, and E) DHTUV 15% CMD scaffolds. The scale bars represent 10 μm (for insets 1 μm). 34

Figure 3-12: TGA of all the 15% CMDD scaffolds in nitrogen gas atmosphere at heating rate of 10°C/min, A) onset and B) offset temperatures of 1st decomposition, and C) weight residue (%) after 1st decomposition of differently treated 15% CMD scaffolds in TGA. 35

Figure 3-13: DSC analysis of 15% CMD scaffolds with different treatments indicating the melting temperature of each treatment. 36

Figure 3-14: Typical FTIR absorption spectra of 15% CDM material with different treatments. Wave numbers defined in blue and dark red are representative for collagen and proteoglycans respectively. The two sharp peaks at 2847 and 2915 on 15%UV are representative for alkane groups formed during UV treatment. 37

Figure 3-15: Alkene to alkane shifts will create new cross-linking bonds.	38
Figure 4-1: Schematic diagram of the A) suspension, B) level and C) overflow methods of measuring volume.....	44
Figure 4-2: components of Microvolumetric liquid level displacement method for porosity measurement: A) magnetic bar, plunger from insulin syringe, and 10 ml glass pipette end sealed with rubber cap 2) Set up and vertical alignment of the measuring pipette and its internal components.....	46
Figure 4-3: Laboratory set up for modified microvolumetric level displacement method for porosity measurement. The measuring glass pipette with its components aligned vertically in between the light source and the digital camera. The monitor shows the liquid level.....	47
Figure 4-4: Microvolumetric level method for porosity measurement: A) Baseline establishment, B) Level calibration with 100 μ l volume and second level establishment, C) V1: level elevation after immersing the sample, and D) V2: Volume depletion after removing the sample.	48
Figure 4-5: Digital photographs (A), Micro-CT 3D rendering images (B), and FESEM micrographs (C-E) of representative porous alumina1, glass, and alumina2 samples respectively.	51
Figure 4-6: Comparison between the measured porosity through micro-volumetric and micro-CT methods with the actual porosities of porous glass, alumina1, and alumina2.	86
Figure 4-7: A) Scatter plot of measured versus actual porosity and the corresponding regression coefficients for Micro-volumetric and Micro-CT methods, and B) scatter plot of difference versus mean porosity of Micro-volumetric and Micro-CT with actual	

porosity, and C) Bland-Altman plots of the data showing the level of agreement between measured and actual porosities. The solid lines indicate the accuracy and the square dotted lines represent the precision of the two techniques. 95% of the data are expected to fall within $\pm 1.96\sigma$ 88

Figure 5-1: Outgrowth method for HDF isolation. A) Full-thickness skin washed in DMEM + 3-10X Antibiotic solution, B & C) Dissecting infradermal fat layer, D & E) Dissecting Epiderm from Derm, F) Mincing the Derm, G, H & I) Putting small minced derm samples in pre-wetted T25 flask. 93

Figure 5-2: The bluish Resazurin passively diffuses into the cells and gets oxidized into pinkish Resurfin which diffuses back into the intercellular space. 96

Figure 5-3: Preparation of serial dilutions of standard DNA. 103

Figure 5-4: Seeding HDFs in 4-Chamber glass slides for adipogenic and osteogenic lineage differentiation. 104

Figure 5-5: Centric cell seeding for Chondrogenic Differentiation. 107

Figure 5-6: Daily serial micrographs [from A) Day 0 to L) Day 11] of HDFs seeded on tissue culture polystyrene at an initial density of $3 \times 10^3/\text{cm}^2$ 112

Figure 5-7: Representative figures of human dermal fibroblasts: A) Typical spindle-shaped morphology of HDF cells in monolayer culture on TCP, B) 3D culture on CMD porous scaffold stained with Live-Dead assay, and C) FESEM micrograph of a single HDF cell spreading its processes and attaching on CMD surface. 113

Figure 5-8: Representative inverted microscope images of HDF cells seeded on TCP at varying densities of: A) 2×10^3 , B) 6×10^3 , C) 2×10^4 , D) 5×10^4 , and E) 10^5 cells per well

4 hours after seeding. The graph F plots the harvested cell number 4 h after seeding against the initial seeding density (n=8 for each cell density).	114
Figure 5-9: Reduction of AlamarBlue-DMEM as function of cell density in monolayer culture at varying incubation times from 1 to 22 hours.	115
Figure 5-10: Reduction of AlamarBlue-PBS as function of cell density in monolayer culture at varying incubation times from 1 to 22 hours.	116
Figure 5-11: Reduction of Resazurin-PBS as function of cell density in monolayer culture at varying incubation times from 1 to 22 hours.	117
Figure 5-12: Reduction of Resazurin-PBS as function of cell density in monolayer culture at varying incubation times from 1 to 22 hours.	117
Figure 5-13: Resazurin Reduction Nomogram as a practical tool for quantification of Human Dermal Fibroblasts cell density in monolayer culture at 1 to 5 hours incubation times. The orders of all 5 curves look reasonable and logical.	118
Figure 5-14: Plotting the relative fluorescence units (RFU) against the DNA concentration ($\mu\text{g/ml}$) yields a linear regression with high R^2 value. This line is used as the DNA standard curve for quantification of DNA containing cell extracts.....	120
Figure 5-15: Growth curves of HDF cells at P5 within 12 days culture based on A) cell count, B) DNA quantification, and C) percentage reduction in Resazurin. The lag, logarithmic and stationary phases are seen in graph A.	121
Figure 5-16: Inverted microscope images of A) HBMSCs at P8, B) HDFs at P2, and C) HDFs at P6, all treated with adipogenic differentiation induction medium for two weeks and after Oil-Red-O staining showing the abundant lipid vacuoles in HBMSCs (A), rare	

vacuoles in HDF cells at low passage No. (B), and no evidence of lipid droplets in HDFs at passage 6 (C).....	122
Figure 5-17: Alizarin-Red staining for Osteogenic differentiation shows numerous calcification signs in HBMSCs (A) and rare ossification signs in HDF cells at P2 (B), but no evidence of osteogenic differentiation in DHFs at P6 (C).....	122
Figure 5-18: Safranin-O staining of A) HBMSCs at P8 treated with chondrogenic differentiation induction medium for 3 weeks, and B) HDF cells at P6 with the same treatment.....	123
Figure 5-19: Flowcytometry scatter plots of HDF cells at P6 stained with Cy5 for CD90. A) unstained HDF cells as control were placed in 3 rd quarter, B) pure population of Cy5 stained HDFs for CD90 as the fibroblast-specific marker, C) Histogram of Cy5 as a single parameter. X axis represents the intensity of the signal in channel numbers while Y axis shows the quantity of the events per channel number.	124
Figure 5-20: Relative quantification of expression of fibroblast-specific marker and stemness genes in primary human dermal fibroblasts (HDF) at passage 5. Human bone marrow stem cells (HBMSC) at P8 and human adipose derived stem cells (HADSC) at P0 were used as controls. GAPDH has been used as the housekeeping gene.	125
Figure 6-1: Scaffold shrinkage test after HDF cell seeding at different time points was tested by measuring the cross-sectional surface area of the scaffolds. Plastic white discs with known constant diameter were used for setting the scale in each picture.....	132
Figure 6-2: Percentage reduction in Resazurin absorption in HDF seeded UV and UVDHT treated CMD scaffolds at different weekly time-points.....	139

Figure 6-3: Confocal laser scanning micrographs of HDF cells seeded on UV and UVDHT treated CMD scaffolds at different weekly time points. All images have been captured after staining with LIVE/DEAD® Viability/Cytotoxicity Kit (green for Calcein and red for Ethidium homodimer). (The scale bars in main and inset images represent for 200µm and 50 µm respectively).	141
Figure 6-4: Continued form Figure 6-3.....	142
Figure 6-5: Total DNA by Hoechst method in papain digested cell seeded UV and UVDHT treated CMD scaffolds (n=5 for each group) at different weekly time-points after subtraction of average DNA in unseeded (blank) samples.....	143
Figure 6-6: FESEM micrographs of unseeded (A&A') and cell seeded UV and UVDHT treated CMD scaffolds at weekly time points from Day 2 (B&B') to Day 42 (H&H'). The scale-bar for image A is 100 µm while for the rest of the images they represent for 50 µm.	145
Figure 6-7: Continued for Figure 6-6.....	146
Figure 6-8: Serial digital images of top view of representative blank (unseeded) and HDF seeded UV and UVDHT treated CMD scaffolds at seeding time and consecutive weekly time points. The white circular plastic discs were used as the constant fixed-dimension scales.....	147
Figure 6-9: Effect of wetting on the dimensions of porous spongy scaffolds.	148
Figure 6-10: Measurements of cross-sectional surface area (top view) of the seeded and unseeded UV and UVDHT treated 15% CMD scaffolds (n=7 for seeded and n=5 for unseeded scaffolds. Significant and non-significant differences are shown by (*: P<0.05) and (†: P>0.0).....	149

Figure 6-11: Percentage of total shrinkage in HDF seeded UV and UVDHT treated CMD scaffolds (n=7 for seeded scaffolds and n=5 for unseeded scaffolds) at different weekly time-points. Part of this shrinkage is due to cell mediated contraction (CMC). Asterix stands for P<0.05.....	151
Figure 6-12: Sulfated Glycosaminoglycan content in cell seeded UV and UVDHT treated CMD scaffolds (n=5 in each group) at different weekly time points after subtraction of the average GAGs in unseeded samples, measured through DMMB method.....	152
Figure 6-13: Correlation between sulfated glycosaminoglycan production and shrinkage rate in cells seeded on UV and UVDHT treated 15% CMD scaffolds.	153
6-14: Correlation between total DNA and shrinkage rate in HDF-seeded UV and UVDHT treated 15% CMD scaffolds.	153
Figure 6-15: Quantitative gene expression of COL1A1 in HDFs seeded on UV and UVDHT treated CMD scaffolds (n=7 in each group) at weekly time points. The data have been normalized to GAPDH. HDF cells were used as Ctrl ⁻	155
Figure 6-16: A) Serial digital images of top view of representative blank (unseeded) and HDF seeded UV and UVDHT treated CMD scaffolds at seeding time and consecutive weekly time points. The white circular plastic discs were used as the constant fixed-dimension scales.....	156
Figure 6-17: Correlation between A) COL2A1 and B) ACAN gene expression, and DNA content, C) the DNA and D) GAGs content, and E) COL2A1 and F) ACAN expression all against shrinkage rate.....	160

LIST OF TABLES

Table 2-1: Biochemical composition of articular cartilage.....	7
Table 4-1: Micro-volumetric and micro-CT porosities compared with the actual porosity, mean and difference between each method and the actual value.	52
Table 5-1: TaqMan® assays used for characterization of human dermal fibroblasts through gene expression.....	110
Table 6-1: TaqMan® Assay Probes Used in QPCR.	137

LIST OF SYMBOLS AND ABBREVIATIONS

CMD	Cartilage Matrix Derived
DBP	Demineralised Bovine Powder
DMEM	Dulbecco's Modified Eagle's Medium
DMSO	Dimethylsulfoxide
EDTA	ethylenediaminetetraacetic acid
FB/CS	Fetal Bovine/Calf Serum
HDF	Human Dermal Fibroblast
HEPES	4-(2-hydroxyethyl) piperazine-1-ethanesulfonic acid
PBS	Phosphate Buffered Saline
Pen/strep	penicillin-streptomycin mixture
TGF	Transforming growth factor

CHAPTER 1: INTRODUCTION

1.1 Introduction

For the past three centuries, it is commonly accepted that cartilage damage results in poor healing. As described by Hunter, "If we consult the standard Chirurgical Writers from Hippocrates down to the present Age, we shall find, that an ulcerated Cartilage is universally allowed to be a very troublesome Disease; that it admits of a Cure with more difficulty than carious Bone; and that, when destroyed, it is not recovered" (Hunter, 1809). Articular cartilage has limited healing capacity following an injury due to low mitotic activity and limited supply of cells (chondrocytes). In addition, the absence of vascular supply and blood perfusion, and limited mobility of chondrocytes to the damaged sites further adds to this insult (Buckwalter & Mankin, 1997; Curl et al., 1997; Kasemkijwattana, Kesprayura, & Chanlalit, 2009; McPherson & Tubo; Shelbourne, Jari, & Gray, 2003). Over the last few decades, physicians and scientists have been working hard to find several different strategies to repair damaged articular cartilage. The target has always been to restore the damaged hyaline cartilage to its original condition. In the past several different procedures have been suggested, however they have been less attractive due to the limited repair outcomes. Arthroscopic lavage and debridement (Finkelstein & Mayer, 1931), marrow stimulation techniques (Pridie, 1959), osteochondral grafts (Hangody & Fules, 2003; Hangody, Kish, Karpati, Szerb, & Udvarhelyi, 1997; Hangody et al., 2004; Jacobs, 1965; Lane, Brighton, Ottens, & Lipton, 1977), and autologous chondrocyte implantation (Peterson, Minas, Brittberg, & Lindahl, 2003) have been the main surgical procedures described, however none has proved to be the ultimate solution for cartilage regeneration.

Tissue engineering repair strategies such as the use of organized delivery of suspended cells by means of scaffold constructs can fill in the voids within cartilage defects. This provides a superior alternative to routine surgical interventions, which has been shown

to produce good mid-term outcomes. To engineer cartilage one must consider the need to fulfil all three prerequisites of the tissue engineering triad: the cells which will function just like chondrocytes, the appropriate extracellular matrix which provides the signalling factors, and the appropriate tissue micro-architecture that recreates the natural state of the cartilage microenvironment.

Tissue engineering solutions for cartilage repair using chondrocytes are limited by the low number of available chondrocytes. This is mainly due to the limited available sources that are required for this treatment. Moreover, additional procedure is needed to retrieve cartilage from a donor region of the patient. In addition, we need to be mindful that allogeneic chondrocytes may not be the most suitable cell of choices due to the immune responses it elicits following transplantation (Hyc, Malejczyk, Osiecka, & Moskalewski, 1997; Kyriacos A. Athanasiou, 2013; Moskalewski, Hyc, & Osiecka-Iwan, 2002). Tissue engineered adult cells have been said to possess chondrogenic differentiation potential. However, harvesting these chondroprogenitors is usually no easy task. Chondroprogenitor cells can be isolated from bone marrow (Longobardi et al., 2006), synovium (Nishimura et al., 1999; Shirasawa et al., 2006), fat (Erickson et al., 2002), and skin (Sommar, 2010) and be used for cartilage tissue engineering (Johnstone, Yoo, & Stewart, 2008).

Different natural (collagen, fibrin, chitosan, hyaluronic acid, alginate gels, agarose, silks, and etc.) and synthetic (PLA-PGA, polyurethanes, polycarbonates, polyfumarates, PEGT-PBT block copolymers, etc.) biodegradable polymers have been used for scaffold fabrication for cartilage tissue engineering. Extracellular matrix components can be included during the fabrication of the scaffold (Mahmoudifar & Doran, 2012). The ideal biomaterials for tissue engineering are supposed to be biocompatible and non-toxic. In addition, they must provide good cell adhesion site, possess high porosity for good cell

penetration, allow nutrient exchange to occur, and are bioresorbable. The biomaterial must also provide a framework that allows proper mechanical properties for migration and proliferation of seeded cells. This in turn allows early weight bearing to occur. A tailored surface chemistry can enhance appropriate cellular responses in order to maintain or promote their phenotypic expression. The scaffold design is also important to assist in the formation of the desired tissue. This can be achieved by using cell culture systems to generate fully functional tissues that support production of ECM components to mimic the biochemical and mechanical properties of native articular cartilage as closely as possible.

1.2 Problem statement

Typical approaches of cartilage tissue engineering have included the seeding of chondrocytes or chondroinducible cells on custom made scaffolds that can simulate chondrocyte to thrive as if these cells live within their native environment. Different hydrogel and porous scaffolds composed of synthetic and/or natural materials have been fabricated previously with the intentions to mimic cartilage extracellular matrix. While different methods have been applied to fabricate biocompatible scaffolds that can support cartilage matrix production, none of the scaffolds has shown to be ideal for cartilage tissue engineering especially when considering these materials lack in the ability to initiate any chondrogenic effects. Therefore, a study was conducted using a novel biomaterial and an unconventional source of cell to demonstrate a superior outcome based on our hypothesis that a good biomaterial using acceptable and more abundant cell source may be adequate for the requirements needed for successful cartilage repair to occur. In the present thesis, a potential biomaterial derived from bovine articular cartilage matrix to induce chondrogenesis in human dermal fibroblasts as potential chondroinducible cells are described and discussed.

1.3 Objectives

- i. Fabrication, characterization, and optimization of bovine articular cartilage matrix derived porous scaffold.
- ii. Isolation, culture and characterization of Human Dermal Fibroblast cells.
- iii. Investigation of the chondrogenic effects of bovine articular cartilage matrix derived porous scaffold on human dermal fibroblast cells in 3D culture.

1.4 Thesis layout

This thesis consists of six chapters. Following the introduction, the second chapter critically reviews the relevance of this study within the current literature. The third section will disclose the underlying theory and the experimental steps involved in the fabrication, characterization and optimization of bovine articular cartilage matrix-derived porous scaffolds. Chapter four outlines the procedures that lead to the isolation, culture and characterization of human dermal fibroblasts (HDFs). The fifth chapter discusses the methodology and rationales of assessment of chondrogenic effects of bovine articular cartilage matrix-derived porous scaffolds on HDF cells. Finally, the sixth chapter provides the discussion, conclusion and the suggestions for future works of the present thesis.

CHAPTER 2: LITERATURE REVIEW

2.1 Introduction

Cell-based therapies in cartilage tissue engineering take advantage of highly porous interconnected three dimensional scaffolds that can provide enough surface area and space for cell attachment, proliferation, extracellular matrix production and deposition to occur; which also includes nutrient and waste exchange. Apart from selecting suitable cells and growth factors, the use of proper scaffolds with appropriate physiochemical structure (Pramanik, Pingguan-Murphy, & Abu-Osman, 2012) will favour cellular biocompatibility and adhesion/proliferation. The scaffolds must possess suitable geometry and mechanical properties (Hutmacher, 2000), has to be highly porous and have interconnectivity between areas, possess stability and consistency in its mechanical strength, and a proper surface micro-morphology that will support cellular differentiation (Pramanik et al., 2012). Different three-dimensional (3D) constructs such as complex branched helical microchannels of microfluidic hydrogels may provide good network structures (G. Huang et al., 2013). Various types of hydrogels, polymers, scaffolds and composites of different materials that can support cartilage matrix production have been previously described. (Hutmacher, 2000; Lu, Zhu, Valenzuela, Currier, & Yaszemski, 2001; Moradi, Dalilottojari, Pingguan-Murphy, & Djordjevic, 2013; Moutos & Guilak, 2008). The material from which the scaffold is fabricated plays a key role in chondroinduction. It has been suggested that modified native extracellular matrix (ECM) may contain bioactive factors that can contribute to cell growth, migration, and differentiation. Different constructs that incorporates bone and cartilage matrix components have been tested for their chondrogenic effects previously. In addition, demineralized bone implants have been used for certain reconstructive procedures since before 1985 (J Glowacki & Mulliken, 1985). Other studies have also described the use of bilayer collagen porous constructs which sandwiches demineralized

bone particles, which demonstrated positive chondroinductive effects on human dermal fibroblasts (J Glowacki, 1996; J Glowacki & Mizuno, 1997; J Glowacki, Yates, Little, & Mizuno, 1998; S Mizuno & J Glowacki, 1996; Shuichi Mizuno & Julie Glowacki, 1996; Shuichi Mizuno, Lycette, Quinto, & Glowacki, 1992). However the issue of ossification formation was observation in these constructs. In general, the closer the material is to cartilage native matrix the higher the probability of achieving a suitable engineered cartilage. For this reason, pure cartilage matrix derived (CMD) scaffolds have recently been suggested as a viable alternative. 3D culture of chondroinducible cells on cartilage matrix components seems logical, as they are expected to provide structural and biochemical signals at the same time (Murphy, Haugh, & O'Brien, 2010; Rowland, Lennon, Caplan, & Guilak, 2013; Q. Yang, Peng, Guo, Huang, Zhang, Yang, et al., 2008; Z. Yang et al., 2009). Human (Q. Yang, Peng, Guo, Huang, Zhang, Yao, et al., 2008) and porcine (Cheng, Estes, Awad, & Guilak, 2009) articular cartilage ECM derived scaffolds have been fabricated and shown promising results with human adipose derived adult stem cells and canine bone marrow stem cells respectively, supporting the hypothesis that a scaffold derived absolutely from cartilage ECM can induce chondrogenesis.

To better understand the nature of cartilage ECM derived scaffolds a brief description of cartilage matrix composition will be described in the subsequent sub-chapters.

2.2 Biochemical Composition of Articular Cartilage

Human cartilage is a semi-solid jelly-like connective tissue which is derived from embryonic mesenchyme. It has four classifications based on the matrix composition: fibro cartilage, elastic cartilage, fibro-elastic cartilage, and hyaline cartilage. The hyaline cartilage which is bluish white when unstained is mainly seen at the diarthrodial joints covering long bones and also forming the growth plates during the longitudinal growth age. Articular cartilage which is composed of hyaline cartilage acts as a low-

friction wear-resistant gliding surface by means of its high compressive strength (Buckwalter & Mankin, 1997). Like all other connective tissues, the hyperhydrated articular cartilage consists of cells and matrix. Extracellular matrix of the articular cartilage consists of water and solids. The precise biochemical composition of the extracellular matrix of the articular cartilage is depicted in the Table 2.2.

Table 2-1: Biochemical composition of articular cartilage.

CONSTITUENT	VALUE BY WEIGHT
Water	66% - 79%
Solids	21% - 34%
Inorganic	
Ash	5% - 6%
Organic	
Collagen	48% - 62%
Protein	8% - 15%
Glycosaminoglycan	14% - 23%
Hyaluronate	< 1%
Lipid	< 1%
Lysozyme	< 1%
Glycoprotein	?

2.2.1 Water

Intracellular and intercellular water account for 65-80% of the articular cartilage wet weight with differences in distribution in superficial and deep zones (Bhosale & Richardson, 2008). The degree of hydration varies with age and species (McDevitt, 1973). The water-macromolecules interaction within the matrix determines the mechanical properties of the articular cartilage tissue(Hunziker, 1990).

2.2.2 Collagens

Collagen forms 10-20% of wet weight(Bhosale & Richardson, 2008), i.e. 60% of the dry weight of adult articular cartilage(McDevitt, 1973). It also forms the endoskeleton of cartilage (Huber, Trattnig, & Lintner, 2000). The most abundant form of collagen and the principal component of the microfibrillar framework is type II collagen (90–95%) which is seen as a microfibrillar framework within cartilage tissue, and is responsible for providing the tensile strength of the articular cartilage (Bhosale & Richardson, 2008).

2.2.3 Proteoglycans

Proteoglycans are heavily glycosylated glycoprotein molecules consisting of core proteins with covalently attached negatively charged long linear glycosaminoglycan (GAG) chains produced inside the chondrocytes and secreted into the cartilage matrix (McDevitt, 1973). Proteoglycans form 10-20% of wet weight of the articular cartilage. They are the filler substances existing between cells forming large complexes, both to other proteoglycans and also to collagen molecules providing the compressive strength of the articular cartilage. They are also involved in binding cations (such as sodium, potassium and calcium) and water; creating a Donnan effect and regulating the movement of fluid and electrolytes through the matrix(Aichroth, Burwell, & Laurence, 1972).

2.3 Rationale of Current Study

Considering the current limitations of cartilage tissue engineering strategies, this thesis is focussed in the development of a biomaterial scaffold derived from bovine articular cartilage extracellular matrix that would promote chondrogenic differentiation of chondroinducible cells and hence providing evidence to the potential development of tissue engineered constructs that closely mimic native articular cartilage.

The source from which the matrix is derived is a major concern. Human sources are impractical due to lack of supplies and the ethical issues related to their procurement. Porcine derived products also have limitations mainly due to religious ethical considerations. More so for a country such as Malaysia where over 60% of the population are predominantly Muslims. Animal sources with high abundance but without ethical issues can be solution of choice.

Preserving the integrity of native cartilage ECM components is a key factor in taking advantage of the total capacity of bioactive factors responsible for chondrogenesis. Therefore non-invasive fabrication methods must be considered when developing this material.

The weak mechanical properties of absolute ECM derived scaffolds accounts for the majority of the disadvantages that arise, especially after seeding the cells. It has been mentioned previously that the tendency of scaffold shrinkage and contraction can be an issue as the result of this. This limits the ability of the scaffold to induce and enhance chondrogenic differentiation of non-chondrocytic cells.

Finally, for cartilage tissue engineering purposes, the scaffold is expected to support the maintenance of chondrocytes or differentiation of other cells with chondrogenic potential. Maintenance of the chondrocyte phenotype is especially important for cartilage tissue engineering, as chondrocytes are particularly quick to lose their phenotype during the expansion process in vitro.

All in all, to help alleviate the above-mentioned issues, four major concerns with cartilage matrix derived scaffolds need to be addressed:

- The source of cartilage harvesting is supposed to be large quantity, easy to access and must be cost-effective.

- The fabrication method is to be non-invasive to an extent that the bioactive components within the cartilage matrix are not lost or damaged.
- Proper fabrication and treatment strategies must be applied to improve the physical architecture and enhance the mechanical properties of the scaffolds.
- Chondrogenic potentials of the scaffolds must be proved through in vitro studies using chondroinducible cells.

Hence, the scaffolds need to be tailored from an abundant, cost-effective, and an ethically acceptable source. The fabrication procedures will not cause significant degradation in ECM components while providing a proper architecture that allows the cells to penetrate deep into the core of the scaffold, attach, proliferate and exert chondrogenic differentiation. In this study, bovine articular cartilage was focussed as the potential source of cartilage matrix harvesting for tissue engineering applications since it fulfils all of the mentioned criteria.

2.4 Bovine Articular Cartilage: A Potential Source of Cartilage Matrix

Articular cartilage with animal source has drawn attention in tissue engineering due to its abundance. Considering that the world cattle population is estimated to be over 1.4 billion animals (Yearbook, 2012), bovine cartilage is a vast potential source of inexpensive matrix acquisition.

Viscoelastic and mechanical properties (Charlebois, McKee, & Buschmann, 2004; Fulcher, Hukins, & Shepherd, 2009; S. Park, Hung, & Ateshian, 2004), the structure of high density proteoglycans (Hunter, 1809), and the three dimensional collagen architecture (Jeffery, Blunn, Archer, & Bentley, 1991) in bovine articular cartilage have already been investigated. However, the suitability of bovine articular cartilage matrix in fabrication of scaffolds with chondroinductive effects remains undetermined. Abundance, inexpensiveness and lack of religious ethical issues (unlike porcine, canine

and murine) are the advantages of tailoring scaffolds derived from bovine articular cartilage for tissue engineering applications.

2.5 Enhancing Mechanical Properties

Achieving a mechanical strength similar to that of native articular cartilage is vital to the success of cartilage tissue engineered constructs, as one of the primary functions of the tissue in vivo is to provide mechanical support. Although CMD scaffolds provide numerous advantages for cartilage tissue engineering, it has been proven that they provide weak resistance to compressive forces (Diekman, Rowland, Lennon, Caplan, & Guilak, 2009), leading to cell mediated contraction and shrinkage of the construct (Zaleskas et al., 2004). As a result, the cells within the construct will have less access to the diffused nutrients and less room for multiplication and matrix production (C. Lee, Grodzinsky, & Spector, 2001). For this reason, various techniques have been developed to improve one or both aspects.

Mechanical properties, resorption kinetics, and biocompatibility of collagen-based biomaterials can be influenced by cross-linking methods (Bellincampi & Dunn, 1997; L. Damink et al., 1995). Different methods of chemical and physical cross-linking treatments have been used extensively to enhance the physio-mechanical and immunogenic properties of matrix derived constructs (Bellamkonda, Ranieri, Bouche, & Aebischer, 1995).

2.5.1 Chemical cross-linking

Chemical cross-linking of collagen fibres in animal hides is an established technique to increase their resistance against decomposition. Collagen is the most abundant matrix protein in the animal kingdom (Lodish et al., 2000). For medical applications, chemical cross-linking is done to decrease collagen degradation through the use of proteinases as well as minimizing immunogenicity of xenografts (Ratner, 2004). Several chemical

cross-linkers have been used in fabrication of biologic grafts and include glutaraldehyde(L. O. Damink et al., 1995), hexamethylene diisocyanate (HDI)(Mendoza-Novelo, Mata-Mata, Vega-González, Cauich-Rodríguez, & Marcos-Fernández, 2014), 1-Ethyl-3-(3dimethylaminopropyl)carbodiimide (EDC, EDAC or EDCI)(J. Lee, Edwards, Pereira, & Samii, 1996). However, chemical cross-linking causes changes in the molecular architecture of the constructs and therefore can decrease cell growth significantly (S. J. Huang & Edelman, 1995; Jarman-Smith et al., 2004; Kimuli, Eardley, & Southgate, 2004).

2.5.2 Physical cross-linking

Physical cross-linking methods have also been applied during the development of matrix derived constructs to enhance their mechanical properties(Charulatha & Rajaram, 2003; Weadock, Miller, Bellincampi, Zawadsky, & Dunn, 1995; Kevin S Weadock, Edward J Miller, Eric L Keuffel, & Michael G Dunn, 1996).Physical cross-linking strategies such as ultra violet (UV) light and dehydrothermal (DHT) treatment for cartilage matrix components have been found to enhance mechanical properties (Haugh, Jaasma, & O'Brien, 2009), although contradictory findings have been reported with the use of chemicals. Carbodiimide treatment was reported to retain the original dimensions of CMD scaffolds (Rowland et al., 2013). However, the use of glutaraldehyde treatment results in higher stiffing effects as compared to DHT treatment (Haugh, Murphy, McKiernan, Altenbuchner, & O'Brien, 2011). Nevertheless, the stiffer carbodiimide or glutaraldehyde treated CMD scaffolds showed higher cell attachment, proliferation and migration with perosteoblast cells compared to DHT treated scaffolds (Haugh et al., 2011) while inhibition of cell attachment and alterations in newly synthesized matrix composition in MSCs seeded on carbodiimide treated CMD scaffolds were reported in another study (Rowland et al., 2013).

Considering the disadvantages of chemical cross-linking, in this study we remained focussed on physical treatments: ultra-violet (UV) irradiation, dehydrothermal (DHT) treatment, and combinations of them.

2.6 Human Skin: A potential source of cells (Fibroblasts)

Scaffolds and hydrogels are mainly composed of type II collagen. It has been due to this that these materials have been shown to induce and support the differentiation of mesenchymal stem cells both *in vitro* and *in vivo*; with and without the addition of growth factors. Many studies have also demonstrated that culturing stem cells in an environment similar to that of *in vivo* cartilage can promote and support chondrogenesis.

Three-dimensional culture of cells for tissue engineering necessitates the seeding of high densities of cells i.e. 10^6 - 10^8 cell*ml⁻¹ on 3D construct (Buckley, Thorpe, O'Brien, Robinson, & Kelly, 2009; C.Y. Charles Huang, P.M. Reuben, G. D'Ippolito, P.C. Schiller, & H.S. Cheung, 2004; R. Mauck, C.-B. Wang, E. Oswald, G. Ateshian, & C. Hung, 2003a). This high number of cells must either be isolated in large quantities or subcultured to reach these numbers. Therefore the cells with easy isolation and rapid proliferation would be the source of choice. While harvesting stem cells from bone marrow and through liposuction are said to be minimally invasive, other more readily available and much easier to extract are presently available. The skin, which has an average surface area of 1.5-2 m² in adult, is one such source.

One issue that needs to be highlighted is that culture of chondrocytes in monolayer yields fibroblastic cells, which may not be ideal to produce cartilaginous repair (Kim, Cho, Hong, Rhie, & Yoon, 2008). It has been demonstrated that aggrecan-sensitive subpopulations of cells isolated from goat dermis demonstrated multi-lineage differentiation potential. These cells were referred to dermis-isolated adult stem cells

(DIAS) have been reported to possess chondrogenic potential (Deng, Hu, & Athanasiou, 2007; Sanchez-Adams & Athanasiou, 2012). What is interesting to note is that it has been shown that some variations of fibroblastic cell lines may be induced to differentiate into various directions (French, Rose, Canseco, & Athanasiou, 2004; Sommar, 2010). Monolayer culture of rabbit dermal fibroblast cell line, pre-treated with IGF-I on aggrecan coated plates have been reported to induce chondrocytic differentiation (French et al., 2004). Human foreskin dermal fibroblasts seeded on collagen/demineralized bone powder constructs have shown chondrogenic differentiation (J Glowacki, 2000; J Glowacki & Mizuno, 1997; J Glowacki et al., 1998; J Glowacki, Zhou, & Mizuno, 2009; S Mizuno & J Glowacki, 1996; Shuichi Mizuno & Julie Glowacki, 1996; S Mizuno & Glowacki, 2005; Shuichi Mizuno et al., 1992; Yates & Glowacki, 2003; Zhou, Yates, Eid, & Glowacki, 2005).

Fibroblast growth factors (FGFs) are a family of growth factors involved in many signalling pathways and the developmental processes of cells (Powers, McLeskey, & Wellstein, 2000; Thisse & Thisse, 2005). Fibroblast growth factor-18 (FGF-18) and Fibroblast growth factor-2 (FGF-2) have been shown to have chondroinductive effects during cartilage repair (Chiou, Xu, & Longaker, 2006; Liu, Xu, Colvin, & Ornitz, 2002; Moore et al., 2005). Fibroblast can be cultivated from embryonic and adult tissues, and they also are able to differentiate into chondrocytes that are cells of mesenchymal origin.

The environment by which cells are cultured is one of the most important of the determining factors in the differentiation of cultured cells. The use of three-dimensional culture of fibroblasts is not enough on its own to produce chondrocytes. Culture of murine embryonic fibroblast cells on perlecan (an ECM cross-linker protein) has been shown to produce massive formation of cartilaginous nodules and expression of chondrocyte markers such as collagen II (COLII), aggrecan (ACAN) and perlecan

(PLC) (French et al., 1999). In addition, the culture of rabbit dermal fibroblast cell lines on aggrecan can lead to the formation of dense cellular aggregates rich in cartilage matrix components (French et al., 2004).

It is possible that the forced expression of several reprogramming factors (Klf4 and c-Myc) and one chondrogenic factor (SOX9) can be achieved through the induction of chondrogenic cells from mouse skin fibroblasts (Hiramatsu et al., 2011; Outani et al., 2013).

Clonal analysis of human dermal fibroblasts isolated from foreskin using standard dermal fibroblast culture system showed that fractions of these cells are unipotent and to certain extent, bipotential (Chen et al., 2007). In all, dermal fibroblasts are no longer assumed to be terminally differentiated cells and hence can possess differentiation capabilities.

The excision of dermal tissue for the isolation of fibroblastic cells is much less invasive than the removal of cartilage. The donor site will usually heal without any complication or resulting from chronic pain. It is preferable that non-sun-exposed areas of the skin like the anterior aspect of thighs and buttock area used for partial thickness graft procedure. For full thickness grafts, skin at the groin is the most commonly used as a donor site. Cubital and postauricular areas are also considered good areas for harvest since they leave minimal scars at the donor sites. However, the size available for harvest is limited and there is a risk for wound infection. It is therefore important that tissues which are aseptically handled which remains undamaged and unexposed to sunlight areas such as the axilla, groin or foreskin are chosen for these reasons. Using Neonatal Foreskin Fibroblasts from newly circumcised Infants is an easy way of obtaining skin tissue (French, Liu, & Athanasiou, 2002). The human foreskin is a very good potential source of cells since many communities around the world practice of circumcision

regularly as part of their culture and religious practices(WHO/UNAIDS, 2007). It is worth noting that the use of the preputial foreskin as an alternative donor site is not a new idea. In any hospital, having an active maternity or paediatric surgery service, one may obtain all the foreskins necessary. Redundant skin and leftovers from cosmoplastic surgeries that are otherwise usually discarded can also be used for tissue engineering applications.

In this study, scaffolds composed of decellularized bovine articular cartilage were fabricated, characterized and optimized by different concentrations and physical treatments. The tissue engineering and chondrogenic potential of two of the optimized scaffold was then tested by seeding the scaffolds with human dermal fibroblasts and evaluating the properties of the constructs and the cells after long-term static culture.

CHAPTER 3: FABRICATION, CHARACTERIZATION AND OPTIMIZATION OF CMD SCAFFOLDS

3.1 Introduction

Attempts to repair and regenerate damaged cartilage through cartilage tissue engineering have failed to meet the needs of most patients. Despite this, tissue engineering techniques using multi-pronged strategies are still promising approaches to solve this problem. Apart from the difficulties in having suitable cells and growth factors, the use of a proper scaffold with appropriate physiochemical structure (Pramanik et al., 2012) that is biocompatible and improves cell adhesion/proliferation appears limited. Scaffolds must not only possess suitable geometry and mechanical properties (Hutmacher, 2000), but also need to demonstrate high porosity and interconnectivity, stability and consistency of mechanical strength, and a proper surface micro-morphology (Pramanik et al., 2012). Different three-dimensional (3D) constructs such as complex branched helical microchannels of microfluidic hydrogels can provide good network structures (G. Huang et al., 2013). The material from which the scaffold is fabricated plays a key role in chondroinduction. Various types of hydrogels, polymers, scaffolds and composites of different materials that can support cartilage matrix production have been described. (Hutmacher, 2000; Lu et al., 2001; Moradi et al., 2013; Moutos & Guilak, 2008). It has been suggested that by modifying native extracellular matrix (ECM) that contains bioactive factors which promotes cell growth, migration, and differentiation can be expected. In general, the closer the material is to cartilage native matrix the higher the probability of it becoming a suitable engineered cartilage. For this reason, cartilage matrix derived (CMD) scaffolds have recently drawn the attention of many researchers. This is especially so since 3D culture of chondroinducible cells on CMD components appears to provide structural and

biochemical signals at the same time (Murphy et al., 2010; Rowland et al., 2013; Q. Yang, Peng, Guo, Huang, Zhang, Yang, et al., 2008; Z. Yang et al., 2009).

Although CMD scaffolds provide numerous advantages for cartilage tissue engineering, it has been shown that they have a weak resistance to compressive loading (Diekman et al., 2009), leading to cell mediated contraction and shrinkage of the construct (Zaleskas et al., 2004). As a result, the cells within the construct will have less access to the diffused nutrients and less room for multiplication or matrix production (C. Lee et al., 2001). In order to improve the mechanical properties, physical cross-linking strategies such as ultra violet (UV) light and dehydrothermal (DHT) treatment are normally recommended (Haugh, Jaasma, et al., 2009). Nevertheless this does not always appear to produce good results. Contradictory findings have been reported with the use of chemical methods. Carbodiimide treatment was reported to retain the original dimensions of CMD scaffolds (Rowland et al., 2013). However glutaraldehyde treatment results in higher stiffness as compared to DHT treatment (Haugh et al., 2011). It has been demonstrated that the stiffer carbodiimide or glutaraldehyde treated CMD scaffolds showed higher cell attachment, proliferation and migration with preosteoblast cells compared to DHT treated scaffolds (Haugh et al., 2011) while a different study showed that culture of MSCs on carbodiimide treated CMD scaffolds resulted in inhibition of cell attachment and alterations in newly synthesized matrix composition (Rowland et al., 2013).

Scaffolds for cartilage tissue engineering are typically polymeric/biopolymeric three-dimensional constructs meant to provide temporary physical, mechanical and biological support for the chondrocytes and chondroinducible cells (Izadifar, Chen, & Kulyk, 2012). The main aim of this chapter is to present the methodology of fabrication, treatment and optimization of bovine articular CMD porous scaffolds for cartilage tissue engineering applications. In this chapter, our study describes that how the physical

structure of the CMD scaffolds is used as the main criteria for scaffold selection. Gross morphology, pore size, porosity, and mechanical properties of the scaffolds will be studied through different tests. Thermodynamic properties, infrared spectroscopy data will be used as complementary tests for further characterization and additional supportive data to rationalize the architectural characteristics of the scaffolds.

3.2 Materials and Methods

3.2.1 Cartilage Matrix Derived (CMD) Scaffold Preparation

Bovine articular cartilage (BAC) was excised from both proximal and distal surfaces of metacarpophalangeal joints of calf hooves procured from a local slaughter house (Figure 3-1).



Figure 3-1: A) lengthwise incision along the cannon bone down to metacarpophalangeal joint, B&C) Peeling the skin off, D) Opening the joint, E) Shaving the cartilage from bone, F) De-cartilaged bone with shaved cartilage flakes in the container.

BAC tissues from 9 cow legs were lyophilized (FreeZone, Lanconco, USA) after weighing. The dry weights were measured using an electronic balance with a resolution of ± 0.0005 g (SHIMADZU AY220 Analytical Balance).

The rest of the cartilage tissue was pooled, minced, shattered and homogenized using a BIOSPEC Tissue TEAROR™ (#985370-395) in 1 X phosphate buffered saline (PBS), 5 mMethylenediaminetetraacetic acid (EDTA) and 0.15 mMphenylmethylsulfonyl fluoride (PMSF) buffer solution at pH 7.4. The resulting slurry was centrifuged at 2000 rpm for 5 min, and the collected supernatant was further centrifuged at 6000 rpm for 5 min. The tissue slurry was decellularized in 1% TritonX-100 (Fisher Scientific) prepared in 0.01M Tris-HCl (Sigma # T5941) and left in a 4°C fridge while gentle agitation was applied for 12 h. After 12 h, the decellularized slurry was centrifuged at 6000 rpm for 5 min, washed with PBS, and incubated for 12h at 37°C in a hybridization oven with a low rotating speed in 50U.ml⁻¹DNase I (Sigma # DN25) and 10 mM TrisHCl (Sigma # 88438). Finally, the slurry was washed twice with PBS and centrifuged at 6000 rpm for 5 min.

The scaffolds were produced by mixing the decellularized slurries with ultrapure water (UPW; conductivity = 0.055 μ S/cm at 25 °C, total organic carbon value < 1 ppb; membrapure Aquinity, Scientech, Taiwan) and placed in cylindrical Teflon molds at 3 mm depth and 7 mm diameter. Scaffolds were prepared at 5%, 15% and 30%(w/v) concentrations, frozen at a constant temperature of -80°C for 2 hours in a freezer, then freeze-dried at -50°C, 0.04 millibar for 16 hours with no additional annealing steps, and post treated by: (A) no treatment (control), (B) exposed to ultraviolet light at an energy concentration of 8 J/cm² for 90min for each side (λ =254 nm) (henceforth 'UV'), (C) dehydrothermal treatment which means heating the scaffolds in a forced-air convection oven (Lab Companion OF-11E, China)at 120°C for 24 h (henceforth as 'DHT'), (D) UV follow by DHT treatment ('UVDHT'), and E) DHT treatment followed by UV

treatment ('DHTUV'). Although all dry scaffolds will be 100% composed of cartilage matrix, codes of the scaffolds are named as 5%, 15% and 30% CMD scaffolds based on the preparation concentration.

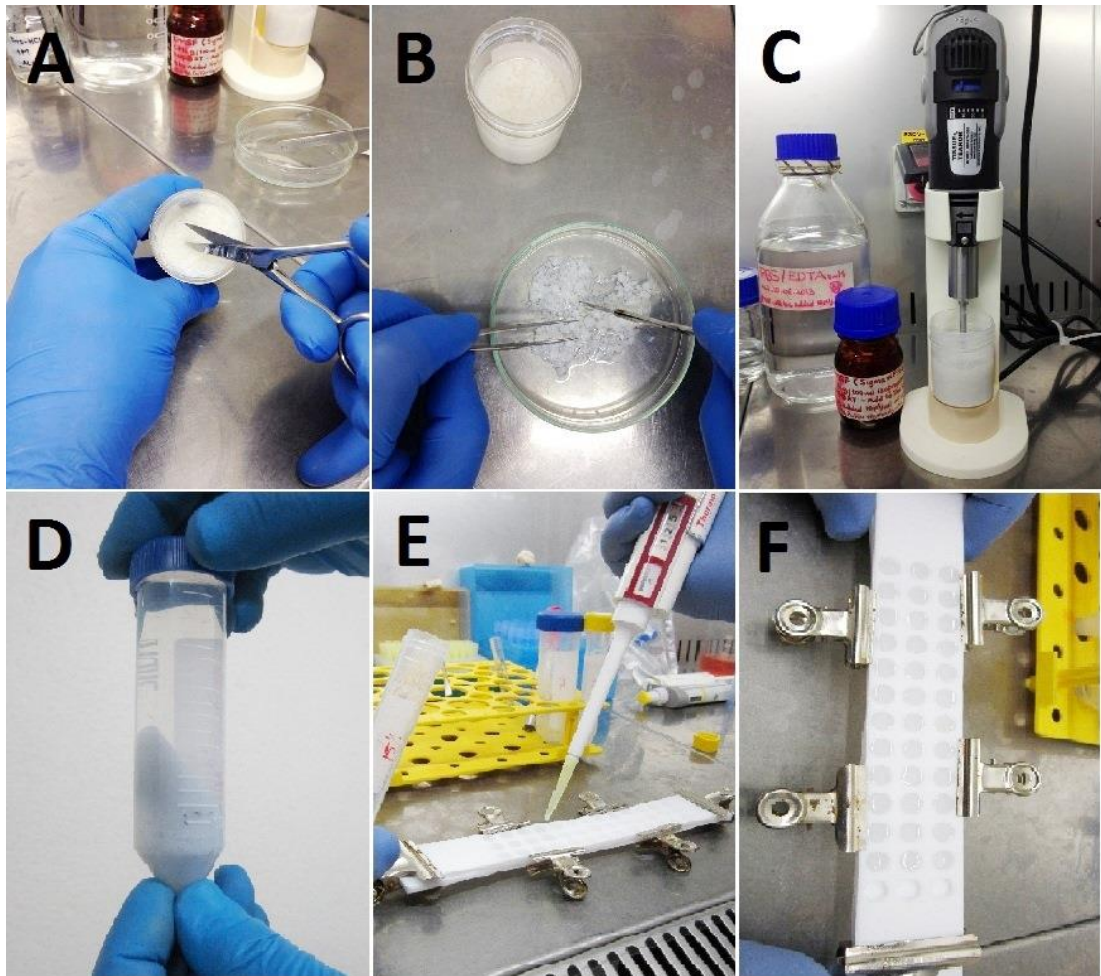


Figure 3-2: Fabrication process of CMD scaffolds consists of the following steps: (A&B) mincing and shattering the cartilage flakes, (C) homogenization in PBS-EDTA-PMSF solution, (D) yielding the slurry after several wash/centrifugation steps, and (E&F) dispensing the diluted slurry into the holes of the Teflon mold.

3.2.2 Characterization of CMD Scaffolds

3.2.2.1 CMD scaffold macro and micro morphologies

A digital camera (Canon PowerShot A570 IS) was used to capture cross-sectional images of the top view of the CMD scaffolds. ImageJ®, version 1.47v software was

used for cross-sectional surface area (A_s) measurement. Percentage of shrinkage was calculated using Eq.1 for each type of scaffold with respect to the constant circular area of the mold (A_m) with a diameter of 7 mm.

$$\% \text{ Shrinkage} = \frac{A_s}{A_m} \times 100 \quad \dots \dots \text{(Eq. 1)}$$

3.2.2.2 Field emission scanning electron microscopy (FESEM)

A field emission scanning electron microscope (FESEM) (QuantaTM 250 FEG – FEI) was used to assess micro-morphology, pore size, and pore distribution. All scaffolds were gold coated (at a thickness of around 450 Å) using a 150 rotary-pumped sputter coater (Quorum Technologies). ImageJ® software was used to calculate the pore sizes. Colour thresholding in ImageJ® facilitates the detection of pore borders and enhances measurement accuracy. FESEM images of n=3 samples from each group of scaffolds at a magnification of 100 x were used for pore size measurement. Since all the identical samples from each concentration and treatment were uniform, the data of a representative scaffold from each group were analysed for pore size measurement. Each image was divided into 9 virtual equal squares. Measurements were done randomly from 3 of the squares. For each sample $n \geq 50$ bidirectional pore diameters were measured. The mean pore diameter was calculated from the average of maximum and minimum diameters of a pore.

3.2.2.3 Porosity measurement

Scaffold porosity was measured using microvolumetric modification of the liquid displacement method based on a novel method developed by the author to meet the requirements of this study, and detailed at length in the following chapter (Moradi, Pramanik, Ataollahi, Kamarul, & Pinguan-Murphy, 2014). Briefly, changes in hexane level in a glass pipette after immersing (V_1) and removing (V_2) of each scaffold

(n≥11 for each type of scaffold) were recorded by a digital camera and analysed by ImageJ® software. The percentage pore volume was calculated using Eq. 2:

$$\text{Total pore volume} = \frac{V_2}{V_1+V_2} \times 100 \dots \dots (\text{Eq. 2})$$

3.2.2.4 Thermogravimetric analysis (TGA)

Thermal stability of CMD scaffolds (n=3 for each type of scaffold) was assessed using a thermogravimetric analyser (TA Instruments, Q500) at a constant heating rate of 10°C/min in over a temperature range of 25 to 825 °C in a controlled nitrogen gas atmosphere.

3.2.2.5 Differential scanning calorimetry (DSC)

Melting temperature and cross-linking of CMD scaffolds (n=3 for each type of scaffold) were analysed using a Mettler DSC820 system (Mettler Toledo, UK) at a constant heating rate of 10°C/min in over a temperature range of 25 to 100 °C in a controlled nitrogen gas atmosphere.

3.2.2.6 Fourier transform infra-red (FTIR) spectroscopy

A FTIR spectrometer (Thermo Scientific® Nicolet iS10) was used to analyse the secondary structure of proteins within the CMD scaffold (Kong & Yu, 2007; Ribeiro et al., 2012). Spectra were acquired from a 1.5 mm diameter sampling area (n=3 for each type of scaffold and n=3 measurements from 3 different spots per each sample) with a diamond crystal at a resolution of 4 cm⁻¹ in the wave number region between 4000 and 650 cm⁻¹.

3.2.2.7 Mechanical properties

Compressive strength and modulus of the scaffolds (n≥7 for each group) with the dimensions of 6 mm in diameter and 2 mm height were measured in compression mode

at a crosshead speed of 500 μ m/min using an Instron 5848 micro tester. The overall Young's modulus was calculated obtained when materials were subjected from 0.7% strain to 95% strain.

3.3 Results

3.3.1 Bovine Articular Cartilage Water Content

Weight measurements of wet and freeze-dried native bovine articular cartilage samples showed at average weight percentage of dry material in bovine articular cartilage to be $31 \pm 3\%$, which is the maximum solid content of BAC samples (Figure 3-3).

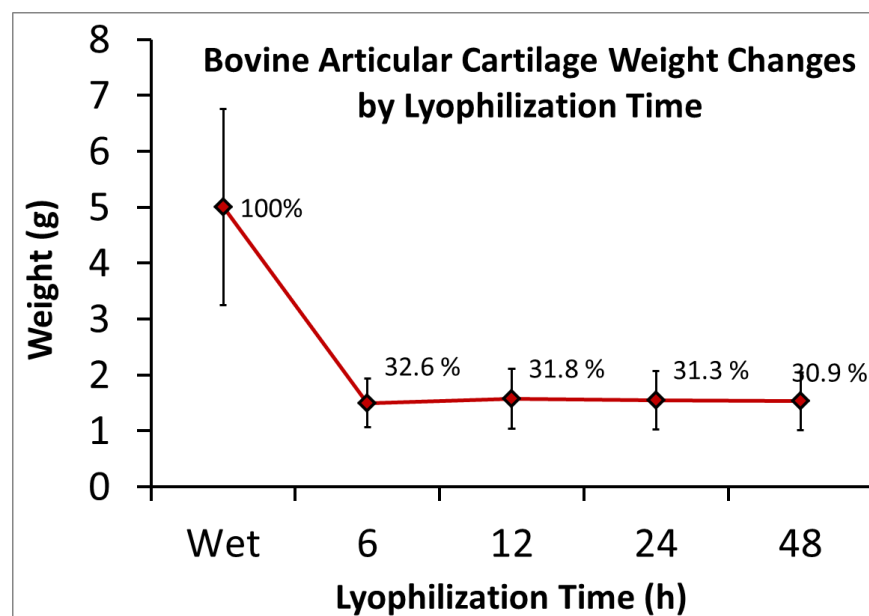


Figure 3-3: Weight measurements of wet and freeze-dried native bovine articular cartilage samples (n=33) showed the average weight percentage of dry material in bovine articular cartilage to be $31 \pm 3\%$, which is the maximum solid content of BAC samples.

3.3.2 Macro and Micro Morphologies of the CMD Scaffolds

Figure 3-4 shows the macroscopic morphologies and surface appearance of non-treated 30% (Figure 3-4: A), 15% (Figure 3-4: B), and 5% (Figure 3-4: C) CMD scaffolds. Samples show a highly porous spongy nature (Figure 3-4: D). While 15% and 30% CMD scaffolds retain their cylindrical shape, the 5% scaffolds look more deformed. Scaffolds showed substantial changes in the size after freeze-drying as compared to

their original mold size (shrinkage after lyophilization). Since there is a greater amount of water present in 5% CMD samples, the amount of total heat extracted from these samples during freeze-drying is much higher than those of 15% and 30% CMD scaffolds, leading to a higher level of shrinkage. However, differently treated samples displayed different rates of shrinkage suggesting that treatment plays a role in determining the shrinkage rate of the CMD scaffolds.

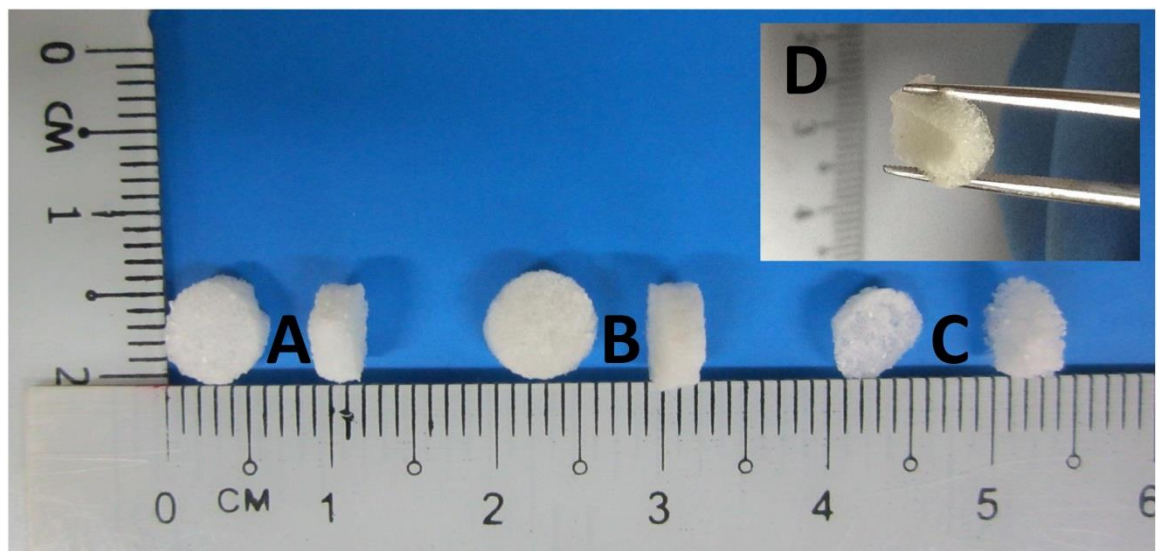


Figure 3-4: Photograph of representative non-treated A) 30%, B) 15% and C) 5% CMD scaffolds. The inset image D) depicts the spongy elastic nature of a 15% CMD scaffold.

15% and 30% UV and 15% UVDHT scaffolds showed the lowest shrinkage ($25.9 \pm 1.5\%$, $25.9 \pm 2\%$, and $25.3 \pm 2.7\%$, respectively) among all treated CMD scaffolds as seen in Figure 3-5. One way analysis of variances showed no significant difference in shrinkage between the three mentioned groups ($p > 0.05$).

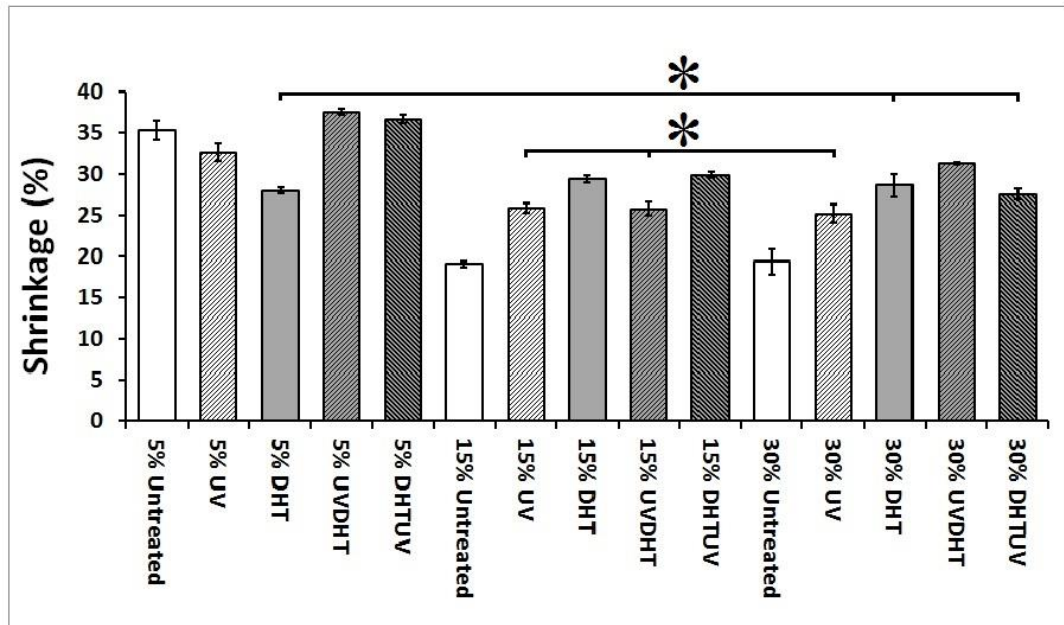


Figure 3-5: Percentage of shrinkage in CMD scaffolds (n≥7 for each group) with different concentrations and treatment methods.*: P>0.05.

FESEM images in Figure 3-6 demonstrate the uneven and irregular shaped highly interconnected pores among the 5%, 15%, and 30% CMD scaffolds as a result of the freeze-drying scaffold fabrication method. Pore size analysis using ImageJ® showed an average pore diameter of $140 \pm 60 \mu\text{m}$ for non-treated 5% CMD scaffolds, and $184 \pm 60 \mu\text{m}$ and $194 \pm 61 \mu\text{m}$ for non-treated 15% and 30% scaffolds respectively (Figure 3-6: A-C). The average pore size in non-treated 5% CMD scaffolds is significantly lower than that of non-treated 15% and 30% CMD scaffolds (Figure 3-7). As it can be seen in the FESEM images of UV treated CMD scaffolds (Figure 3-6: D-F), UV treatment did not affect the pore size of 5% scaffolds, but did demonstrate a moderate and mild increase in the pore sizes of 15% and 30% scaffolds respectively. The correlation between the shrinkage and pore sizes of the CMD scaffolds was small ($R^2=0.097$). Shrinkage of the scaffolds during freeze-drying is not necessarily associated with a change in pore size since this is determined by the rate of cooling and annealing during the lyophilization process (Haugh, Murphy, & O'Brien, 2009). However, an increase in the pore size of 15% and 30% scaffolds was coincident with an increase in shrinkage,

suggesting that the degrading effect of UV on loose bands results in smaller scaffolds with bigger pore sizes.

Image analysis of DHT treated scaffolds (Figure 3-6: G-I) shows a significant drop in pore sizes of 5% and 30% scaffolds as compared to a decrease in 15% scaffolds.

As observed in Figure 3-9: J-L, UVDHT treated 15% and 30% scaffolds show the biggest pore sizes while the pore sizes of 5% UVDHT are smaller than the non-treated 5% scaffolds. FESEM images of DHTUV samples (Figure 3-6: M-O) indicate big pore sizes for 15% samples, which are almost the size of those for the 15% UVDHT. However, a decrease in the pore sizes in 30% DHTUV scaffolds was observed. Interestingly, 5% DHTUV samples showed the biggest pore sizes.

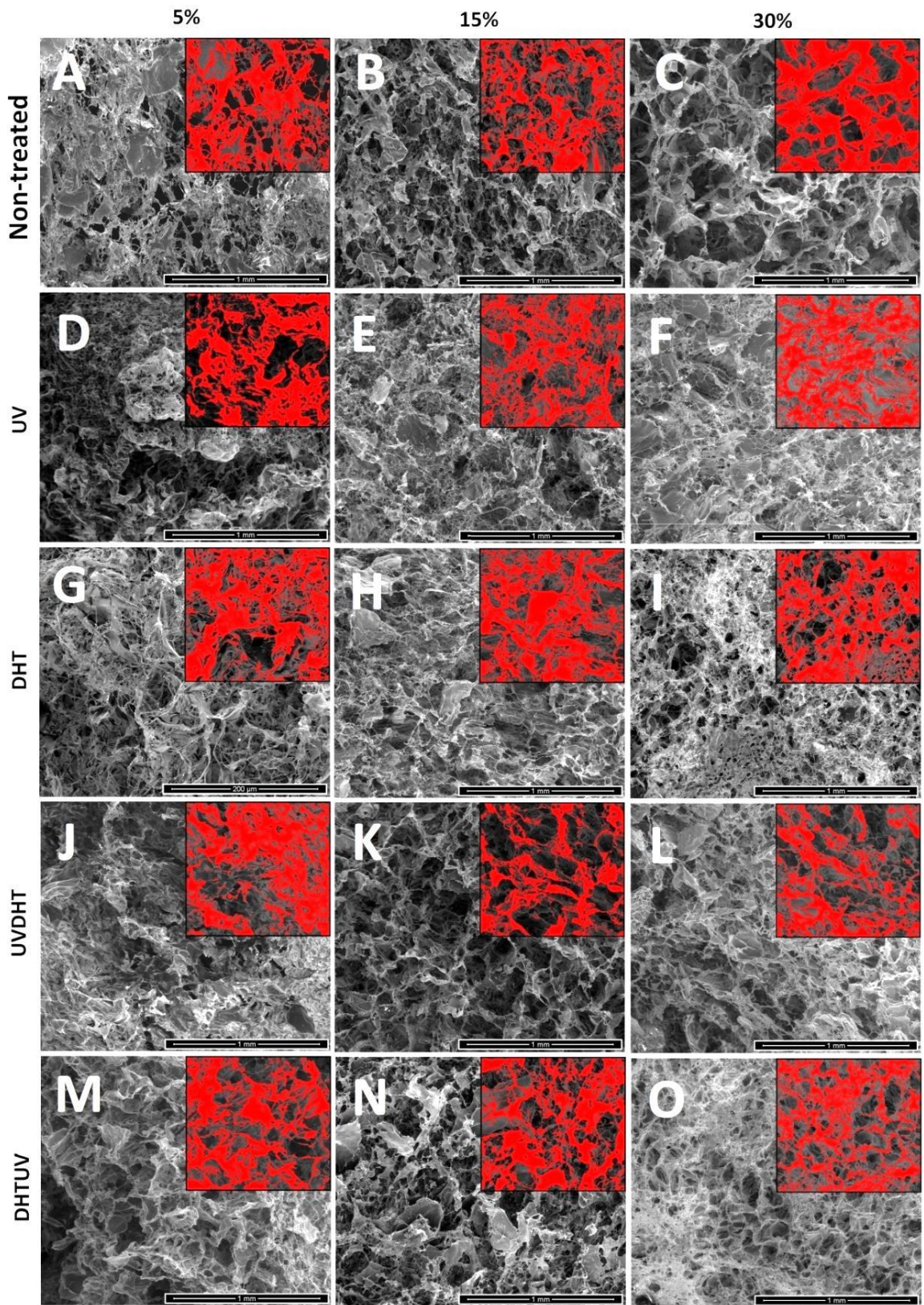


Figure 3-6: FESEM images of CDM scaffolds with different concentration and treatments. The scale bars represent 1 mm. Inset images with the same scale bars are representative of colour thresholding through ImageJ® software used for pore size measurement.

Figure 3-7 shows the average pore sizes of CMD scaffolds with different concentrations and treatments ($n \geq 50$ for each group) derived from FESEM images using ImageJ® software. The 5% DHTUV, 15% UV, UVDHT and DHTUV, and 30% UV scaffolds showed the biggest mean pore diameters. However, one way analysis of variances between the five mentioned groups revealed no significant difference between them ($P > 0.05$).

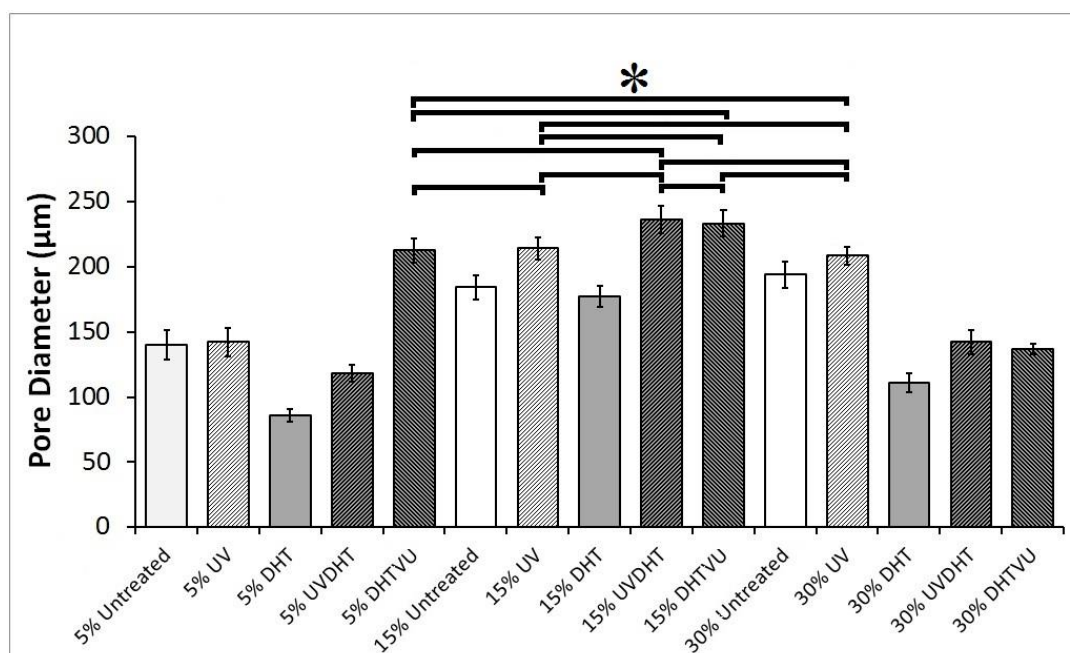


Figure 3-7: Pore sizes of non-treated and treated CMD scaffolds with different concentrations and treatments ($n \geq 50$ for each group), calculated from FESEM images using ImageJ® software. Asterix stands for $P > 0.05$ (non-significant difference).

3.3.3 Porosity of CMD scaffolds

Porosity measurement using a modified microvolumetric Archimedes method showed an average porosity of 94% and above for all the different CMD scaffolds (Figure 3-8). Considering that the biggest difference between the porosities is still less than 4% among all the different groups, it is suggested that scaffolds may still be porous. In

addition, since these differences were significant, it may be that the resultant increase in surface area may provide better cell attachment and migration.

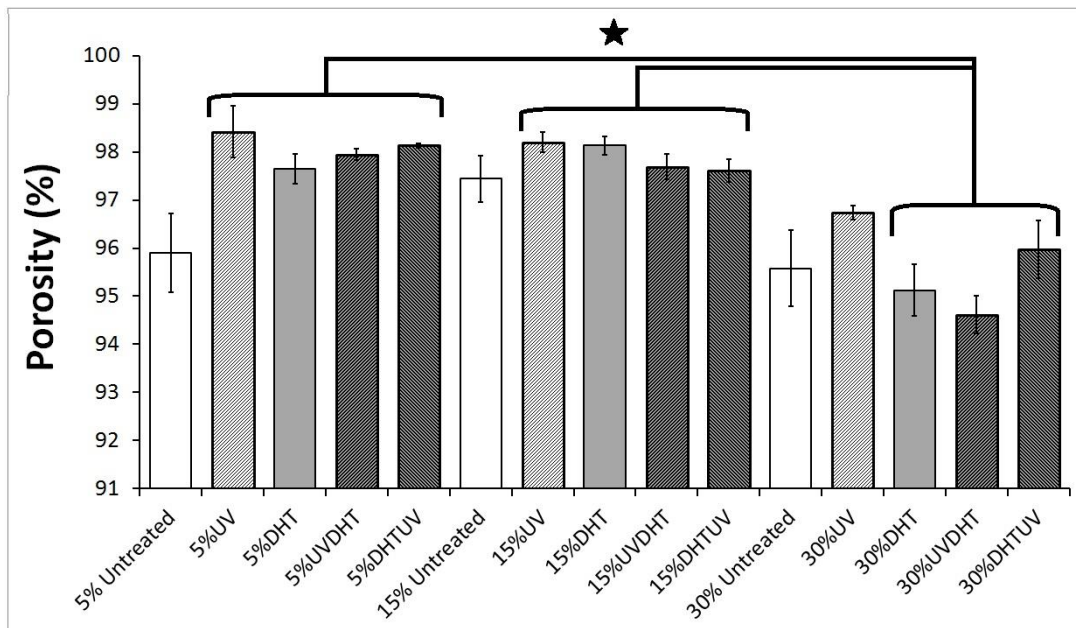


Figure 3-8: Percentage of porosity of different scaffolds consisting of varying cartilage matrix concentrations and different treatments (n≥11 for each group). Porosity measurements have been done through microvolumetric modification of liquid displacement method.*: P<0.05.

Plotting the shrinkage against the porosity shows that by increasing the concentration of CMD from 5% to 15% the porosity of all treated and untreated scaffolds, the outcomes are not affected significantly ($P>0.05$). In contrast, a decrease in the shrinkage ($P<0.05$) except for DHT ($P>0.05$) can be observed. However, increasing the CMD concentration from 15% to 30% does not result in significant changes in the material shrinkage except for the DHT group, while the differences in porosity of different treatments remain significant ($P<0.05$). The results suggest that 15% CMD concentration is a critical value beyond which significant changes in porosity and shrinkage occurs (Figure 3-9).

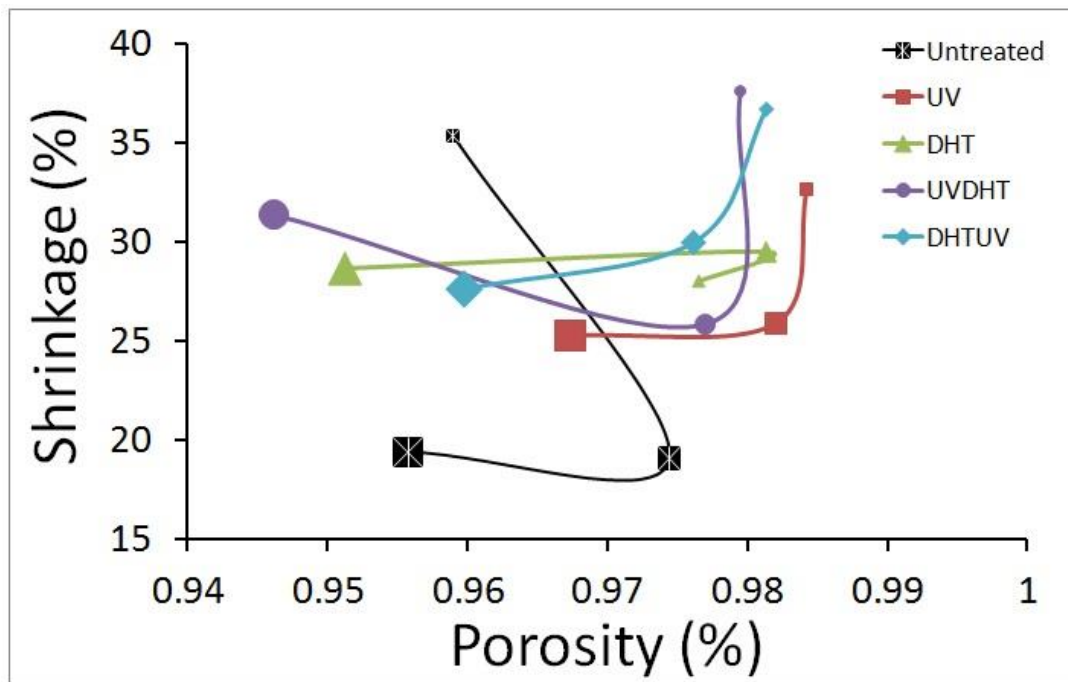


Figure 3-9: Correlation between shrinkage and porosity among CMD scaffolds with different concentrations and treatments. Markers with small, middle, and big sizes indicate for 5%, 15%, and 30% cartilage matrix concentrations respectively.

All 5% and 15% treated scaffolds showed a porosity of 98%, while the highest porosity among the 30% group was observed in UV treated scaffolds $96.7 \pm 0.5\%$. This result indicates that when the scaffolds were shrinking, the shape and size changed significantly without much change in total number of pores, resulting in a homogeneous porosity of over 94% for all specimens. Furthermore, the higher porosity in few treated 5% CMD scaffolds is indicative of breaking of the surface (as revealed in thresholding inset images in Figure 3-6 for 5% scaffolds) as a result of increased open porosity. Since 30% CMD concentration is more than a critical value, which is in this pure water media 15% CMD, the total number of pores also decreases with greater amount compared with 5 or 15 % CMD scaffolds.

Pluralization of shrinkage, pore size, and porosity data as major criteria in scaffold engineering suggests that although 5% and 15% DHTUV groups show big pore sizes,

but simultaneously show high percentages of shrinkage which fails them for selection as good scaffolds.

On the other hand, the 15% and 30% UV and also 15% UVDHT groups show the lowest shrinkages, proportionally biggest pore sizes, and high porosities, and hence all three groups can be scaffolds of choice from the view of architecture.

Considering all the above characteristics, including shrinkage, pore size and porosity of the entire CMD scaffolds and to confirm our selection, the other data of all 15% CMD scaffolds was assessed and characterized further.

3.3.4 Compressive tests

Figure 3-10 shows the results of mechanical testing in compression mode for all treatments of 15% along with 30% UV treated CDM scaffolds. UV and UVDHT treated scaffolds showed the highest compressive modulus (E_c) among other scaffolds, while one way analysis of variances showed that the Young's modulus of DHT treated 15% scaffolds was not significantly different from that of UVDHT scaffolds ($p=0.874$). On the other hand, the 30% UV treated scaffolds exerted weak compressive strength and low Young's modulus. Considering the maximum physiologic load applied on knee joint cartilage which is said to be 0.84-3.0 MPa for an average person, the Young's moduli measured for 15% UVDHT and UV treated CMD scaffolds (0.274 ± 0.05 MPa and 0.355 ± 0.06 MPa respectively) falls between the range of 10-42% of compression moduli values of natural cartilage (Izadifar et al., 2012). The Young's moduli for 15% UVDHT and UV treated CMD scaffold are significantly higher than untreated 15% CMD scaffolds and significantly higher than the compressive moduli reported for potential scaffold substitutes such as 1.5% and 2% agarose (9.0 ± 0.3 KPa and 76 ± 5 KPa respectively) and mechanically enhanced agarose/PEG-dimethacrylate (51 ± 3 kPa - 93 ± 4 kPa) hydrogels (G. Huang et al., 2012).

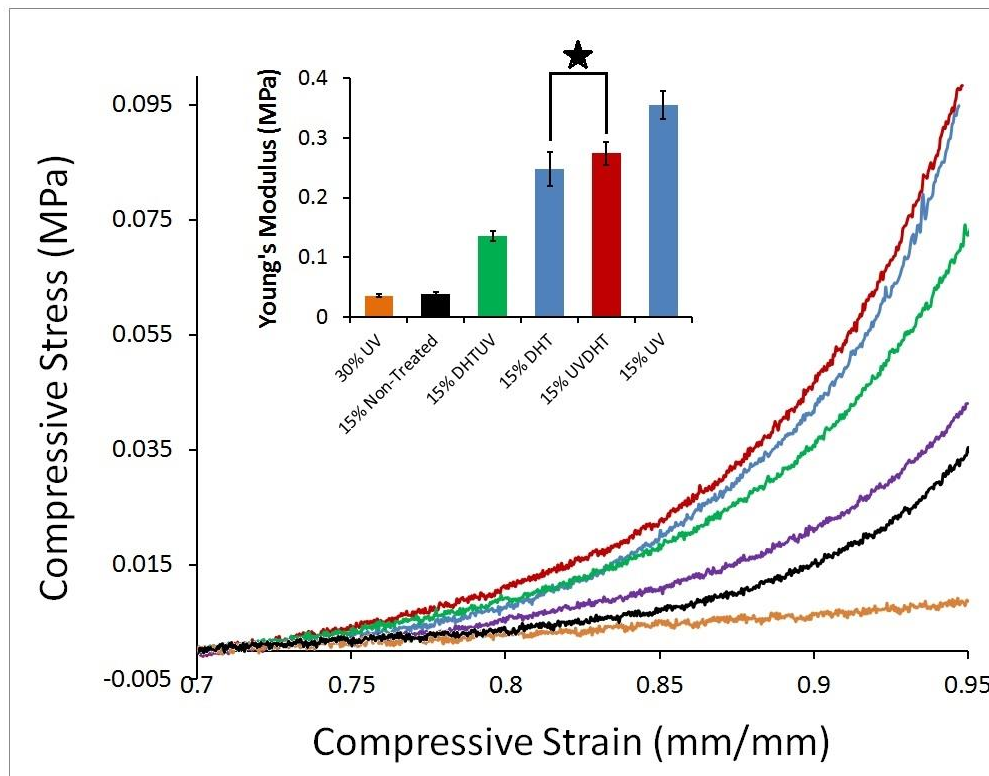


Figure 3-10: The compressive stress/strain representative curves of untreated and treated 15% and 30% UV treated CMD scaffolds. The inset graph compares the Young's modulus (n=7) of differently treated 15% CMD scaffolds. (*: P>0.05)

3.3.5 Surface Morphology

Figure 3-11 illustrates the surface topography changes in 15% CMD scaffolds after different cross-linking treatments, compared to the non-treated sample at higher magnification. The typical nano-structure of collagen fibrils, with their bands, is revealed in all samples by the very high magnification inset images in Figure 3-11. A ramous surface morphology can be seen in all treated samples while non-treated material shows no signs of dehiscence. It indicates that more cross-linking between the collagen polymer chains in the fibrils has occurred due to the different physical treatment. The DHT sample shows more surface cracks compared to other materials (Figure 3-11: C). On the other hand, UV and DHTUV treated materials (Figures 3-11: B & E) show the fewest cracks. In addition, the UV treated scaffolds show many network structures indicative of maximum cross-linking, and the UVDHT treated scaffolds are

moderately ramous. Considering these results, UV and UVDHT appear to have the more optimal surface morphologies, compared to the other treated or non-treated scaffolds.

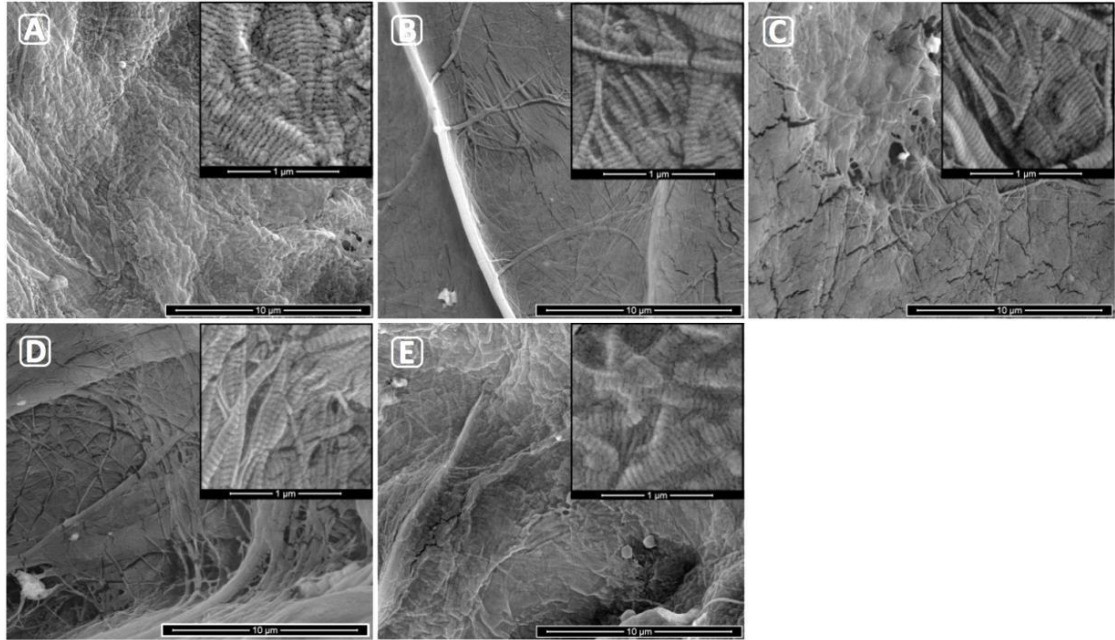


Figure 3-11: FESEM images of fibrous surface morphology of A) Non-treated, B) UV, C) DHT, D) UVDHT, and E) DHTUV 15% CMD scaffolds. The scale bars represent 10 μm (for insets 1 μm).

3.3.6 Thermogravimetric Analysis (TGA)

All CMD materials show two main decomposition temperatures according to the two major weight losses (Figure 3-12). The first weight loss (10-16 wt %) appears at around 265°C and is due to adsorbed moisture, adsorbed water and also collagen present in the material. The next decomposition (56-66 wt %) occurs at almost 720°C and represents the inorganic components in cartilage.

Increases in thermal stability, which is measured in terms of the first decomposition temperature, is a result of and proportional to formation of cross-linked structures (Rodríguez-Baeza, Neira, & Aguilera, 2003). The 15% UV scaffold group showed the highest thermal stability of all treatments. The onset and offset temperatures of the first decomposition of 15% UV treated sample computed at 300.85 and 393.7 °C

respectively, which is higher than those of other treatments (see the inset in Figures 3-12: A & B). The average weight residue after the first decomposition is 36 ± 4 % regardless of treatment for all 15% samples (see the inset in Figure 3-12: C).

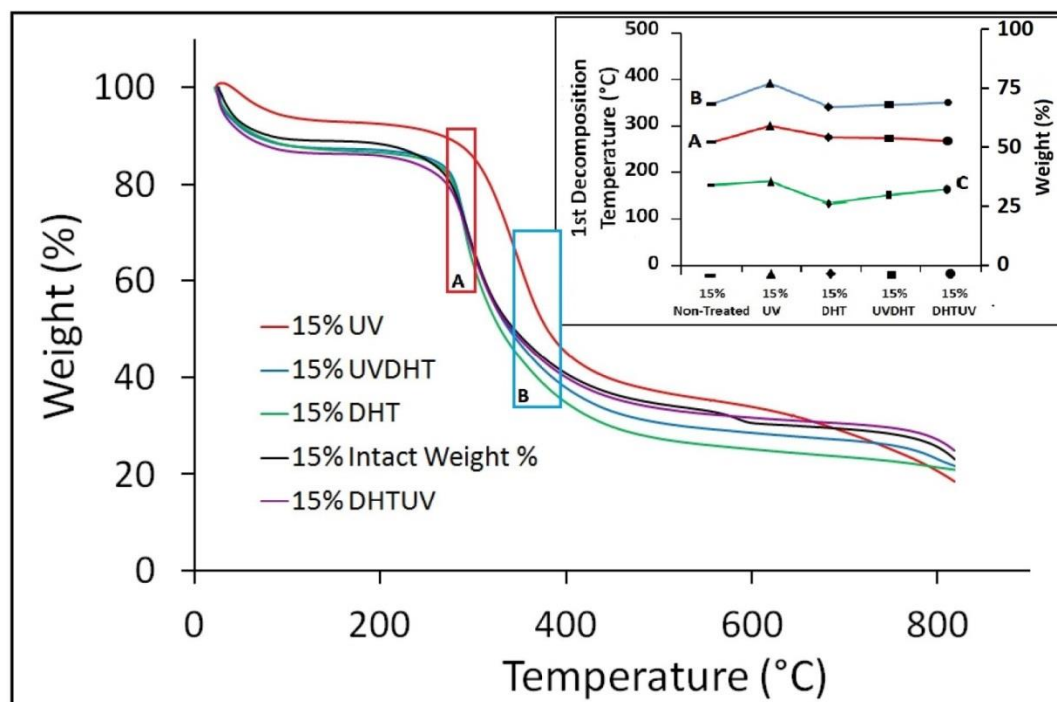


Figure 3-12: TGA of all the 15% CMDD scaffolds in nitrogen gas atmosphere at heating rate of $10^{\circ}\text{C}/\text{min}$, A) onset and B) offset temperatures of 1st decomposition, and C) weight residue (%) after 1st decomposition of differently treated 15% CMD scaffolds in TGA.

3.3.7 Differential Scanning Calorimetry (DSC)

Figure 3-13 shows the DSC results and indicates melting points (T_m , in $^{\circ}\text{C}$) of the 15% CMD scaffolds with different treatments. The 15% UV treated scaffold shows a significantly higher melting temperature compared to the other treated and non-treated scaffolds, indicating that it may have better mechanical properties which has already been shown in mechanical study. A higher melting point occurs due to the more cross-linking present in the 15% UV treated scaffolds than in other non-treated or treated scaffolds. The cross-links may have been damaged due to thermal energy in other treated scaffolds or by other treatments.

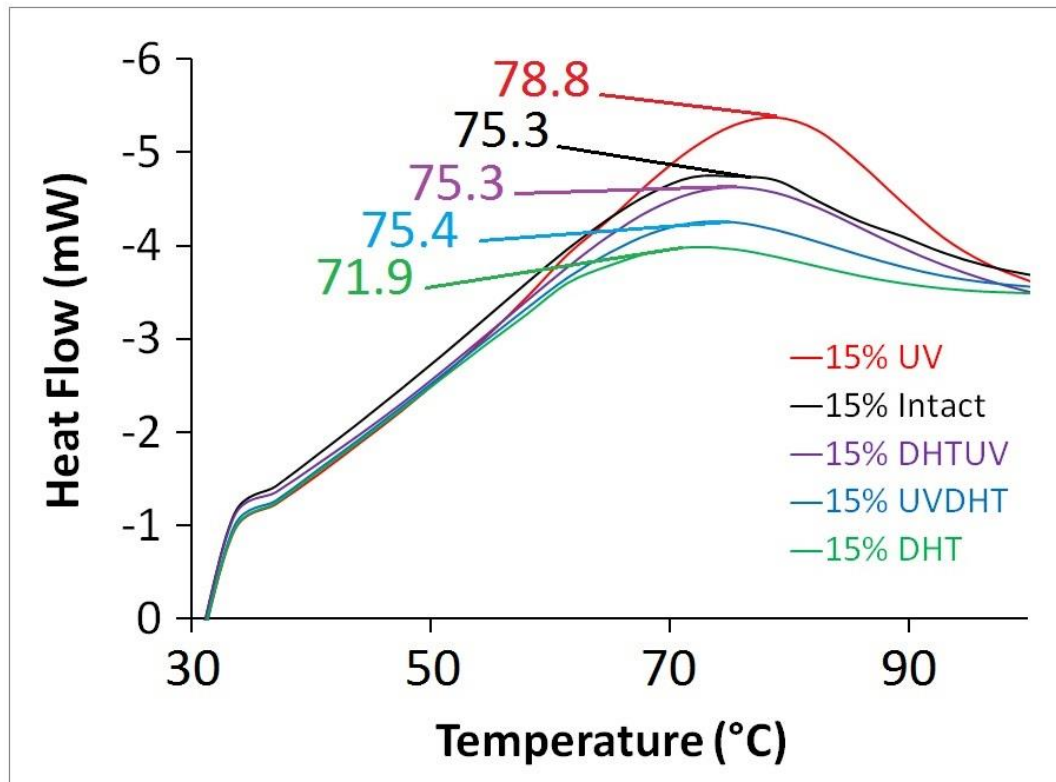


Figure 3-13: DSC analysis of 15% CMD scaffolds with different treatments indicating the melting temperature of each treatment.

3.3.8 FTIR

The FTIR spectra of 15% CDM scaffolds with different treatments are shown in Figure 3-14. Articular cartilage extracellular matrix (ECMD) derived scaffolds mainly consist of collagen II and proteoglycans. Amide I (C = O stretch), Amide II (N – H stretch, N – H bend combination), Amide III (C – N stretch, N – H bend, C – C stretch) and Amide A (N = H stretch) at wave numbers 1655, 1550, 1250 and 3330 cm^{-1} , respectively are the representative bonds of collagen, while sulphate stretch (C – O – S stretch) occurred at 1125-920 and 850 cm^{-1} , Amide I (C = O stretch) at 1640 cm^{-1} and Amide II (N – H stretch, N – H bend combination) at 1545 cm^{-1} are characteristic of Proteoglycans (Camacho, West, Torzilli, & Mendelsohn, 2001; Petra, Anastassopoulou, Theologis, & Theophanides, 2005; Ribeiro et al., 2012; Saarakkala, Rieppo, Rieppo, & Jurvelin,

2010). All the characteristic FTIR peaks, including Amides I, II, III, and A as well as sulfate groups for collagen and proteoglycans are shown in Figure 3-14.

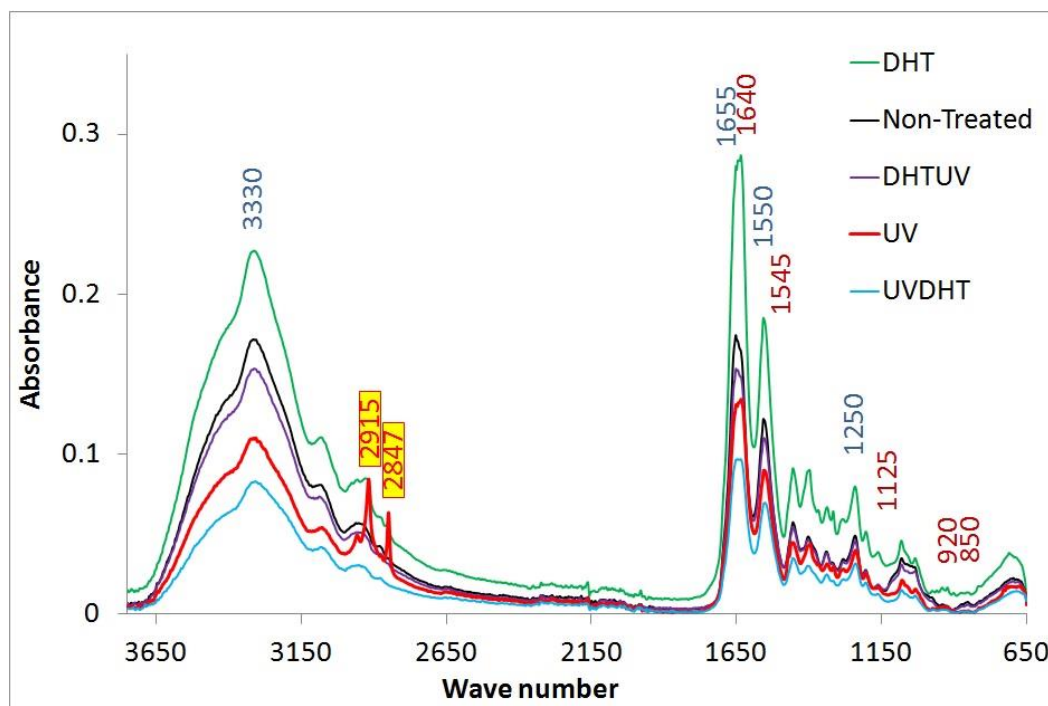


Figure 3-14: Typical FTIR absorption spectra of 15% CDM material with different treatments. Wave numbers defined in blue and dark red are representative for collagen and proteoglycans respectively. The two sharp peaks at 2847 and 2915 on 15%UV are representative for alkane groups formed during UV treatment.

The two sharp peaks at 2847 and 2915 wave numbers on 15%UV group spectrum are due to new alkane group formation from alkene groups during UV cross-linking treatment (Figure 3-14). The broken bonds from the alkenes in turn help the alkanes to make more crosslinks with the other chains of polymer collagens, as shown in Figure 3-15. The more cross-links through UV in 15% CMD scaffolds would restrain the scaffold structure during cell culture study better than other treated scaffolds.

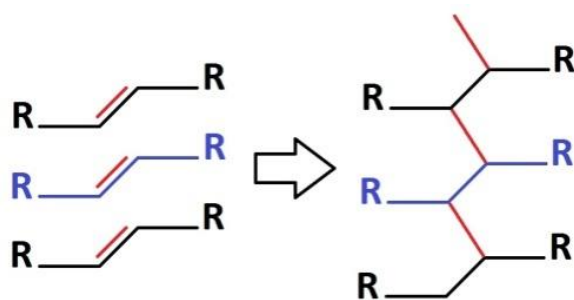


Figure 3-15: Alkene to alkane shifts will create new cross-linking bonds.

Considering the sensitivity of the Amide III band at 1235 cm^{-1} to native collagen tertiary structure and C-H deformation related insensitivity of the absorbance at 1450 cm^{-1} , the $1235/1450\text{ cm}^{-1}$ ratio can help in quantification of degradation (Gilbert, 1988; Jus et al., 2011). The ratio was 1.022 in untreated 15% CMD scaffolds and showed a decrease after treatment with UV (1.011) and UVDHT (1.008), indicating higher cross-linkage in initially UV treated samples, while increasing in DHT (1.030) and DHTUV (1.023) treated scaffolds resulting from a partial degradation in samples first treated with DHT.

Our FTIR findings show that the effectiveness of physical treatment of CMD constructs is highly dependent on the concentration of CMD content in the construct. At low CMD concentrations (e.g., 5% CMD in our case) UV treatment causes more cross-linking, reconfirming the findings of Bellincampi and Dunn (Bellincampi & Dunn, 1997). When the CMD concentration is increased to 15% the DHT treatment forms a higher cross-linking while UV treatment has more denaturation effects, which replicate the findings of a study on collagen fibers conducted by Weadock et al (K. S. Weadock, E. J. Miller, E. L. Keuffel, & M. G. Dunn, 1996). At the same time, alkene to alkane transitions provide supportive cross-linkings.

3.4 Discussion

ECM-based strategies are already established in tissue engineering (Benders et al., 2013). Native cartilage ECM-derived scaffolds have been shown to support

chondrogenesis (Cheng, Estes, Young, & Guilak, 2011). Also, the effects of physical (UV and DHT) and chemical (carbodiimide) cross-linking treatments on chondrogenic differentiation and cell-mediated contraction of porous CMD scaffolds have already been studied (Rowland et al., 2013). However, the purpose of the current study was quantitative assessment of changes in the architectural and mechanical properties of physically cross-linked CMD scaffolds.

Considering other studies done were only based on 3% (Q. Yang, Peng, Guo, Huang, Zhang, Yao, et al., 2008) and 10% (Cheng, Estes, Awad, & Guilak, 2008); CMD scaffolds and according to the proportional weight of dry material content in native fresh bovine articular cartilage, we produced bovine CMD scaffolds with three different concentrations of CMD material: 5%, 15% and 30% concentrations.

The scaffolds underwent one of the five physical treatment conditions for cross-linking (Non-treated, UV, DHT, UVDHT, and DHTUV). Remarkable deformation and shrinkage after treatment, and small pore size were the major criteria to eliminate the 5% scaffold group. UV and UVDHT treated 15% scaffolds as well as UV treated 30% scaffolds showed the biggest pore sizes as compared to all other samples. Although UV treated 30% scaffolds have the same concentration of dry material as the native cartilage, they showed a lower porosity, a relatively higher shrinkage, and a very low compressive strength compared to UV and UVDHT treated 15% scaffolds. Structural stability, sufficient surface area for cell attachment, adequate space for diffusion of nutrients, cell migration and matrix deposition have been accounted as beneficial features of scaffolds with 95-97% porosity (Seal, Otero, & Panitch, 2001). UV and UVDHT treated 15% CMD scaffolds showed high porosity rates ($\approx 98\%$) and high Young's moduli. The compressive moduli of these scaffolds appeared to be higher than pure and enhanced agarose and agarose/PEG (G. Huang et al., 2012), cell seeded porous scaffolds derived from native porcine articular cartilage (Cheng et al., 2011), and close to PEG

hydrogels(Bryant & Anseth, 2002) as potential alternative constructs for cartilage tissue engineering.

While both UV and UVDHT treated 15% scaffolds showed high pore sizes, low shrinkages, and high porosities; UV treated 15% scaffolds showed a higher compressive strength, better thermal stability in TGA and DSC analyses as well as newly formed alkane peaks in FTIR which are obvious indicative of a higher degree of cross-linking.

Crosslinking changes the mechanical strength of the scaffold due to breaking of unsaturated bonds and converting to primary bonds between the polymer chains as confirmed by FTIR study. The breaking of unsaturated bonds and consequent transformation into the primary bonds are mainly responsible to change the porosity in the CMD scaffolds as revealed in the SEM micrographs. The surface morphology of UV treated 15% scaffolds also showed an optimal intertwined collagenous surface that favours better cell attachment.

DHT treatment has been reported to have beneficial effects in terms of providing bigger pore volume favouring cell attachment, proliferation, matrix production and cell-matrix interactions (Rowland et al., 2013). DHT treatment was also reported to increase the mechanical properties of collagen-glycosaminoglycan scaffolds (Haugh, Jaasma, et al., 2009). Our findings indicate that although the compressive profile of DHT treated 15% CMD scaffolds as well as its porosity are as good as UVDHT treated CMD scaffolds, DHT treatment results in higher shrinkage and smaller pore sizes at 15% cartilage matrix concentration as compared to UV and UVDHT treatments. UV and UVDHT treatments on 15% CMD scaffolds can yield stiffer CMD scaffolds with low shrinkage rates that simultaneously possess optimal microstructure and biocompatibility. Our study employed 5%, 15% and 30% CMD scaffolds and, based upon data obtained suggests that 15% CMD concentration is a critical value beyond, which results in significant changes in porosity and shrinkage.

Therefore, fairly simple, feasible and cost effective UV and UVDHT treatments on 15% CMD scaffolds are promising candidates to provide the desired architecture while preserving bioactive factors, both of which are major concerns in the tissue engineering of scaffolds.

Future studies are required to elucidate the particular chondroinductive capabilities of physically treated CMD scaffolds, and to further characterise the results of the present study.

**CHAPTER 4: DEVELOPMENT OF MICROVOLUMETRIC
MODIFICATION OF LIQUID DISPLACEMENT METHOD
FOR POROSITY MEASUREMENT**

4.1 Introduction

As discussed in Chapter 3, the measurement of porosity for light and highly porous materials has required the development of a novel technique. In this chapter we detail the wider background to such an undertaking, and the development of this technique.

Porous materials find widespread applications almost in all the areas, covering engineering to medicine (Bertoldi, Farè, & Tanzi, 2011; H. Park & Miwa, 2003; Parrilli, 2010; Pramanik et al., 2012). For these applications, the porosity and pore size have significant effect on different properties of porous materials. For instance, porosity is a highly determinant factor in fabrication of three-dimensional (3D) scaffolds in tissue engineering to mimic the extracellular matrix as templates onto which cells of various tissues attach, proliferate, move and function (Johnson, Bahrapourian, Patel, & Mequanint, 2010; Pramanik et al., 2012). Pore density is important in the fabrication of synthetic materials used in various applications such as filtration, bioreactors, analytical devices, prostheses etc. (Bradham, 1960; Fry, DeWeese, Kraft, & Ernst, 1964; Furneaux, Rigby, & Davidson, 1989). Therefore, it is essential that characterizations of the porosity of these materials be conducted accurately.

Due to the importance, various methods have been developed to characterize the porosity, such as (BET) which uses the Archimedes' principle based and computerized tomographic imaging techniques. Archimedes' principle based liquid (Calvo, Bottino, Capannelli, & Hernández, 2008; Peinador et al., 2011) and gas (Szepes, Kovács, & Szabóné, 2005; Westermarck, 2000; Westermarck, Juppo, Kervinen, & Yliruusi, 1998) displacement as well as computerize tomographic imaging (Vergés, Ayala, Grau, &

Tost, 2008) methods of porosity measurement are routinely used for porous material characterization. Eligibility of application of each technique for different porous materials depends on their physiochemical properties. Although micro-CT is assumed as a gold standard technique for porosity measurement especially in biomedical field, it is not applicable to non-opaque materials. Cost and time-consuming process of data acquisition especially at high resolution rendering and the need for high performance imaging machinery and users are still important concerns and hence measuring the porosity through other methods is considered. Probable invalid equation due to absence of a truly linear region, shrinkage of some samples, need of degassing thermal preparations, limited nitrogen gas adsorption with highly porous solid samples(Kissa, 1999) and restrictions with the minimum sample size(Sharif, DiMemmo, Davidovich, & Sarsfield) and cost are some limitations with BET surface area analysers. Cost-effectiveness and feasibility have been the main reasons that Archimedes' principle based liquid displacement methods are still favourable. However, determining the porosity of non-opaque small sized highly porous light materials through these methods has always been a big concern. However Archimedes' principle based and micro-computerized tomography (micro-CT) techniques are comparatively better. In micro-CT, pore distributions from several tomographical images, generally developed by X-ray, are combined together to get total porosity of small 3-D scaffolds. Variations of Archimedes' principle based liquid displacement method are still favourable due to their simplicity, inexpensiveness and ease of use for determination of porosity of solid materials with irregular shapes. Suspension (Figure 4-1: A), level (Figure 4-1: B), and overflow (Figure 4-1: C) methods are three different modifications of liquid displacement using the same Archimedes' principle. It has been shown that suspension technique is the most preferred method in terms of accuracy and precision(Hughes, 2005).

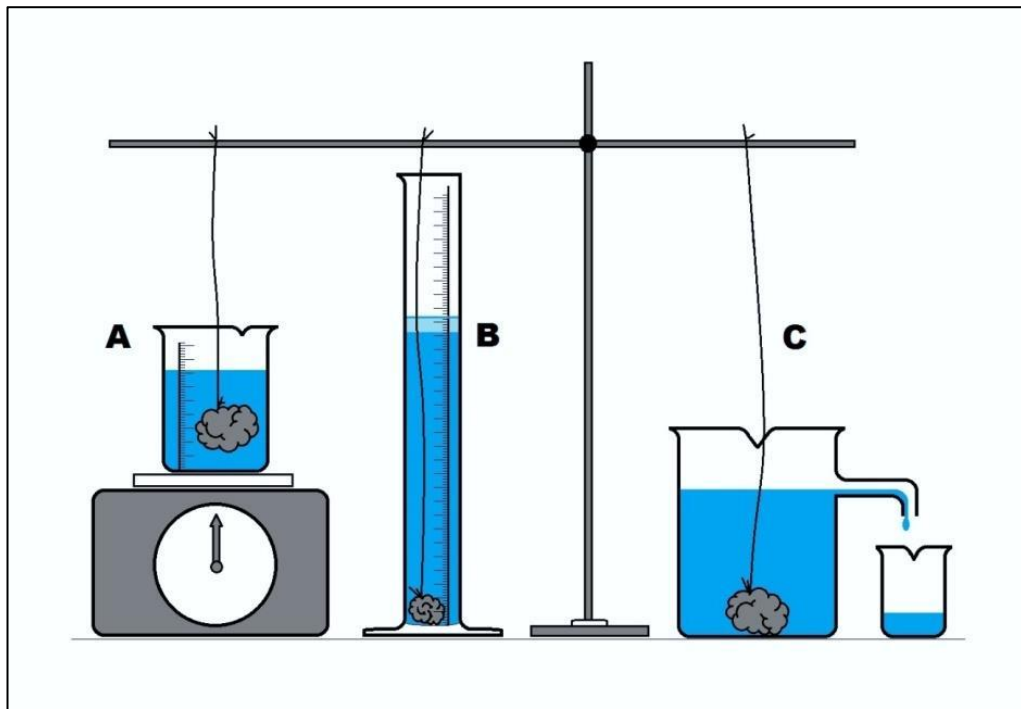


Figure 4-1: Schematic diagram of the A) suspension, B) level and C) overflow methods of measuring volume.

However, there are several limitations associated with these methods. For instance, the accuracy of each method depends on how delicate the weight or volume changes are read. On the other hand, precision and accuracy of the method depend on the readability of the weighing scale or volumetric readings. Moreover, the sample is to be suspended stationary in the liquid by means of a string line, which can affect the readings by exerting a tension effect. Considering the weight and geometry of the sample, the string weight and volume may also not be negligible. Thus, suspension method cannot be used for small and very lighter objects. Overflow method on the other hand may not be applicable to very light and highly porous materials due to their geometry and the limitations caused by surface tension.

Therefore, there is still an unmet need for a much precise method for porosity measurement of ultra-light highly porous materials. In this study, we aim to develop a very precise and accurate modification of the “Level” method, which is consistently

applicable for very small and light objects up to the volume of only few microliters such as those used within this thesis.

4.2 Materials and Methods

4.2.1 Experimental Set up

A 10 ml glass pipette with an internal diameter of 7.2 mm was used for the experiment. The narrow tip of the glass pipette was cut and the other side was sealed with a rubber cap. A small magnetic bar (29x6 mm, 3 g) along with a modified insulin syringe plunger was inserted in the pipette to assist in taking out the soaked sample from the glass pipette. (Figure 4-2)

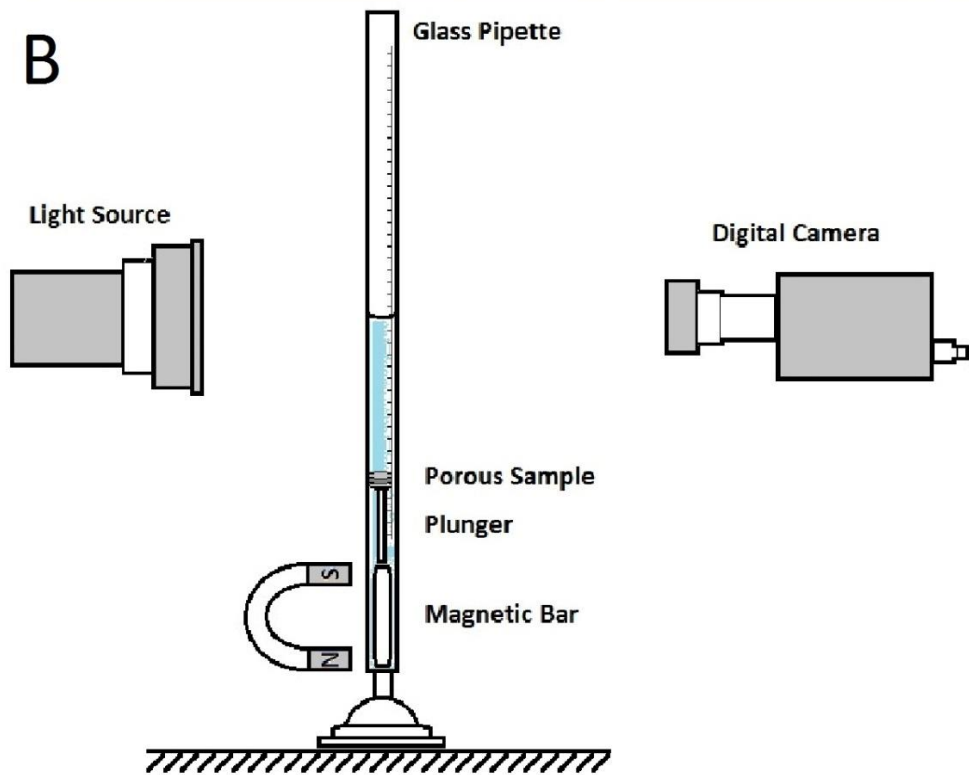
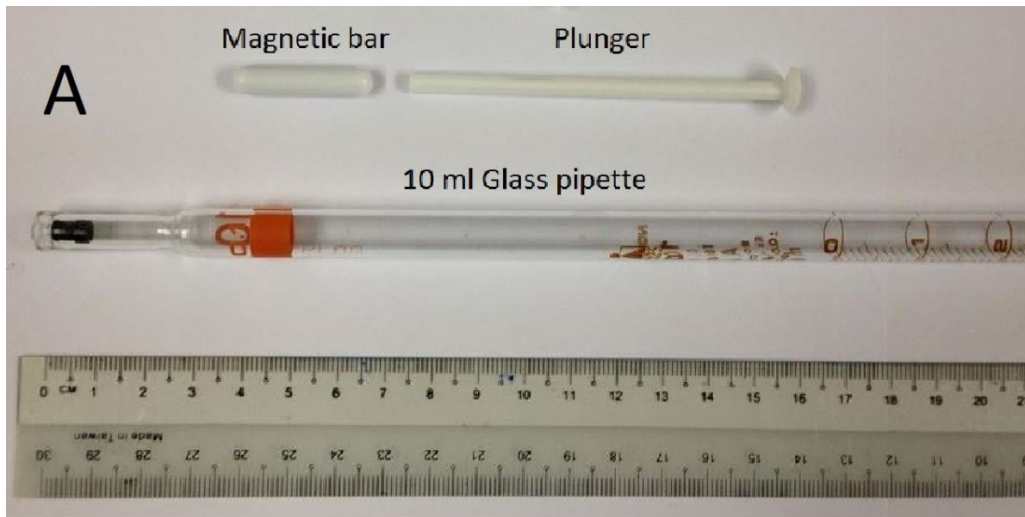


Figure 4-2: components of Microvolumetric liquid level displacement method for porosity measurement: A) magnetic bar, plunger from insulin syringe, and 10 ml glass pipette end sealed with rubber cap 2) Set up and vertical alignment of the measuring pipette and its internal components.

An *OCA 15EC* optical contact angle measuring instrument, *dataphysics*®, Germany was used to capture the images more perfectly during test. The sample table for contact angle measurement was replaced with the glass pipette, which was totally aligned and fixed vertically in between light source and the camera. (Figures 4-2: B and 4-3)

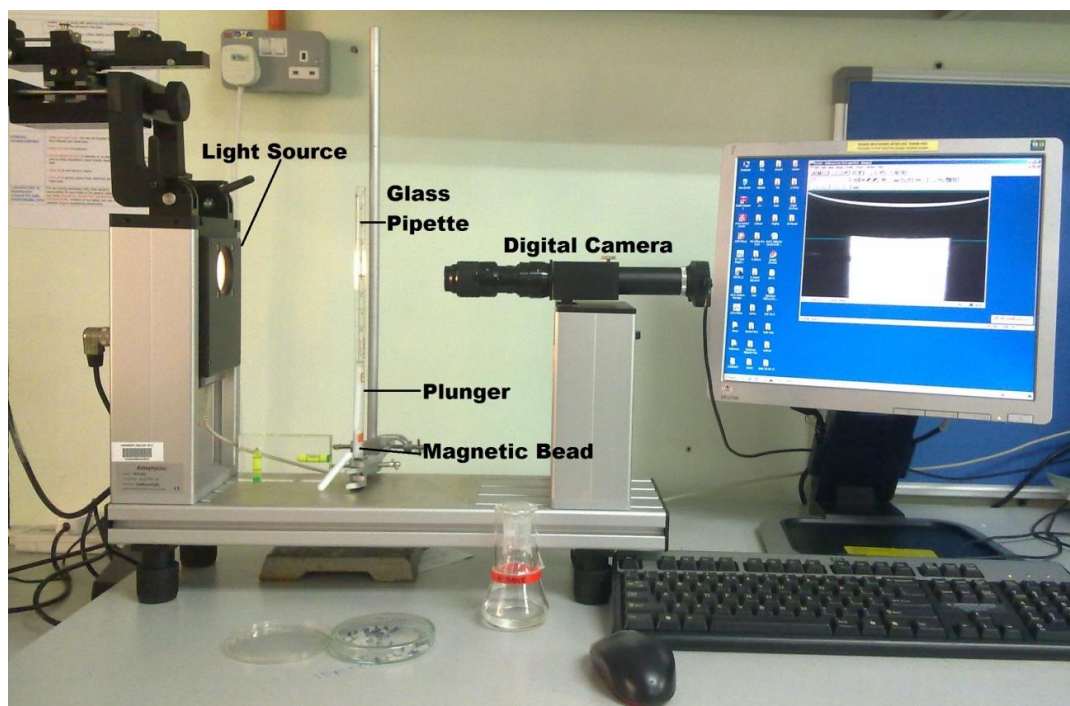


Figure 4-3: Laboratory set up for modified microvolumetric level displacement method for porosity measurement. The measuring glass pipette with its components aligned vertically in between the light source and the digital camera. The monitor shows the liquid level.

The glass pipette was filled up to the lens vision level with liquid hexane (Fisher Scientific # H/0421/PB17), which can be clearly observed on the computer monitor. Hexane is as an inert, cheap, relatively safe and colourless liquid. The digital level marker was adjusted at the liquid level after proper focusing and the image was captured on the computer screen (Figure 4-4: A). Using a micropipette, 100 μl of hexane was added to the previous level (Figure 4-4: A) and the second image was captured with a new liquid level marker. The distance between the two markers was later used for scale calibration with the image processing software (Figure 4-4: B). This calibration step is most important to validate our technique as precise and accurate. The new level was assigned as the new reference baseline.

4.2.1.1 Microvolumetric Measurements

Using a fine tip tweezer and side pinching with agility, the sample was moved into the standing pipette and let to sink. Once the sample was sat on the plunger surface, the

elevation of the liquid level inside the pipette from the baseline was marked with a level cursor on the computer and the image was captured (Figure 4-4: C). An external U-shaped permanent magnet was used to pull up the suspended sample, which was sitting on top of the plunger, with help of inside magnetic bar in the glass pipette, and then it was removed with the tweezers from the glass pipette. The plunger was left to settle back down the pipette. The liquid level marker was established and the last image was captured (Figure 4-4: D).

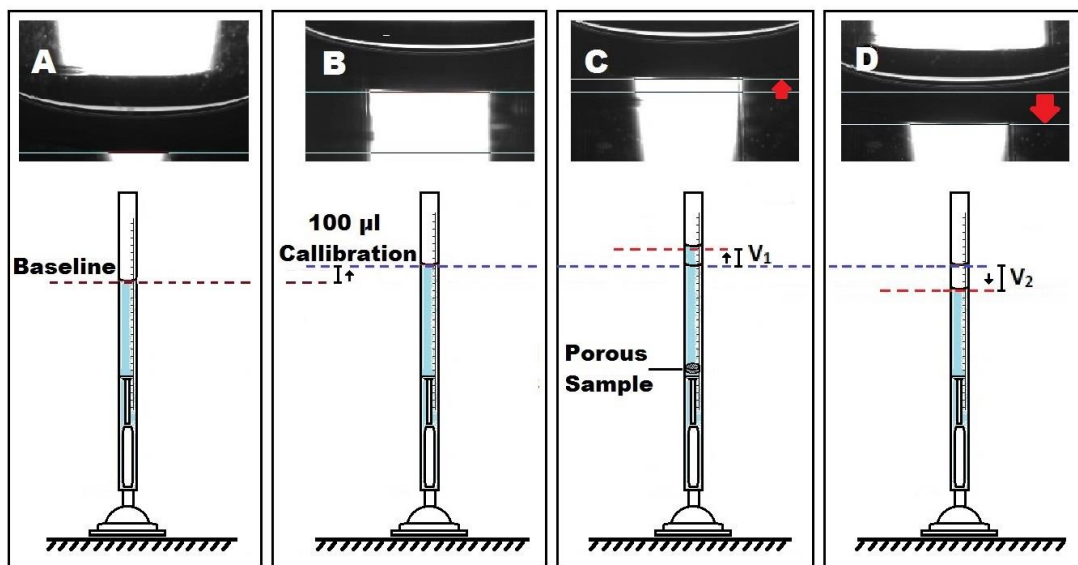


Figure 4-4: Microvolumetric level method for porosity measurement: A) Baseline establishment, B) Level calibration with 100 µl volume and second level establishment, C) V_1 : level elevation after immersing the sample, and D) V_2 : Volume depletion after removing the sample.

Changes in the hexane level in the pipette from the baseline after calibration were recorded. When the sample was immersed in the pipette, it sank into the hexane and sat on top of the plunger surface and the hexane level elevated to a higher level compared to the baseline. This volume change was recorded by the digital camera and called (V_1), representing the absolute volume of the sample. After removing the sample the hexane level dropped to a lower level compared to the baseline. The image of this volume depression which was called (V_2) and represented the pore volume in the sample was

captured by the camera using a SCA20 software version 4. 2. 4. (*dataphysics*® Instruments). Changes in the hexane level were precisely measured through length measurement using ImageJ® 1.47v software. The volume calibration image was used to convert length to volume through imageJ® software.

Percentage of total pore volume was calculated as:

$$\text{Total pore volume} = \frac{V_2}{V_1+V_2} \times 100 \%$$

Where, V_1 is volume change after immersing the sample (absolute volume = volume of solid matter without pores) and V_2 is volume change after removing the sample (pore volume).

4.2.2 Validation of Microvolumetric method

To assess the accuracy and precision of the microvolumetric method of porosimetry three standard porous samples were prepared. Two groups of porous alumina made of alumina/poly-(ethylene oxide) composites with different ratios were fabricated by means of sintering. Briefly, 5.45 g and 5.62 g of poly(ethylene oxide) (density: 1.21 g/cc) were mixed homogeneously with 0.86 g and 0.81 g of Al_2O_3 (density: 3.95 g/cc), respectively and then the mixture powder was pelletized in a stainless steel mould at room temperature at 100 MPa uniaxial pressure using a hydraulic press. The pellets ($\phi 10 \text{ mm} \times 5 \text{ mm}$) were then sintered at 1000°C temperature for 3 hours in nitrogen atmosphere to get 65% and 70% porous alumina structures, called alumina1 and alumina2, respectively. Sintered porous glass bars (R & H Filter Co. Inc, Georgetown, USA) with dimensions of 4 mm x 5 mm x 50 mm and porosity of 61.5%, as supplied by manufacturer, also were selected as the third standard porous material (Figure 4-5: A). Porosity measurement of standard porous samples was carried on through both microvolumetric method and micro-CT imaging.

4.2.2.1 Field Emission Scanning Electron Microscopy (FESEM)

FESEM was performed using a Quanta™ 250 FEG – FEI microscope to confirm the outer surface porosity of the fabricated porous samples.

4.2.2.2 Micro-CT

Micro-CT has been widely used as one of the best techniques to show the total pore volume and porosity present in a material with complex geometry (Bertoldi et al., 2011; H. Park & Miwa, 2003; Parrilli, 2010; Zhang Yang & Xiaofeng, 2007). Therefore, three replicates of each standard porous group were subjected to micro-CT imaging for porosity analysis using a SkyScan-Bruker 1076 *in vivo* micro-CT (parameters: voltage: 59 kV, current: 100 uA, filter: Al 0.5 mm, resolution: 18 μm, rotation angle: 180°, rotation step: 0.7°, and number of scan slice: 100). Samples were mounted on polystyrene foam prior to CT scanning.

4.2.3 Statistical Analysis

A Bland-Altman analysis(Altman & Bland, 1983; Bland & Altman, 1986) was used to assess agreement between two methods of porosity measurement with the actual values. XLSTAT® version 2014.1.05 package for Excel® (2007) was used for data analysis. A range of agreement was defined as mean bias ± 2 standard deviation (SD).

4.3 Results

Actual size of the sintered porous pellets from three different porous materials is shown in Figure 4-5(A). Micro-CT and FESEM images shown in Figures 4-5(B) and 4-5(C-E) clearly show the porous structure of representative porous alumina1 and alumina12, and glass samples.

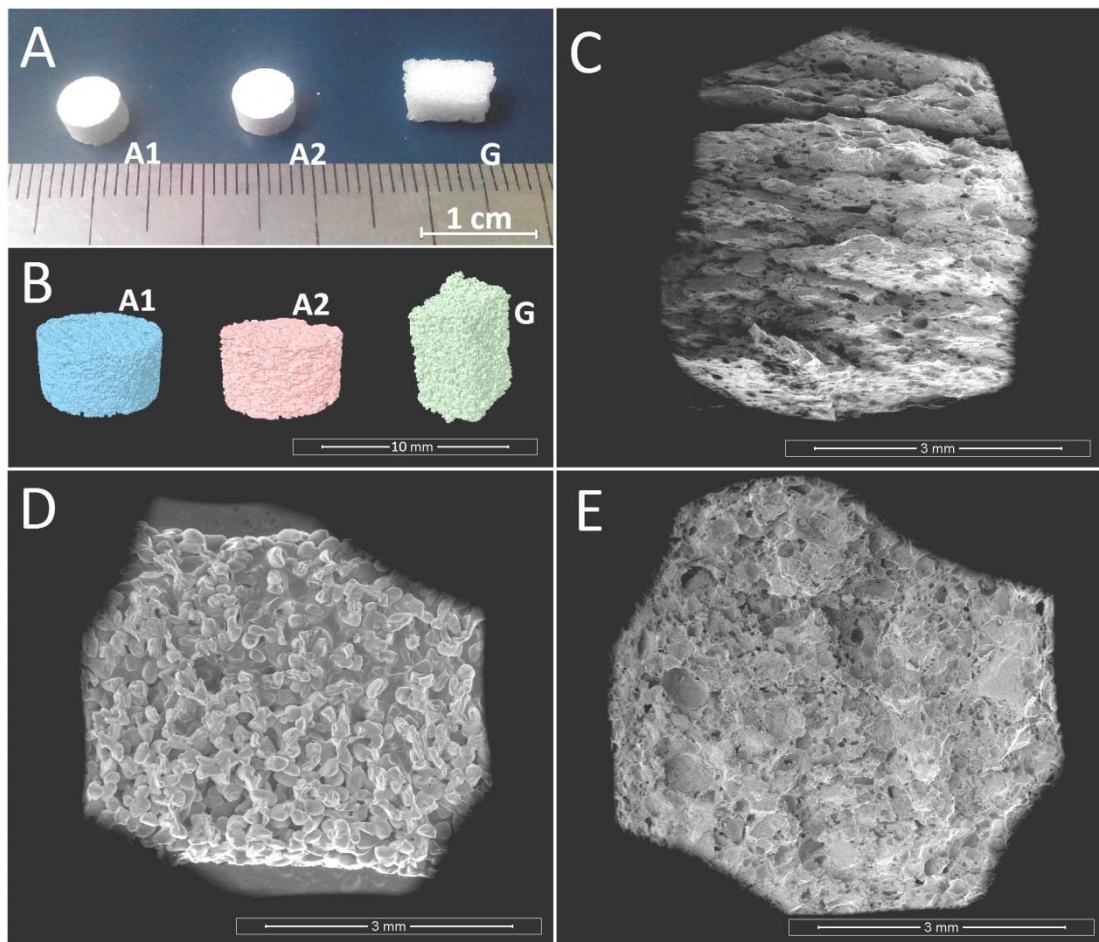


Figure 4-5: Digital photographs (A), Micro-CT 3D rendering images (B), and FESEM micrographs (C-E) of representative porous alumina1, glass, and alumina2 samples respectively.

The original results of porosity measurement by micro-volumetric and micro-CT methods along with the actual porosities for two types of porous different sintered alumina scaffolds and glass scaffolds are illustrated in Table 4-1. As it can be seen, total mass volume of the samples are to the scale of only few hundred microliters and volume measurements have been done to the resolution of less than one microliter.

Table 4-1: Micro-volumetric and micro-CT porosities compared with the actual porosity, mean and difference between each method and the actual value.

Samples	V ₁ (μ l)	V ₂ (μ l)	Actual Porosity (%)	Porosity from micro-volumetric (%)	Mean: Actual and Micro- volumetric	Difference: Actual and volumetric	Porosity from micro-CT (%)	Mean: Actual and Micro- CT	Difference: Actual and Micro- CT
Alumina 1-1	59.2	112.5	65	65.5	65.3	-0.5	40.6	52.8	24.4
Alumina 1-2	55.6	107.5	65	65.9	65.5	-0.9	74.1	69.6	-9.1
Alumina 1-3	56.6	109.5	65	65.9	65.5	-0.9	79.1	72.0	-14.1
Alumina 2-1	66.7	142.2	70	68.1	69.0	1.9	73.3	71.6	-3.3
Alumina 2-2	61.9	131.9	70	68.0	69.0	2.0	83.4	76.7	-13.4
Alumina 2-3	55.6	119.4	70	68.3	69.1	1.7	84.3	77.1	-14.3
Glass 1	172.8	274.5	61.5	61.4	61.4	0.1	55.9	58.7	5.6
Glass 2	241.4	389.9	61.5	61.8	61.6	-0.3	70.9	66.2	-9.4
Glass 3	107.5	170.8	61.5	61.4	61.4	0.1	79.6	70.5	-18.1

Figure 4-6 compares the measured porosity through micro-volumetric and micro-CT methods with the actual porosity of porous glass, alumina1, and alumina2 materials. While the values obtained from micro-volumetric method are almost equal to the actual porosities, with small standard deviations, the values gathered from micro-CT are different from actual porosity and have very big standard deviations.

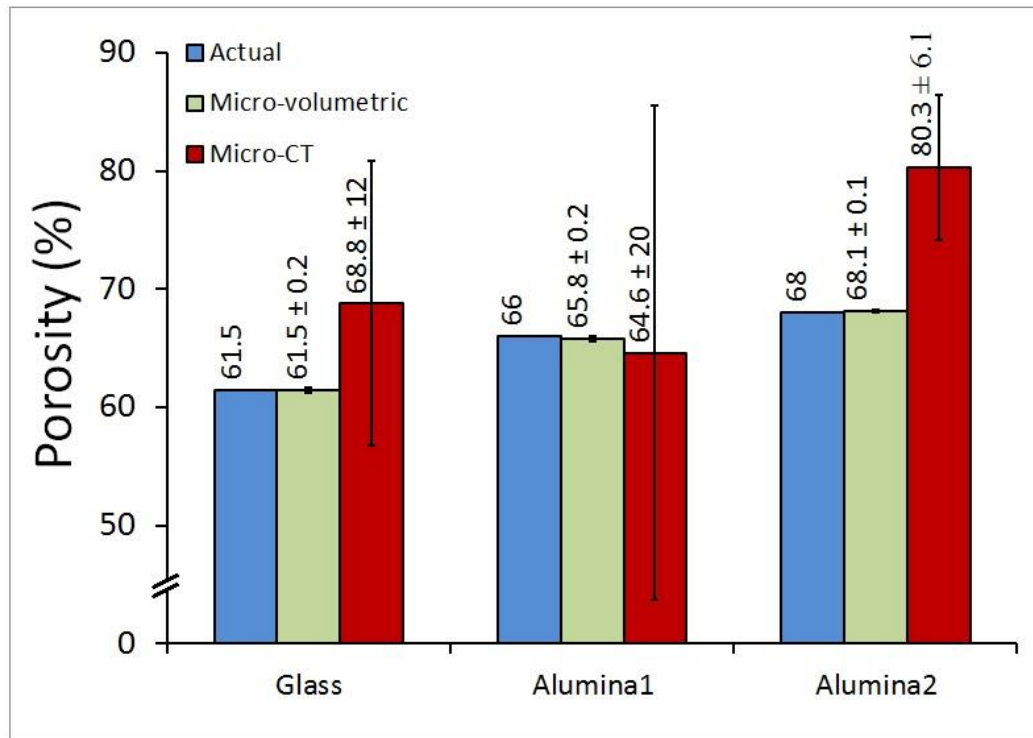


Figure 4-6: Comparison between the measured porosity through micro-volumetric and micro-CT methods with the actual porosities of porous glass, alumina1, and alumina2.

Figure 4-7(A) shows the scatter plot of measured porosity through micro-volumetric and micro-CT methods versus actual porosity values. There is a strong correlation coefficient of $R^2=0.92$ for micro-volumetric and actual porosities while that of micro-CT method and the actual porosities is only 0.14, indicating a weak correlation between the micro-CT and actual porosities. Figure 4-7(B) represents the Bland-Altman plot of the difference versus mean porosities of each pairs of data, indicating an almost consistent difference at various average porosities between the micro-volumetric and

actual porosity compared to the changing difference for different values of mean porosity between micro-CT and the actual.

Figure 4-7(C) also shows the Bland-Altman plots of the data with the bias and precision lines for both micro-volumetric and micro-CT methods. The accuracy (bias= -0.023) and precision (confidence interval: -0.459, 0.413) for micro-volumetric method is much higher than that of micro-CT method (Bias = 6.1, CI: -21, 33.1).

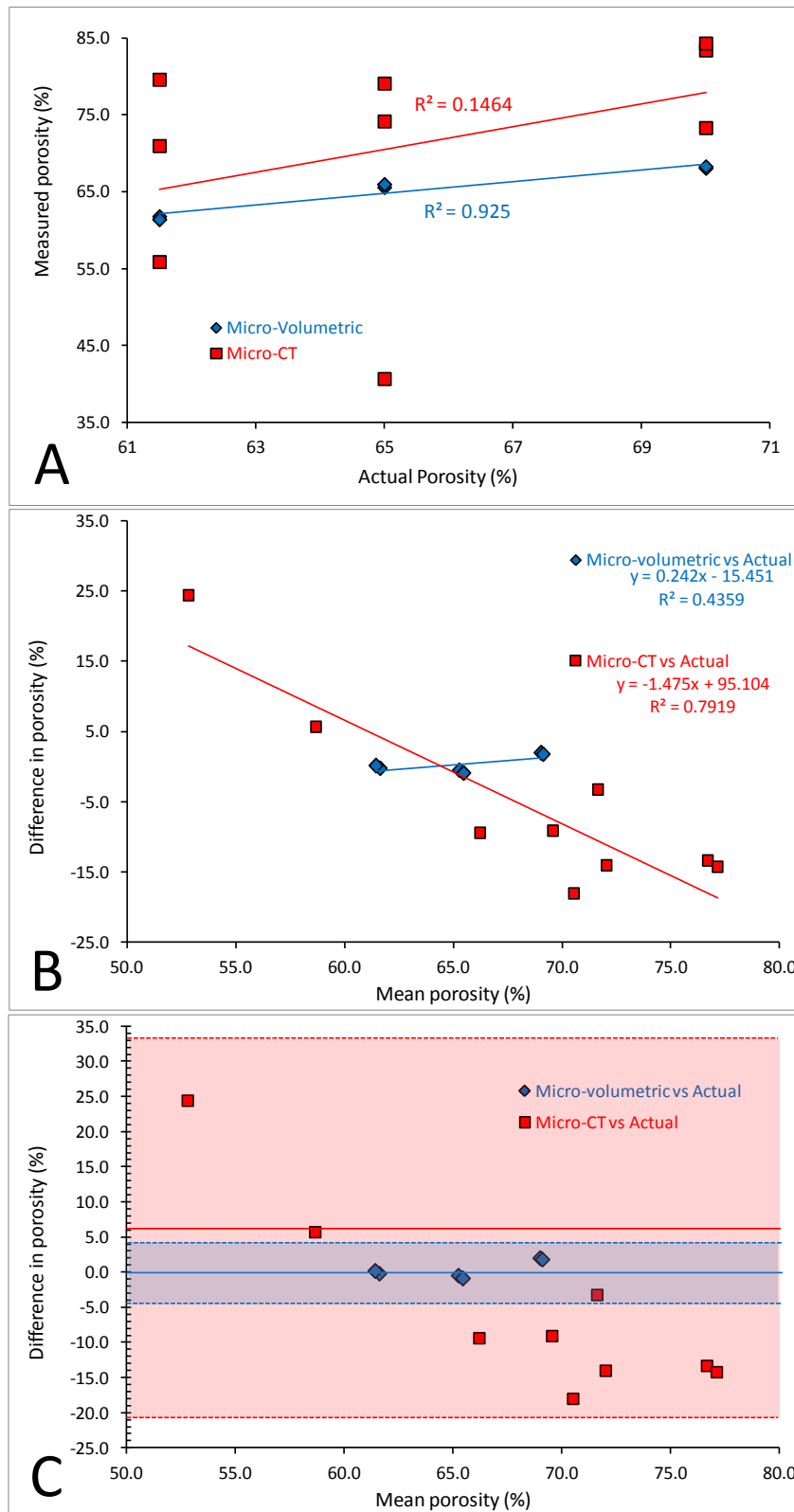


Figure 4-7: A) Scatter plot of measured versus actual porosity and the corresponding regression coefficients for Micro-volumetric and Micro-CT methods, and B) scatter plot of difference versus mean porosity of Micro-volumetric and Micro-CT with actual porosity, and C) Bland-Altman plots of the data showing the level of agreement between measured and actual porosities. The solid lines

indicate the accuracy and the square dotted lines represent the precision of the two techniques. 95% of the data are expected to fall within $\pm 1.96\sigma$.

4.4 Conclusion

In this chapter, a revised modification of Archimedes' principle based liquid level displacement method to increase the accuracy and precision of porosity measurements of small light highly porous materials for many advanced applications is hereby presented. Our method consists of using a pipette as a more delicate measuring cylinder along with the improved sample loading and removal system, and taking advantage of digital imaging and computer assisted image processing to increase the performance of liquid level change readings.

Our findings show that the precision and accuracy of our modification of Archimedes' method of porosity measurement is much higher than that of Micro-CT. Although each group of our standard samples were fabricated with constant conditions, microvolumetric method shows similar results with a small standard deviation for each type of construct, while micro-CT method fails to do so. We achieved an excellent precision and accuracy in porosity measurements. The readability of microvolumetric method is down to 1 μl volumes.

This method is applicable to any porous material regardless of opacity, lightness, shape and degree of porosity. Taking advantage of the magnetic bead/plunger escalator technique instead of a variable size string to suspend the sample, high performance lens with integrated continuous fine focusing ability, and adjustable observation and camera tilt angle, minimize the measurement errors and brings in a high precision and accuracy to the measurements.

Microvolumetric level method is one of the most accurate and precise methods of porosity measurement for ultra-light highly porous materials. Simple design, feasibility,

open source ImageJ® software and straight forwarded results all are the benefits of this modification.

CHAPTER 5: ISOLATION, CULTURE AND CHARACTERIZATION OF HUMAN DERMAL FIBROBLASTS

5.1 Introduction

There are two main strategies for isolation of human dermal fibroblast cells: enzymatic digestion of skin samples and the outgrowth (explant) method. Whilst enzymatic digestion can shorten the HDF production time, it often yields a non-homogeneous population of fibroblasts, therefore, the explant method is preferred when one seeks to isolate a pure population of HDF cells within 3 to 4 weeks (Froget et al., 2003). Further, the explant method can yield high motility cells, which are more suitable for tissue engineering applications in terms of their better penetration into the scaffolds (Rittié & Fisher, 2005).

In this chapter we explain the explant method for HDF cell isolation with minor modifications. Subculture and preservation of HDF cells as well as characterization are also described.

5.2 Materials and Methods

5.2.1 Cell Isolation

Ethical approval for this study was obtained from the University of Malaya Medical Centre (UMMC) ethics committee (PPUM/MDU/300/04/03, 22 April 2011). Redundant human skin from cosmoplastic surgery was procured from the UMMC operating theatre. Preferably, skin from non-sun-exposed areas of the body of female subjects was used for cell cultivation. The average age of the subjects was 27.5 ± 15 years. The minimum and maximum ages were 8 and 42 years respectively. Preoperative antimicrobial preparation (prep and drape) was done as the routine technique prior to incision. After excising the extra full-thickness skin, in some occasions along with the underlying fat tissue, the tissue was dipped in Povidone Iodine and then 70% ethanol,

each for 5-10 seconds. The skin sample was then washed with sterile saline and immediately transferred to a cell culture clean room in a sterile container with saline and 3-5X Antibacterial-Antifungal solution (Penicillin 100 IU/mL, Streptomycin 100 µg/mL, and Amphotericine B 0.25 µg/mL). The rest of the work was carried out inside a laminar flow biological safety cabinet. The skin samples were transferred to another sterile container with wash medium containing DMEM-HG (4.5g/l glucose) with L-glutamine and Sodium Pyruvate [cellgro® #10-013-CM] and 3X Penicillin-Streptomycin-Neomycin Solution [GIBCO # 15640]. Any remaining Infradermal fat was removed (Figure 5-1, A-C). The skin was first cut into strips of 0.5-1 cm². The epidermis was dissected from dermis using scalpel and surgical blades (Figure 5-1, D). The dermis then was minced to 0.5-1 mm² pieces (Figure 5-1, E&F). Nunc EasYFlask™ Nunclon™ T25 tissue culture flasks were pre-wetted with working medium (DMEM with 4.5g/l glucose, L-glutamine and Sodium Pyruvate [cellgro® #10-013-CM] supplemented with 20% FBS [SIGMA # F1051] and PSN [GIBCO # 15640]) and left to dry out inside the laminar flow biological safety cabinet. 5-10 minced dermal pieces were transferred to each flask and incubated (Figure 5-1, G-I). 30-45 minutes later 1-2 drops of working medium per each skin piece was gently added to the flasks on top of each sample. The flasks were incubated in 5% CO₂ at 37°C. The flasks were checked for possible drying of medium and 1-2 drops of working medium was added on top of each skin sample when necessary. After 3 days, and thereafter every 2-3 days, the medium was changed, until the cells started to grow, then the concentration FBS in working medium was decreased to 10%.

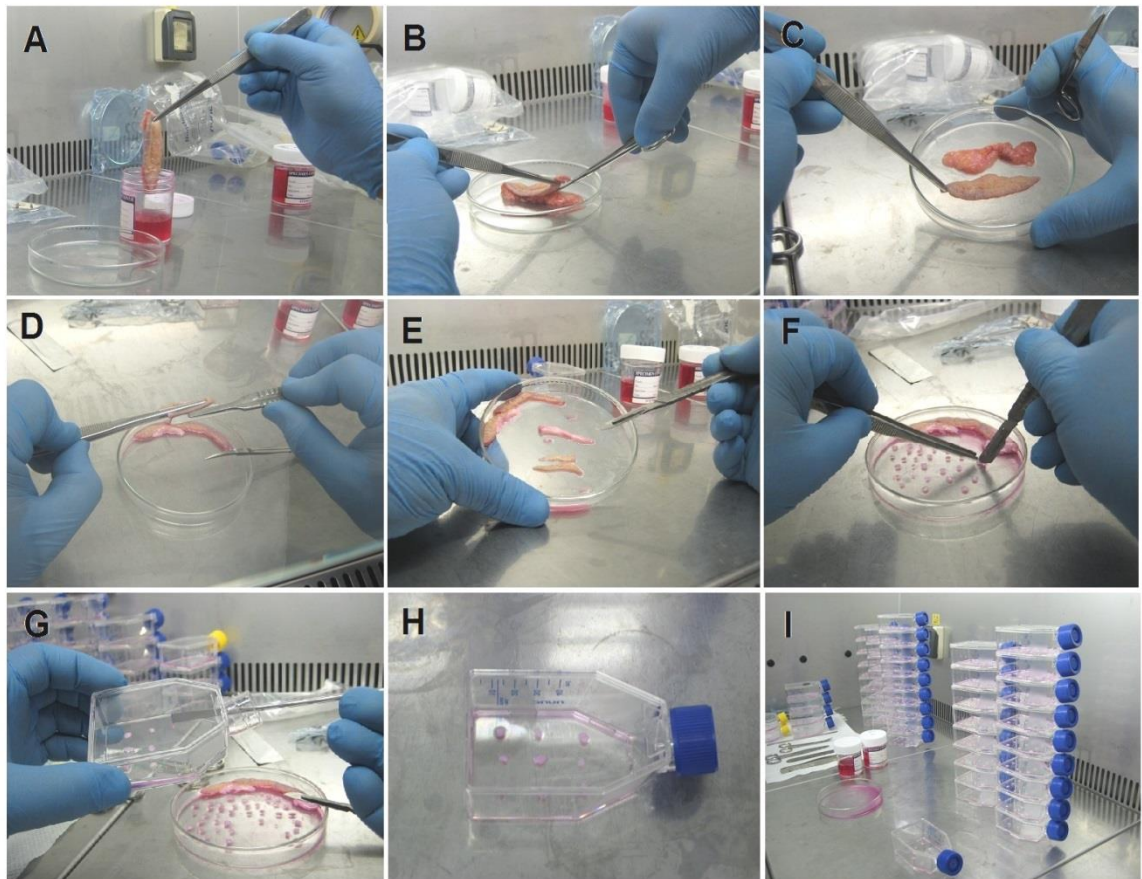


Figure 5-1: Outgrowth method for HDF isolation. A) Full-thickness skin washed in DMEM + 3-10X Antibiotic solution, B & C) Dissecting infradermal fat layer, D & E) Dissecting Epiderm from Derm, F) Mincing the Derm, G, H & I) Putting small minced derm samples in pre-wetted T25 flask.

5.2.2 Cell Harvesting

After the cells started to grow, the skin pieces were removed and cultured in new flasks with the same described method, and the same process was followed again. Cell isolation from the same skin pieces was repeated up to six times. After the flasks reached confluence of up to 70-100% passaging was done using TryPLE Select® [GIBCO# 12563011]. Briefly, the medium was removed and discarded and cells were gently washed with pre-warmed (37°C) PBS. After discarding the PBS, 2ml of TryPLE Select® was added to each T25 flask and incubated at 37°C for 3-15 minutes with intermittent monitoring under an inverted phase microscope (Nikon ECLIPSE TS100)

for cell detachment. Cell detachment was enhanced by tapping the flask. 5 ml working medium was added to each T25 flask to inactivate the TryPLE Select®. The cell suspension was transferred to 15 ml centrifuge tubes and spun at 220 RCF for 5 minutes. The supernatant was gently removed and the cell pellet was resuspended in 1ml fresh medium.

5.2.3 Cell Count and Viability (Dye Exclusion Method)

Preparation of Trypan Blue Solution

0.2 gm Trypan Blue (Sigma Catalog # F-7378) was dissolved in 99.8 ml Ultra-pure water and filtered through a 0.45µm hydrophobic membrane syringe filter (Thermo SCIENTIFIC Catalog # 9057). 0.2% Sodium Azide (Sigma Catalog # S2002) was added to make a stock solution. 2 ml stock solution was added to 0.43 gm Sodium Chloride (NaCl) in 9.58 ml Ultra-pure water to make the Trypan Blue working solution.

Cell Count and Viability

20 µl of the cell suspension was transferred to a 1.5 ml micro-centrifuge tube and topped up with the same amount of Trypan Blue working solution. After placement of a cover slip (Hausser Scientific, Horsham, PA) on a Bright-line Haemocytometer, 20 µl of Trypan Blue/cell suspension mixture was transferred to each of the two chambers of the haemocytometer.

The unstained (viable) and stained (nonviable) cells were counted separately in the haemocytometer. The total number of viable cells was multiplied by 2 (the dilution factor for trypan blue) to obtain the total number of viable cells per ml, and the total number of viable and nonviable cells were added up to obtain the total number of cells per ml.

5.2.3.1 Subculture of HDFs

According to the cell count results 5×10^3 cells per square cm were transferred to new T75 flasks. 12-15 ml fresh working medium was added to each flask and incubated at 37° in a 5% CO_2 humidified incubator. Sub-culturing the HDF cells was continued up to Passage 4 and then cryopreservation was done.

5.2.3.2 Cryopreservation

At passage 3, when the cells reached confluence, the medium was discarded and the cells in the T75 cell culture flask were washed twice with 10-15ml pre-warmed Phosphate Buffered Saline (PBS). PBS was discarded and cell harvesting was carried out using TryPLE Express[®] through the previously described method. After spinning the cell suspension at 220 RCF for 5 minutes and discarding the supernatant, the cell pellet was resuspended in 1 ml of working medium. Cell counting was performed. The cell suspension, with a density of 10^6 - 10^7 cells/ml, was transferred to a 2 ml cryovial and 7% Dimethyl sulfoxide (DMSO) [SIGMA#2650] was added to each vial. The cryovial was labelled, kept at room temperature for 30 minutes for equilibration, placed in a Mr Frosty[™] freezing container (Thermo Scientific), and moved to a -80°C freezer and left overnight. The next day, the cryovial was shifted to a liquid nitrogen tank for long-term conservation.

5.2.4 Resazurin Standard Curve for HDFs

Determining cell number and viability without the need to harvest or digest cells provides certain advantages. It allows the researcher to track the changes in cell number precisely, without the need of inference, and also to see the changes to cells as the result of external factors in real time. Resazurin (7-Hydroxy-3*H*-phenoxazin-3-one 10-oxide) has been used as a non-toxic cell number/viability quantifying assay with a variety of cell types (Dienstknecht et al., 2010; Gago et al., 2009; Jeney, Bazsó-Dombi, Oravecz, Szabó, & Zs-Nagy, 2000), bacteria (Lorenz et al., 2008; Riekstina, Muceniece, Cakstina, Muiznieks, & Ancans, 2008; Rutherford et al., 2002) and fungi (Xu, Rao, Zhu, & Chai, 1993) since the reagent was first introduced in 1929 (Pesch & Simmert, 1929). The indigo blue and non-fluorescent Resazurin can easily diffuse through cell membranes without harming the cells. A significant overtime reduction of AlamarBlue® dye co-incubated with post-mitochondrial fractions of murine hepatic cells has shown the role of microsomal, mitochondrial and cytosolic enzymes in intracellular metabolism of Resazurin (R.J. Gonzalez, 2001). Resazurin is oxidized inside the cells and turns into pink fluorescent Resurfin (Figure 5-2).

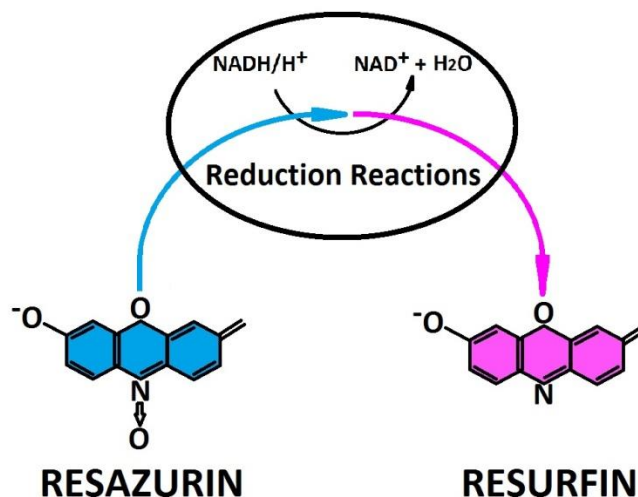


Figure 5-2: The bluish Resazurin passively diffuses into the cells and gets oxidized into pinkish Resurfin which diffuses back into the intercellular space.

Both Resazurin reduction and Resurfin production can be measured through colorimetric and fluorometric readings respectively. This helps to visually identify the metabolic activity of the cells which suggests that cells are indeed viable. Cost-effectiveness, safety, ease and feasibility of long term use and good correlation to other reference cell viability assays as well as feasibility of the application of other chemiluminescent assays are the reasons of the superiority of Resazurin among other assays (Chen et al., 2007; Dienstknecht et al., 2010; Rampersad, 2012).

Although Resazurin has been used to assess viability in a wide range and number of animal and human cells including Swiss 3T3 mouse fibroblasts (Voytik-Harbin, Brightman, Waisner, Lamar, & Badylak, 1998), rat hepatocytes (O'Brien, Wilson, Orton, & Pognan, 2003), Retinal Pigment Epithelial Cells (RPEs) (Yu, Chung, Yu, Seo, & Heo, 2003), and Mesenchymal Stem Cells (MSCs) (Dienstknecht et al., 2010), its suitability for use with primary HDFs has not yet been shown.

In this study, varying densities of primary HDF cells in monolayer culture on TCP were subjected to four different formulations from two commercial brands of Resazurin dye at varying incubation times. We show HDF attachment rate on TCP 4 hour after cell seeding. We report a detailed method to determine the most reliable formulation for dye preparation, Resazurin standard curve for primary HDFs, and also suggest a “Resazurin Reduction Nomogram” as a graphic tool for quantification of monolayer cultured primary HDFs based on Resazurin absorbance.

5.2.4.1 Cell Seeding

HDF cells at passage 5 were seeded at different densities (2, 6, 20, 50, and 100 x10³ cells/well) in quadruplicates in six separate Nunc® 24-well plates pre-wetted with working medium. The last well in each row was left unseeded as blank. Wells including the blank were topped up to a final volume of 500 µl with working medium and incubated in 5% CO₂ at 37°C for 4 hours.

5.2.4.2 Cell Attachment

Four hours after cell seeding two of the 24-well plates with different cell densities were removed from the incubator and subjected to trypsinization and cell harvesting. The cells from each well were collected in separate 1.5 ml microcentrifuge tubes and spun for 5 min at 220 RCF. After removing the supernatant, the cell pellets were resuspended in 200 μ l of fresh medium and cell count using the Trypan-blue and haemocytometer method was performed. The average \pm SD cell number attached on TCP surface, 4 hours after seeding varying cell densities was calculated.

5.2.4.3 Dye Preparation

To prepare the stock solutions, the Resazurin sodium salt powder (Sigma-Aldrich # R7017) was dissolved in Phosphate Buffered Saline (Sigma-Aldrich # P4417) solution and Phenol red-free Dulbecco's Modified Eagle's Medium (DMEM) (Sigma-Aldrich, Cat No.: D5921) separately at a concentration of 140mg/liter according to the instructions from Sigma technical support team. AlamarBlue[®] (Life Technologies # DAL1100) readymade stock solution was also purchased from a local company. The stock solutions were then re-diluted with either PBS or Phenol red-free DMEM to make 10% working solutions.

5.2.4.4 Resazurin Assay

4 hours after cell seeding and incubation the 24-well plates were also checked under an inverted microscope for cell attachment. The working medium was removed gently and discarded. 3ml of either pre-warmed 10% AlamarBlue[®] in PBS or AlamarBlue[®] in DMEM or Resazurin in PBS or Resazurin in DMEM was added to each well and the well-plates were re-incubated. After 50 minutes all four well-plates were wrapped in aluminum foil and shaken at 60 rpm for 10 minutes on an orbital shaker. Duplicates of 100 μ l of the dye from each well were transferred to a TPP 96-well-plate and the

absorbance was measured in the plate reader (FLUOstar OPTIMA (BMG LABTECH) at 570nm and 595 nm. Measurements were repeated every 1-2 hour up to 22 hours. The following manufacturer's formula (Gang et al., 2004) was used to calculate the percentage of AlamarBlue®/Resazurin dye reduction:

$$\frac{(\epsilon_{OX})_{\lambda 2} A_{\lambda 1} - (\epsilon_{OX})_{\lambda 1} A_{\lambda 2} \text{ of test agent dilution}}{(\epsilon_{OX})_{\lambda 2} A^{\circ}_{\lambda 1} - (\epsilon_{OX})_{\lambda 1} A^{\circ}_{\lambda 2} \text{ of untreated positive growth control}} \times 100$$

Where:

ϵ_{OX} = molar extinction coefficient of AlamarBlue oxidized form (BLUE)

ϵ_{RED} = molar extinction coefficient of AlamarBlue reduced form (RED)

A = absorbance of test wells

A° = absorbance of positive growth control well

$\lambda 1$ = 570nm

$\lambda 2$ = 600nm

% reduction in Resazurin at different cell densities was plotted against time to get the Resazurin Standard Curve for Human Dermal Fibroblasts.

5.2.5 HDF cell doubling time

Cells in culture proliferate on a binary fission basis; on the other hand each cell cleaves into two equal cells at an invariant rate. When the duration of time per cell repartition is known, population sizes can easily be predicted. The mean generational time (the time the cells need to double) can be calculated from population sizes at given times.

Generation of a growth curve is useful in evaluating the growth characteristics of the cells particularly when growth kinetics of cells on a special material is considered. From a growth curve, the lag time, logarithmic population doubling time and the stationary phase (saturation) density can be determined. The results are plotted on a log-linear scale, then the population-doubling time can be determined by identifying the cell

number along the exponential phase of the curve, tracing the curve until that number has doubled, and calculating the time between the two.

Methods

HDF cells were seeded at a density of 25×10^3 cells/well in pentaplicates in 6-well plates (TPP, Switzerland) pre-wetted with 500 μ l of working medium. The last well in each plate was left unseeded as the blank. After 4 hours of incubation in 5% CO₂ and 37°C all wells including the blank were topped up to a final volume of 3ml with working medium and re-incubated.

Five aliquots of cell suspension with the same density (2.5×10^4) were also prepared for total DNA quantification through Hoechst 33258 method.

Resazurin reduction test, cell count, and DNA quantification were performed at 24 h intervals every day.

DNA Quantification

Preparation of EDTA/PBE solution

10 mM (0.02922g) Ethylenediaminetetraacetic acid (EDTA) white powder (SIGMA #E6758) was dissolved in 100ml PBE (pH=7.8) and labelled properly, then autoclaved and left to cool down. (The EDTA will not dissolve in PBE unless its pH is adjusted to 7.8)

Preparation of DNA Standard

5 mg Deoxyribonucleic acid sodium salt from calf thymus Type 1 fibres (SIGMA #D1501) was weighed using a SHIMADZU AY220 Analytical Balance in sterile condition and dissolved in 5.00 ml of EDTA/PBE solution in a small sterile glass container inside the laminar flow hood. The container was left in a 0-4°C fridge overnight (≥ 16 hours). Once in a while the container was shaken gently. After around

12 hours the DNA started to make a gel. To shear the DNA, it was pipetted up and down several times using a sterile glass pipette. The DNA was filtered through a 0.45 µm syringe filter (minisart SRP15, Sartorius, Germany) after it was fully dissolved. The precise DNA concentration was checked with a Nanodrop ND2000 (Thermo Scientific). As DNA tends to be absorbed onto the plastic surfaces, it was aliquoted in 1-2ml bijoux tubes and frozen at -20°C. (This way the DNA standard solution can be stored for several months without significant degradation)

Hoechst Stock Solution

50mg of Hoechst 33258 (SIGMA #861405) was dissolved in 25.00 ml of ultra-pure water in a light-tight bottle to make 2mg/ml Hoechst stock solution.

Preparation of TEN Buffer

A mixture of 10 mM Tris, 0.2 M NaCl, and 1 mM EDTA in PBS was prepared, autoclaved, and the pH was adjusted to 7.4. The TEN buffer was used for diluting the Hoechst stock solution to a working solution of 0.2 µg/ml.

Papain Digestion

At each daily time point, pentaplicates of cells in the 6-well plate were trypsinized and harvested and subjected to Papain digestion after performing a Resazurin test and cell count.

1 ml of digest buffer with the following formula was added to each cell pellet.

Digest buffer ingredients:

- L-Cystein HCl (Sigma # C1276) 0.1576 g
- EDTA (Sigma # E6758) 0.0806 g
- PBS 100.00 ml

3 μ l (~5 KU) of Papain (Sigma # P5306) was added to each tube and incubated in a 65°C oven for 1 hour with intermittent vortex-mixings. The digests were centrifuged at 10,000 RPM for 10 min to sediment the residual debris. The supernatants were then ready for DNA quantification.

Standard DNA Curve

Serial dilutions of standard DNA were made at 50, 25, 12.5, 6.25, 3.125, 1.5625, and 0.78125 μ g/ml with PBE (Figure 5-3). Triplicates of 40 μ l of each dilution along with triplicates of each cell digest sample were transferred to a black, flat dense bottom 96-well-plate (Falcon, Corning # 3916). 200 μ l of the working Hoechst solution (0.2 μ g/ml) was added to each well in a dark room. Wrapped in Aluminium foil the 96-well-plate was transferred to the microplate reader (FLUOstar OPTIMA BMG LABTECH) and absorbance was read at excitation: 570 nm and 595 nm. An R^2 -value of ≥ 0.95 for the standard DNA dilution concentration against optical density was accepted.

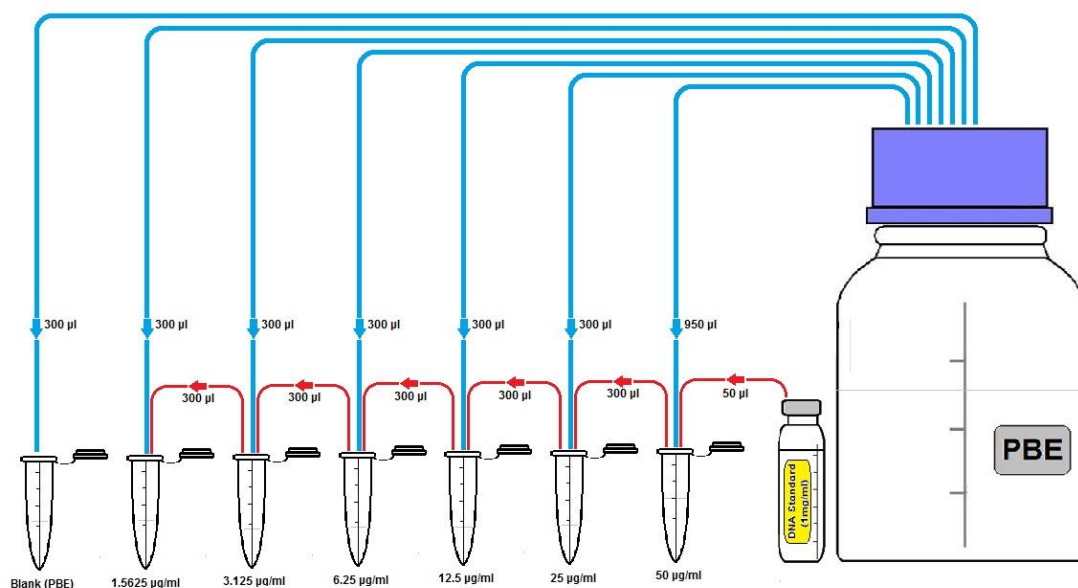


Figure 5-3: Preparation of serial dilutions of standard DNA.

5.2.6 Characterization of HDFs

5.2.6.1 Morphology:

The morphology of HDFs on tissue culture polystyrene was studied using an inverted phase microscope. Also Confocal and FESEM micrographs of HDFs seeded on collagen scaffolds (precisely described in Chapter 5) were used for HDF cell morphology.

5.2.6.2 Tri-lineage Differentiation

Tri-lineage differentiation was performed to rule out the possibility of presence of stem cells in HDF population. HDF cells at passage 4 were used for Tri-lineage differentiation. Human Bone Marrow Stem Cells (HBMSC) was also used as the positive control group. Immediately after thawing the cells they were washed with fresh medium and centrifuged at 220 RCF for 5 minutes. The supernatant was discarded and the cell pellet was resuspended in 1 ml of fresh medium. Cell count and viability test was done using Trypan Blue solution and Neobar Hemocytometer.

Adipogenic Differentiation

Cells were plated in Lab-Tek®II 4-Chamber glass slides (Figure 5-4) at a density of 2500-3500 cells per cm^2 (≈ 6000 cell/chamber) and incubated at 37° in a 5% CO_2 humidified incubator for 2 hours, then topped up with working medium.

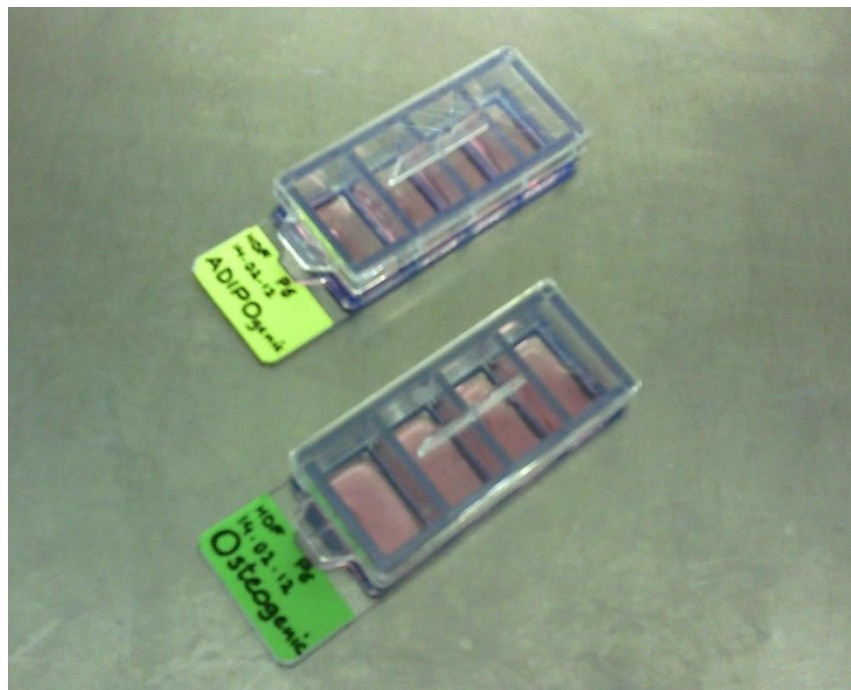


Figure 5-4: Seeding HDFs in 4-Chamber glass slides for adipogenic and osteogenic lineage differentiation.

The medium was replaced every 3 days until the cells were 100% confluent. Upon reaching a state of confluency, the medium was replaced by Adipogenesis induction medium (STEMPRO® Adipogenic Differentiation Kit- A10070-01) and this medium change is made reference to differentiation day 1. The adipogenic differentiation medium was changed every 2-3 days for up 21 days. Inverted phase microscopic monitoring for lipid droplets was performed every day for both test and control groups. At day 21 the medium was discarded and the cells were washed very gently with pre-warmed PBS and then Oil-Red O staining was carried out.

Oil-Red O Staining

Dye Preparation

0.5g Oil-Red-O (Sigma # O0625) was dissolved in 100 ml Isopropanol (Fisher # P/7500/17) in a warm water bath to prepare stock solution. Three parts of Oil-Red-O stock solution were mixed with 2 parts of ultra-pure water to make the work solution.

Staining

The medium was removed and discarded. Cells were washed with PBS. Fixation was carried on through incubating the cells with 4% Paraformaldehyde for 30 minutes at room temperature. After discarding the fixing solution the cells were washed with PBS three times and then 0.5 ml ultra-pure water one time. 0.5 ml of Oil-Red-O working solution was added to the cells in each chamber and incubated for 50 minutes at room temperature. Removal of the dye was followed by gentle washing with ultra-pure water three times. 0.5 ml Hematoxylin was added to each chamber and incubated for 10 minutes at room temperature. Hematoxylin was removed and cells were washed with ultra-pure water again. Stained cells were watched under inverted phase microscope and pictures were snapped.

Osteogenic Differentiation

Cell seeding was done with the same method described for adipogenic differentiation. After getting confluency the working medium was replaced with Osteogenesis induction medium (STEMPRO[®] Osteogenic Differentiation Kit- A10072-01) and this medium change corresponded to differentiation day 1. The Osteogenesis differentiation medium was changed every 2-3 days for 21 days. Inverted phase microscopic monitoring was performed every day for both test and control groups. At day 21 the medium was

discarded and the cells were washed very gently with pre-warmed PBS and then Alizarin-Red staining was carried out.

Alizarin-Red Staining

Dye Preparation

2.0 g Alizarin-Red (Sigma # A5533) was dissolved in 100 ml ultra-pure water and filtered through a 0.45 µm filter paper. pH was adjusted to 4.2 using 10% Ammonium Hydrochloride.

Staining

After discarding the medium the cells were washed with PBS, and then fixed through incubating with 10% Formaldehyde for 30 minutes at room temperature. Fixative removal was followed by gentle washing with PBS three times and ultra-pure water one time. Addition of 1 ml Alizarin Red to each chamber was followed by incubation at room temperature for 30 minutes. The dye was removed and cells were washed with ultra-pure water three times, each time with gentle shaking for 5 minutes. Image acquisition was done after addition of 1 ml ultra-pure water.

Chondrogenic Differentiation

Small droplets of cell suspension were put in a centric order in previously medium coated 6-well plate (Figure 5-5) at a total density of 10^3 cells per square cm and incubated.

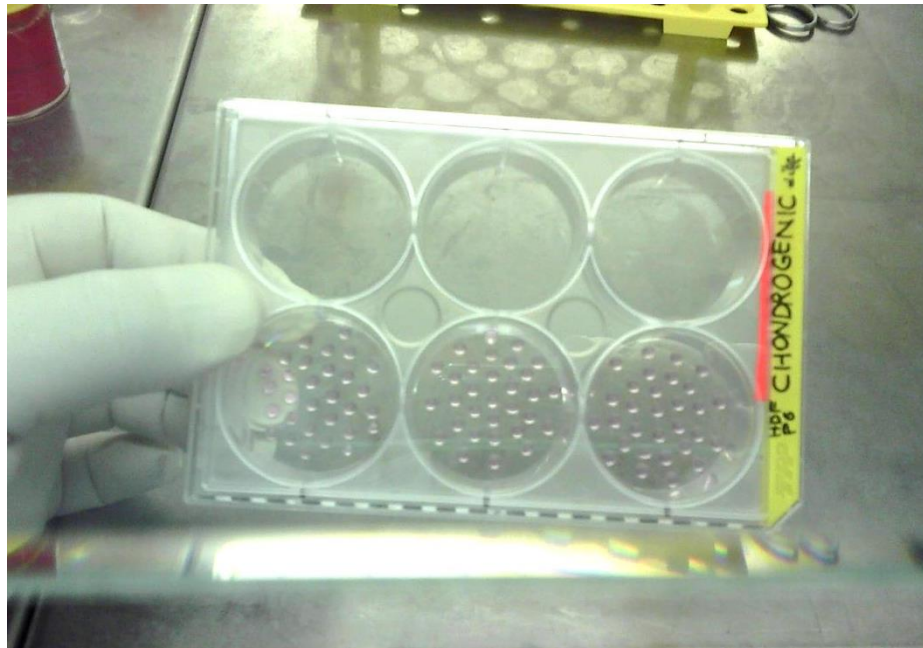


Figure 5-5: Centric cell seeding for Chondrogenic Differentiation.

Two hours later, 2 ml of chondrogenesis differentiation medium (STEMPRO[®] Chondrogenic Differentiation Kit- A10071-01) was added to each well and incubated. The Chondrogenesis differentiation medium was changed every 2-3 days for up to 21 days. Inverted phase microscopic monitoring was performed every day for both test and control groups. At day 21, the medium was discarded and the cells were washed very gently with pre-warmed PBS and then Safranin O staining was carried out.

Safranin-O Staining

Cells were rinsed with PBS and then fixed with 10% Formaldehyde for 30 minutes at room temperature. Washing the cells with ultra-pure water was followed by putting 2 ml 1.5% aqueous Safranin-O for 40 minutes. The dye was removed and cells were washed with ultra-pure water three times. 2 ml of 0.02% alcoholic fast green was added and removed after 30 seconds. 2 ml of 1% acetic acid was added and removed after 3 seconds and cells were rinsed quickly with ultra-pure water and watched under an inverted phase microscope.

5.2.6.3 Immunologic Differentiation

Flowcytometry

Cryopreserved HDF cells at P6 were used for flowcytometry. Bovine Aortic Endothelial Cells (BAECs) were used as negative control. Immediately after thawing the cell suspension was diluted with fresh pre-warmed complete work medium and centrifuged at 220 rpm for 5 minutes. The supernatant was discarded and the cell pellet was resuspended in 1ml fresh medium. Cell count was performed through Trypan Blue and Haemocytometer chamber method. Cells were washed with 15 ml of wash medium (0.5% Bovine Serum Albumin [aMReSCO # 0332-25g] in PBS) and centrifuged at 2000 rpm 5 minutes. The cell pellet was resuspended again in 12 ml wash medium and filtered through a 70 μ M BD FalconTM nylon cell strainer [REF 352350]. Filtered cells were counted again and then divided into three separate tubes along with one tube for BAECs, each containing $\geq 10^6$ cells and incubated on ice at 4°C for 20 minutes. After centrifuging at 2000 rpm for 5 minutes, the supernatants were discarded. The BAECs sample as the negative control and one of the HDF tubes were planned to be stained with CD90 (Anti-Fibroblast Antigen Mouse monoclonal Antibody) (AS02) [Calbiochem® # CP28] as the primary antibody. The second HDF tube was aimed to be stained with FITC conjugated CD31 CO.3E1D4 IgG2a antibody [GeneTex # GTX43622] as the negative control-2 and the last HDF was meant to remain unstained. The BAEC negative control-1 and HDF Sample were resuspended respectively in 85 μ l of sheath fluid [BD FACSTFlowTM # 342003] + 3 μ g/15 μ l of CD90. The HDF negative control-2 cells were resuspended in 90 μ l of sheath fluid + 10 μ l of CD31, and the last HDFs were resuspended in 100 μ l of sheath fluid. All tubes were incubated at room temperature for 45 minutes. (Saalbach et al., 1996; Saalbach, Aust, Haustein, Herrmann, & Anderegg, 1997) After removing the primary antibody, cells were washed two times with sheath fluid and centrifuged at 2000 rpm 5 minutes. BAEC negative control-1 and

HDF Sample were resuspended in 90 μ l of Sheath fluid and 10 μ l of Cy5 conjugated Goat Anti-Mouse IgG Secondary Antibody [Thermo SCIENTIFIC # PA1 -28523], wrapped in Aluminium foil and incubated for another 45 minutes at room temperature. After washing out the secondary antibody all samples were centrifuged at 2000 rpm and resuspended in 500 μ l of sheath fluid and taken for flowcytometry. The final evaluation was done by using the FACS CANTO II.

QPCR

In the present study, two fibroblast specific markers along with four stemness markers were used for fibroblast characterization through gene expression. Table 3-1 shows the particulars of different gene assays used for QPCR.

Table 5-1: TaqMan® assays used for characterization of human dermal fibroblasts through gene expression

Markers	Gene name	Abbrev.	NCBI Ref. Seq.	Assay No.
Endogenous Control	Glyceraldehyde 3-phosphate dehydrogenase	GAPDH	NM_001256799.1	Hs02758991_g1
Fibroblast Markers	Fibroblast Specific Protein 1	S100A4	NM_002961.2	Hs00243202_m1
	Fibroblast Surface Antigen	THY1	NM_006288.3	Hs00264235_s1
Stemness Markers	Octamer-binding transcription factor	OCT4	NM_001173531.1	Hs04260367_gH
	Sex Determining Region Y-Box 2	SOX2	NM_003106.3	Hs01053049_s1
	NANOG	NANOG	NM_024865.2	Hs04260366_g1
	Rex1	ZFP42	NM_174900.3	Hs01938187_s1

- Fibroblast-specific protein 1 (FSP1) is a cyto/nucleoplasmic and extracellular calcium-binding protein that is encoded by S100A4 gene. FSP1 is assumed as a fibroblast marker in different organs (Österreicher et al., 2011; Strutz et al., 1995).
- Fibroblast surface antigen, known also as CD90 and Thy-1 (thymocyte differentiation antigen 1) is a heavy cell surface protein which is encoded by THY1 gene. In humans, Thy-1 is expressed by endothelial, smooth muscle, some of bone marrow cells, and also of fibroblasts of most vertebrate species studied (Saalbach et al., 1997; Vaheri et al., 1976).

- OCT4 is a protein encoded in human by POU5F1 gene and is involved in the self-renewal of undifferentiated embryonic stem cells.
- Sex Determining Region Y-Box 2 (SOX2) is a transcription factor responsible for pluripotency of stem cells.
- NANOG is also a transcription factor in embryonic stem cells and is responsible for maintaining the pluripotency and self-renewal.
- REX1 is protein encoded by ZFP42 gene and is responsible for maintaining the pluripotency of mesenchymal stem cells.

5.3 Results

5.3.1 HDF Cell Morphology

Fibroblast cells are known for their spindle shape morphology. Although they bear irregular round shapes when suspended, they start spreading when attaching on plastic surfaces. They align parallel while featuring wavy whirling arrangements in confluent states (Figure 5-6).

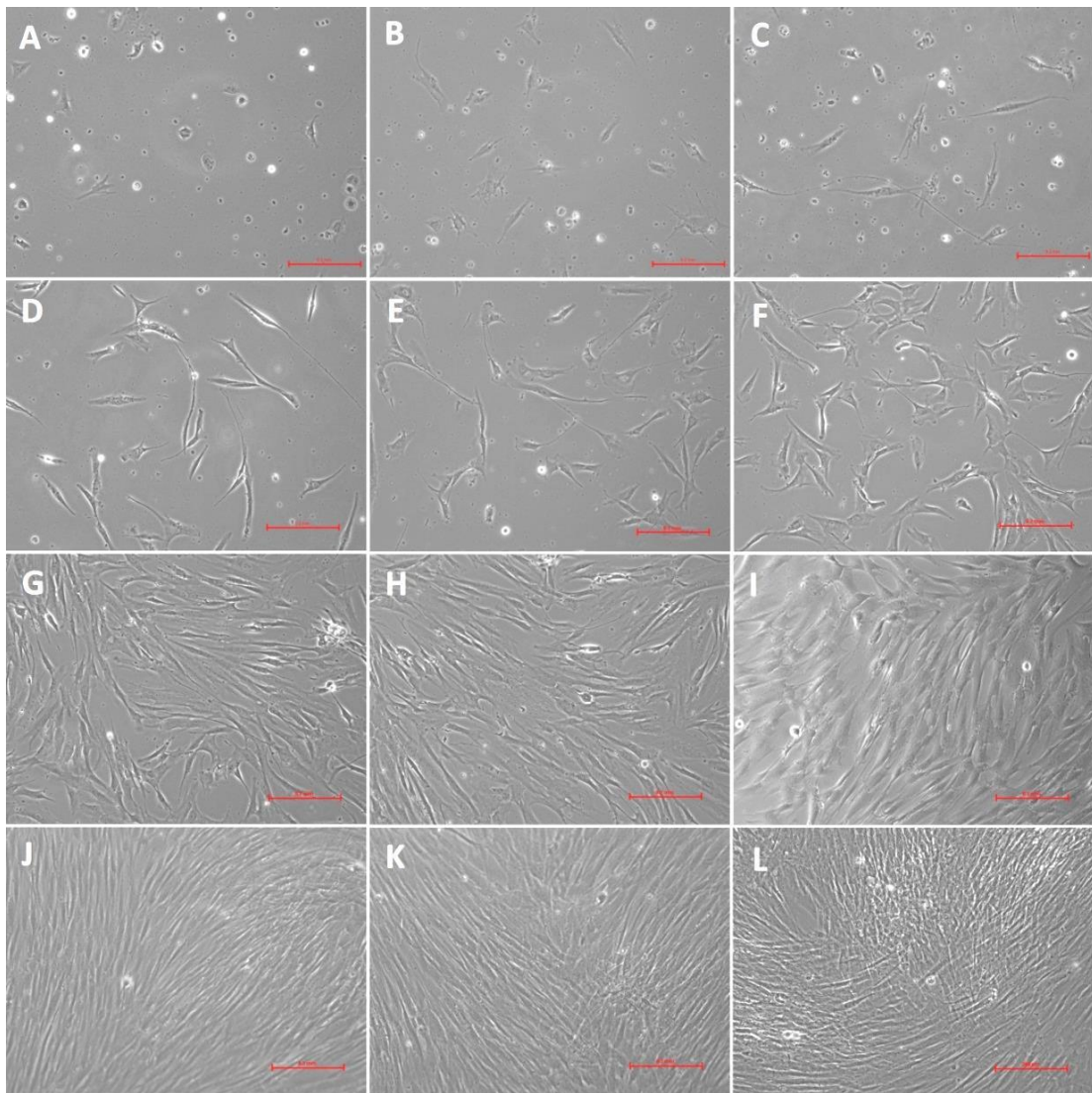


Figure 5-6: Daily serial micrographs [from A) Day 0 to L) Day 11] of HDFs seeded on tissue culture polystyrene at an initial density of $3 \times 10^3/\text{cm}^3$.

Confocal laser scanning micrographs of HDFs in 3D culture on CMD porous scaffolds also shows their spindle-shaped morphology (Figure 5-7: B). FESEM micrograph of a spreading HDF cells with its cell processes is shown in Figure 5-7: C.

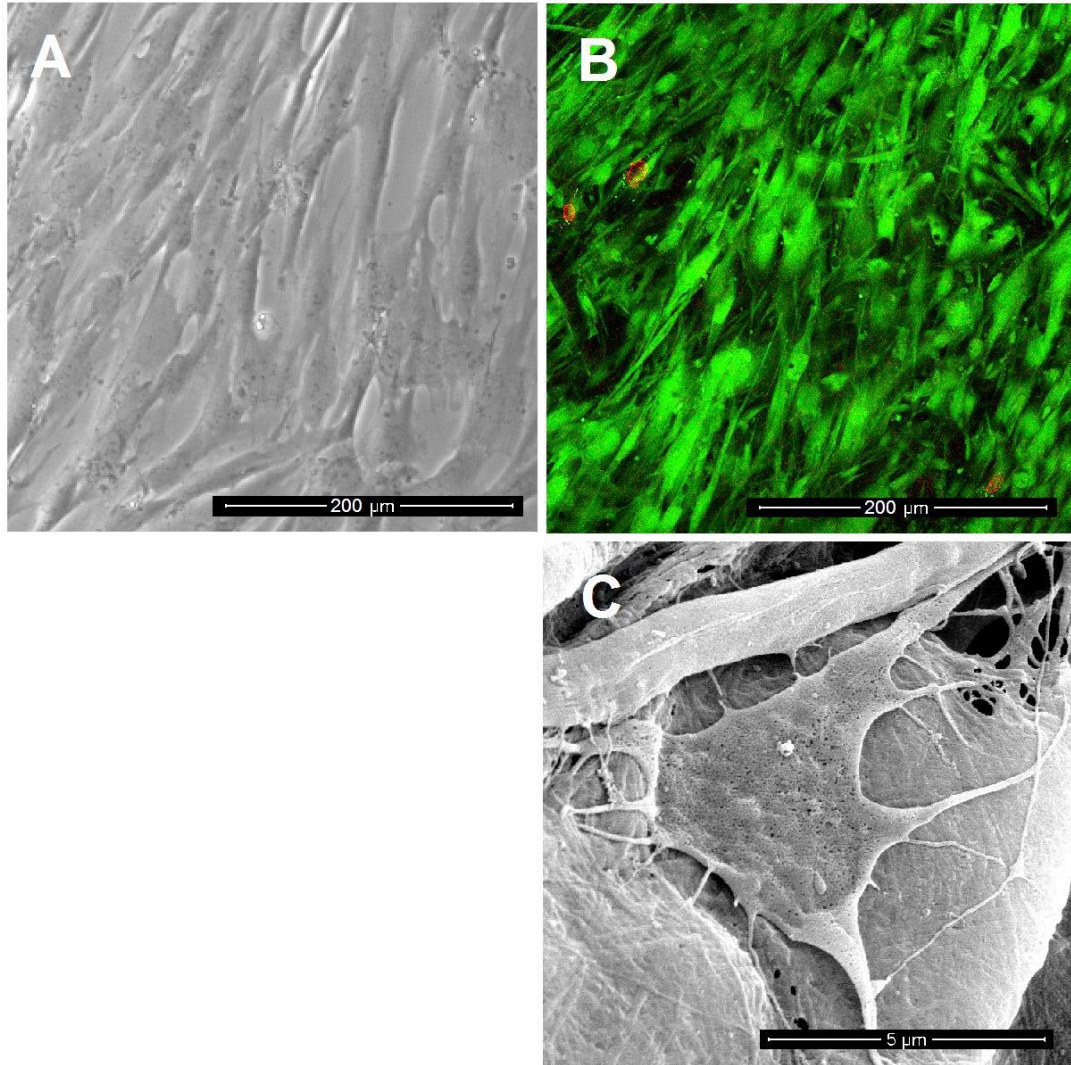


Figure 5-7: Representative figures of human dermal fibroblasts: A) Typical spindle-shaped morphology of HDF cells in monolayer culture on TCP, B) 3D culture on CMD porous scaffold stained with Live-Dead assay, and C) FESEM micrograph of a single HDF cell spreading its processes and attaching on CMD surface.

5.3.2 HDF Resazurin Standard Curves

Four (4) Hour HDF Cell Attachment on TCP

Cell attachment on tissue culture polystyrene plates four hours after seeding 2×10^3 HDFs was found to be $35.9 \pm 7.8\%$ (Figure 5-8). Based on this data, the Resazurin standard curves were plotted on the basis of the number of the attached cells rather than the seeded density.

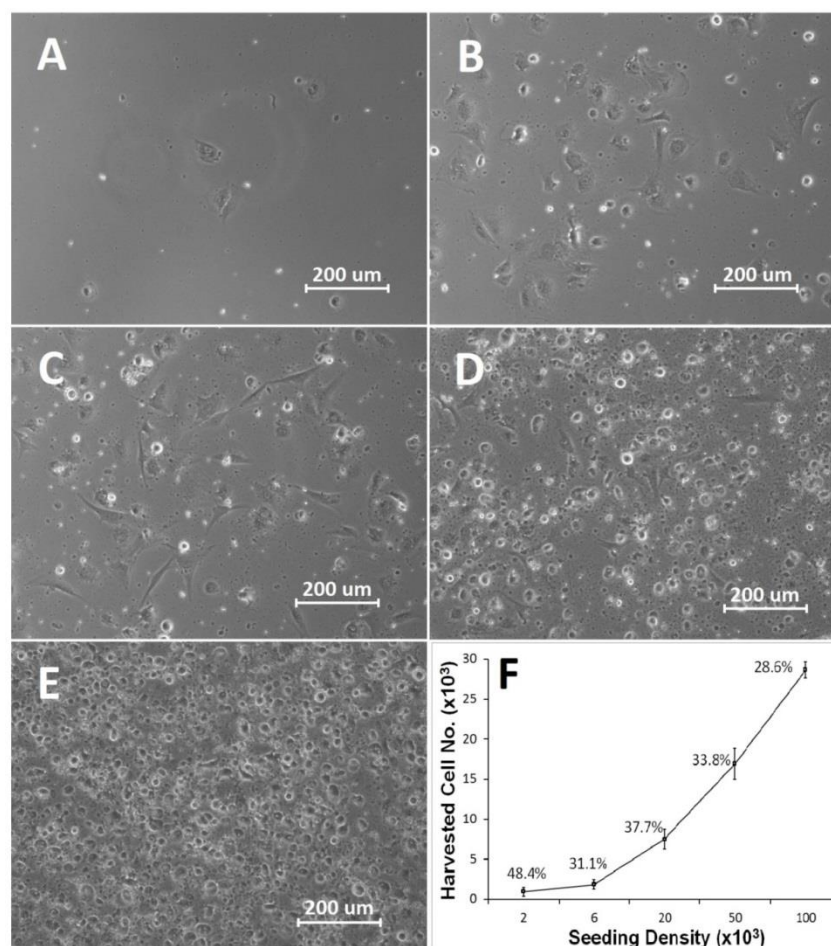


Figure 5-8: Representative inverted microscope images of HDF cells seeded on TCP at varying densities of: A) 2×10^3 , B) 6×10^3 , C) 2×10^4 , D) 5×10^4 , and E) 10^5 cells per well 4 hours after seeding. The graph F plots the harvested cell number 4 h after seeding against the initial seeding density (n=8 for each cell density).

HDF cell number quantification in a wide incubation time and cell density range was feasible through AlamarBlue®/Resazurin dye diluted with either PBS or Phenol-red-free DMEM.

Our data did not follow a normal distribution pattern. As such, Kruskal-Wallis Test was conducted and revealed no statistically significant difference in % reduction of the dye among four different formulations at each cell seeding density ($P > 0.05$).

When % reduction in AlamarBlue[®]-DMEM was plotted against the cell number at different incubation time points the standard curve remained linear with correlation coefficients almost above 0.95 except for 1 and 4 hours (0.62 and 0.82 respectively), while regression lines showed overlappings at 1 and 2 hours and at 3 and 4 hours, and also dislocations at 3, 4, 6, and 12 hours (Figure 5-9).

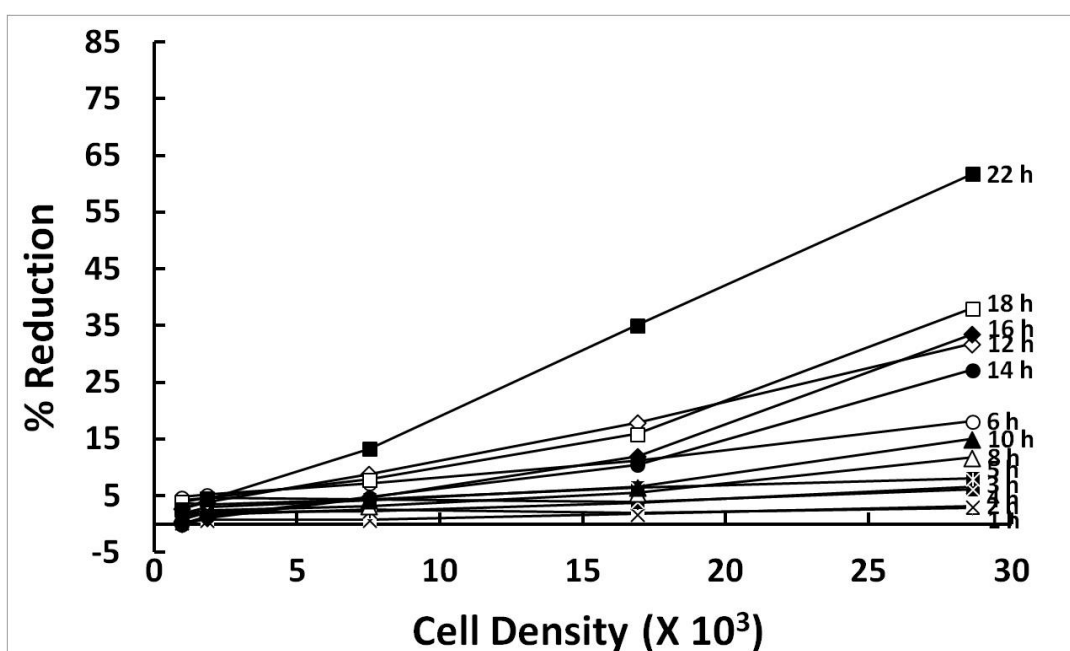


Figure 5-9: Reduction of AlamarBlue-DMEM as function of cell density in monolayer culture at varying incubation times from 1 to 22 hours.

The correlation obtained between % reduction in AlamarBlue[®]-PBS and cell number at different incubation time points remained linear with correlation coefficients almost all above 0.95 except for 1, 6 and 22 hours, which were 0.75, 0.91, and 0.89 respectively,

while regression lines showed overlapping at 1 and 2 hours and at 4 and 6 hours, and also dislocations at 2, 5, and 12 hours (Figure 5-10).

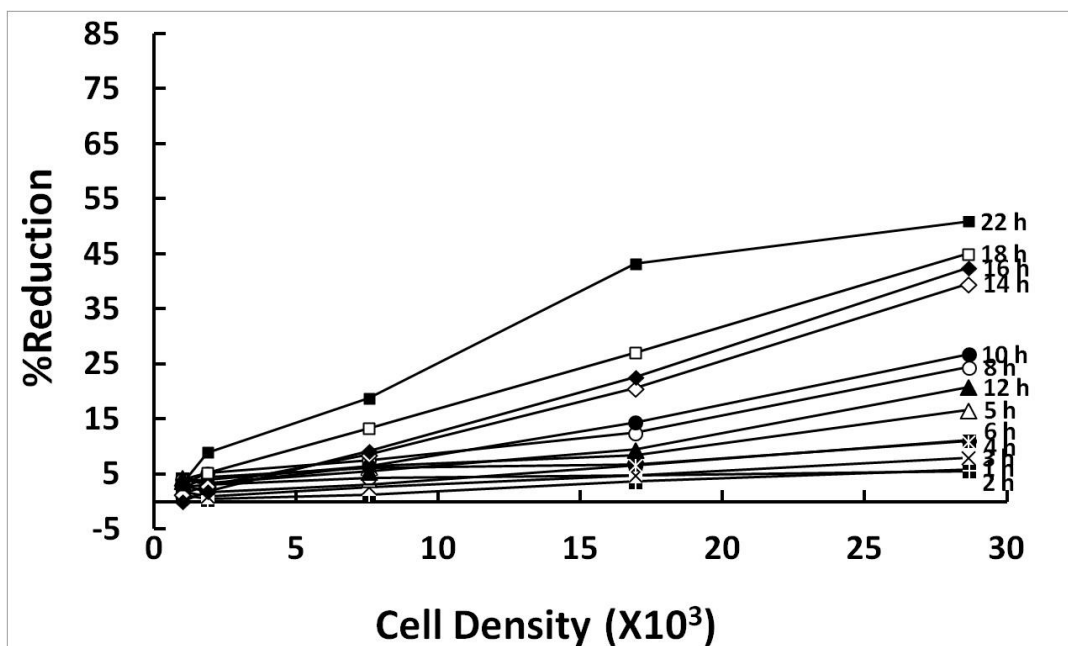


Figure 5-10: Reduction of AlamarBlue-PBS as function of cell density in monolayer culture at varying incubation times from 1 to 22 hours.

Plotting % reduction in Resazurin-DMEM versus cell number at different incubation time points showed linear correlation with coefficients almost above 0.94 except for 1, 3, 4, and 6 hours (0.83, 0.83, 0.85 and 0.92 respectively), while regression lines showed overlappings at 3 and 4 hours and at 5 and 6 hours, and also dislocation at 4, 6, and 14 hours (Figure 5-11).

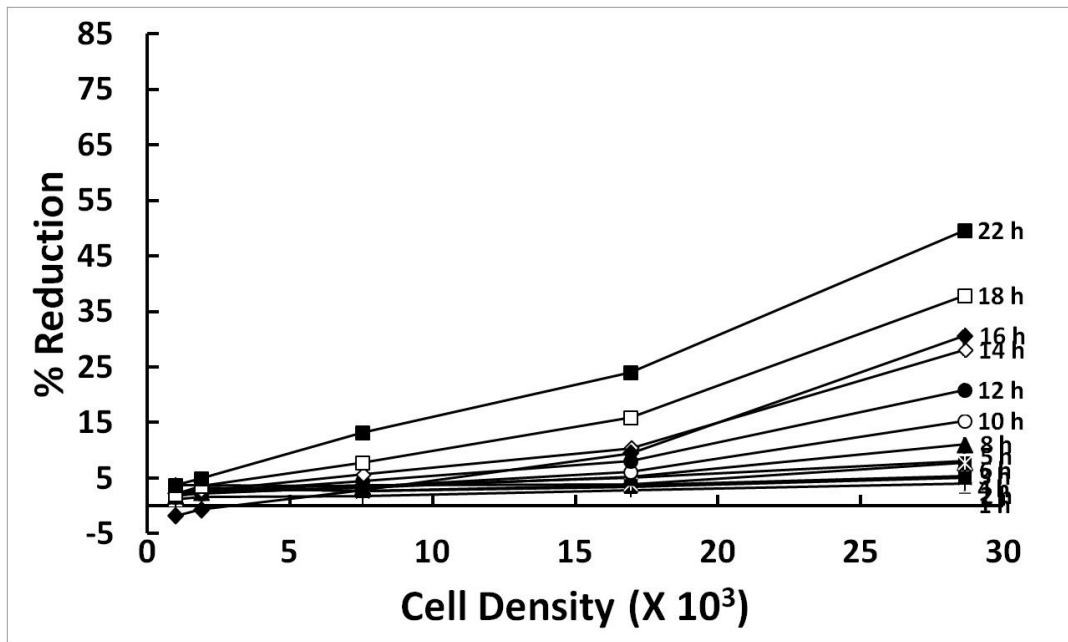


Figure 5-11: Reduction of Resazurin-PBS as function of cell density in monolayer culture at varying incubation times from 1 to 22 hours.

The correlation between % reduction in Resazurin diluted in PBS and cell number at different incubation time points remained linear with correlation coefficients all above 0.95 with almost no significant overlapping or dislocation (Figure 5-12).

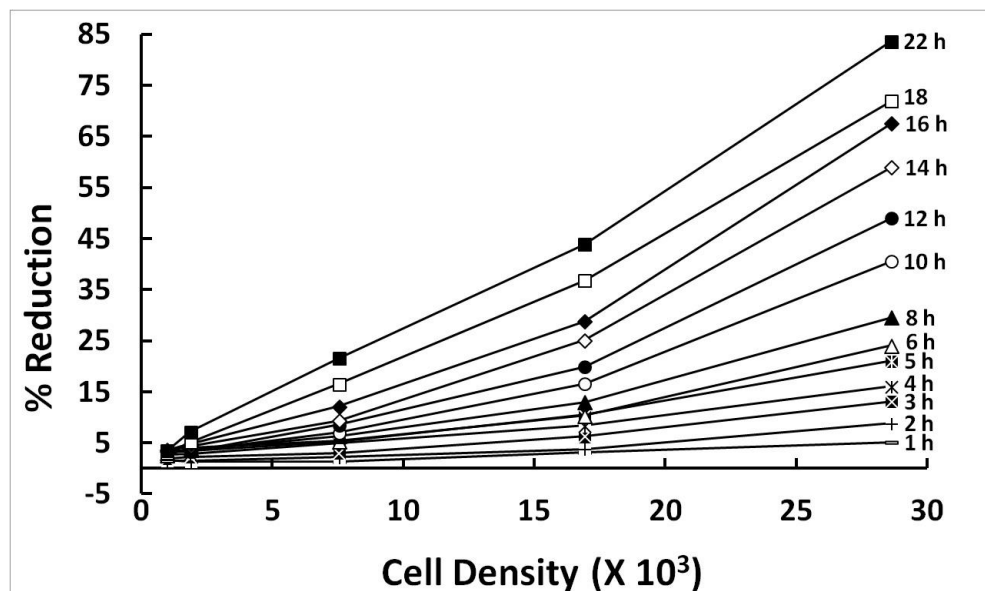


Figure 5-12: Reduction of Resazurin-PBS as function of cell density in monolayer culture at varying incubation times from 1 to 22 hours.

The Friedman Test showed a significant difference between all the first 5 time points at every given cell density in the Resazurin-PBS group ($P < 0.05$) (Figure 5-13).

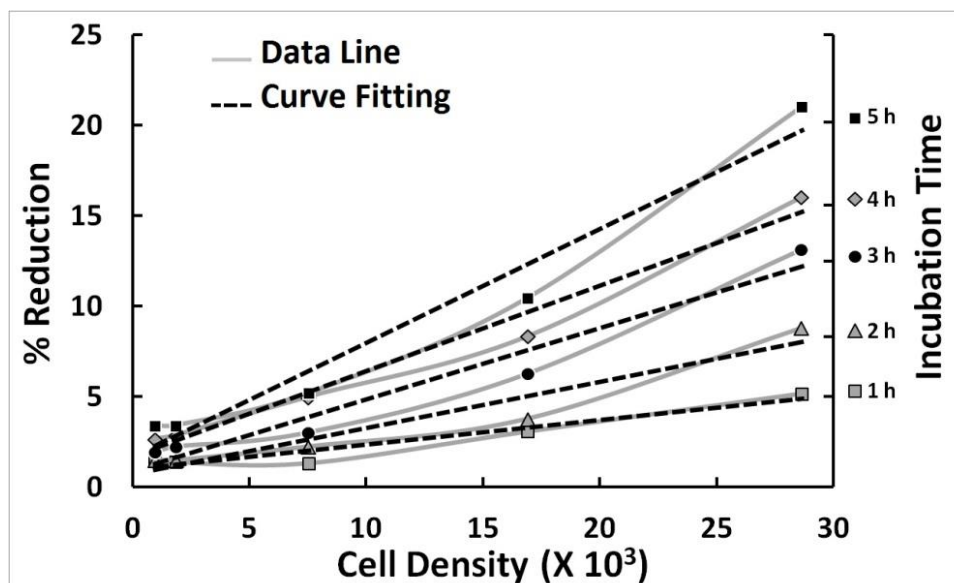


Figure 5-13: Resazurin Reduction Nomogram as a practical tool for quantification of Human Dermal Fibroblasts cell density in monolayer culture at 1 to 5 hours incubation times. The orders of all 5 curves look reasonable and logical.

Our results confirm that the % reduction in Resazurin/ AlamarBlue® has a linear correlation with HDF cell number and that there is no statistically significant difference between the two different commercial dyes regardless of the dye preparation formulation is. Although there was no significant difference in the % reduction of the dye among four different formulations at every cell density, however, considering the correlation coefficients, the order and the regularity of the curves, Resazurin-PBS reduction nomogram is suggested as a practical graphic tool for determination of HDF cell number at different incubation times from 1-5 hours (Figure 5-13).

The linearity of the correlation between the Resazurin reduction and HDF cell number appears to support the previous findings (Al-Nasiry, Geusens, Hanssens, Luyten, & Pijnenborg, 2007; Voytik-Harbin et al., 1998; Yu et al., 2003). Although our findings

showed similar features to the previous studies, however, the wide dye concentration as well as the cell density and type in our study are the advantages of our results.

The correlation between the Resazurin dye absorption and the cell number has been studied with different cell types. AlamarBlue® dye has been shown to have a good constant correlation with Swiss 3T3 Mouse Fibroblast cell number in a wide range of dye concentration and cell density (Voytik-Harbin et al., 1998). The correlation between the optical density of AlamarBlue® dye and Retinal Pigment Epithelial Cell number has been reported to be linear with a correlation coefficient of 0.951 through absorbance method at 2, 4, 6, 9, 12, and 24 hour time points (Yu et al., 2003), and eventually plotting the AlamarBlue® % reduction against the logarithm of choriocarcinoma cell density ($16.6 - 500 \times 10^3$) was also reported to be linear with regression coefficients of 0.73 – 0.81 (Al-Nasiry et al., 2007).

Although comparison between the four different dye formulations showed no significant difference between the four formulations at any given cell density, the correlation graphs look quite different in terms of the order of the curves and their correlation coefficients (Figure 5-12). As mentioned in the results section, several curve displacements and overlappings can be seen in both AlamarBlue® groups while curves in both Resazurin groups are more regular, with less overlapping/displacements. Correlation curves in Resazurin-PBS group look even more attenuable. Instructions from different companies generally recommend 2 to 4 hours of cell-dye incubation. Our results also show the lowest correlation coefficients for the 1st hour of incubation ($0.62 \leq R^2 \leq 0.83$) among all groups except for the Resazurin-PBS group ($R^2=0.95$).

Although the correlations between % reduction in Resazurin diluted in PBS and cell concentrations at different incubation time points were high- R^2 linear, the nomogram was modified, summarized and focused on the first 5 hours of incubation as most researchers prefer shorter incubation times.

All in all, Resazurin-PBS shows the best graph in terms of order, accuracy, and correlation coefficients. Our findings suggest the Resazurin-PBS reduction nomogram as the practical choice tool for determination of primary HDF cell number in monolayer cultures. HDF cell number can easily be determined with a high accuracy by having the % reduction of Resazurin at any incubation time between 1 to 5 hours using the suggested nomogram.

5.3.3 DNA standard Curve

The micro-plate readers are designed to present the data from serial dilutions of standard DNA in the form of a scatter graph plotting the relative fluorescence units against DNA concentration. In a short range between 1-50 $\mu\text{g/ml}$ of DNA the regression line is linear with a high correlation coefficient. An $R^2 \geq 0.95$ is usually acceptable (Figure 5-14).

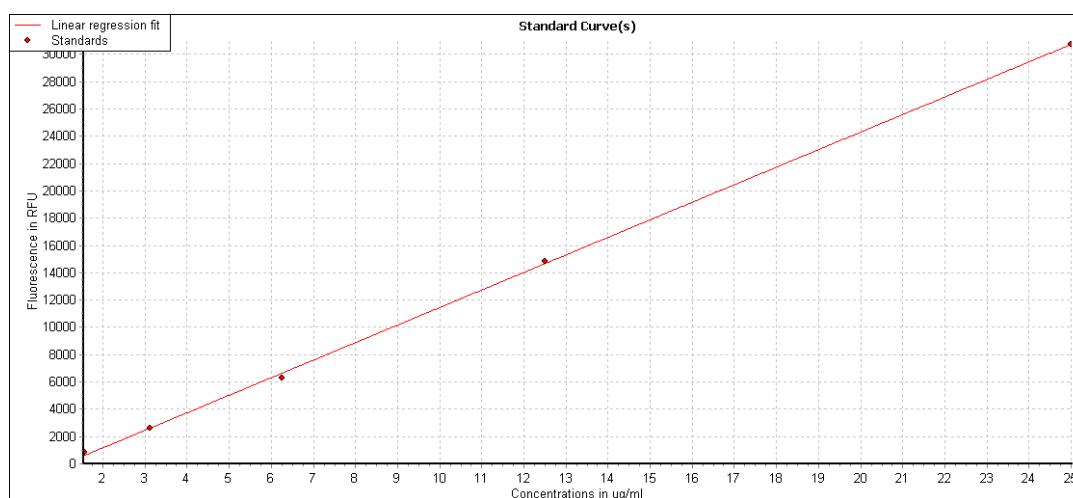


Figure 5-14: Plotting the relative fluorescence units (RFU) against the DNA concentration ($\mu\text{g/ml}$) yields a linear regression with high R^2 value. This line is used as the DNA standard curve for quantification of DNA containing cell extracts.

5.3.4 HDF Cell Doubling Time

Figure 5-6 depicts the daily serial inverted microscopic images of HDF cells seeded at a density of 3×10^3 cells/cm² on tissue culture polystyrene. As it can be seen in Figure 5-15(A) HDF cells show a lag period of 2-3 days after seeding. The logarithmic phase starts at the 3rd day and continues until 7-8th day.

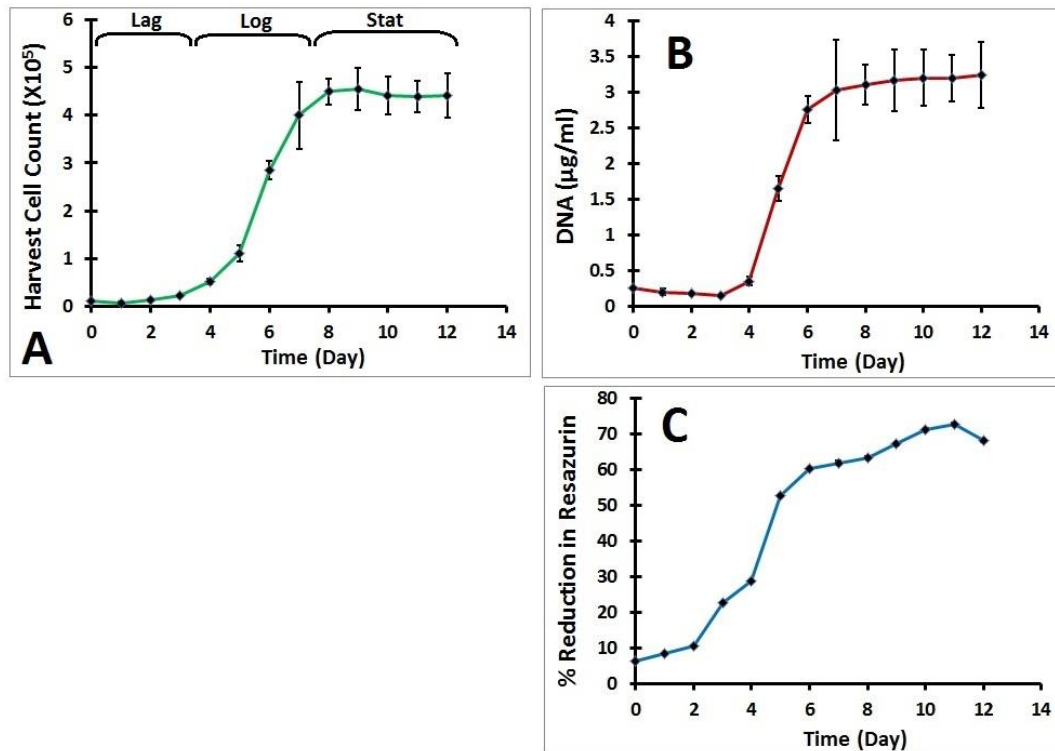


Figure 5-15: Growth curves of HDF cells at P5 within 12 days culture based on A) cell count, B) DNA quantification, and C) percentage reduction in Resazurin. The lag, logarithmic and stationary phases are seen in graph A.

5.3.5 Tri-lineage differentiation

The adipogenic differentiation medium tends to induce stem cells to produce lipid vacuoles while having no effects on non-stem cells. Oil-Red-O staining of HDF cells fed with Adipogenic differentiation induction medium for two weeks showed few lipidification signs in HDF cells at passage 2 due to cell contamination with fat cells at low passages while no signs of lipidification in HDF cells at Passage 6. Human bone

marrow stem cells (HBMSCs) as the positive control cells showed lipid vacuoles after staining (Figure 5-16).



Figure 5-16: Inverted microscope images of A) HBMSCs at P8, B) HDFs at P2, and C) HDFs at P6, all treated with adipogenic differentiation induction medium for two weeks and after Oil-Red-O staining showing the abundant lipid vacuoles in HBMSCs (A), rare vacuoles in HDF cells at low passage No. (B), and no evidence of lipid droplets in HDFs at passage 6 (C).

Alizarin red staining of HDF cells at P2 and P6 and HBMSCs at P8 treated with osteogenic differentiation induction medium for two weeks shows vast calcification signs in HBMSCs and few in HDF cells at P2 while no signs of ossification are seen in HDFs at P6 (Figure 5-17).

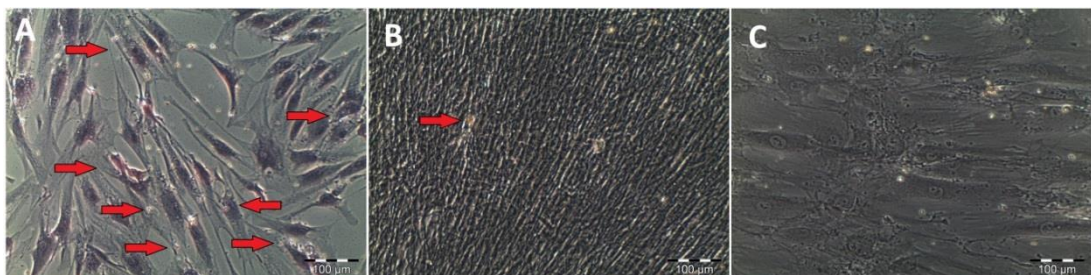


Figure 5-17: Alizarin-Red staining for Osteogenic differentiation shows numerous calcification signs in HBMSCs (A) and rare ossification signs in HDF cells at P2 (B), but no evidence of osteogenic differentiation in DHFs at P6 (C).

Chondrogenic differentiation medium also failed to induce HDF cells to go through chondrogenesis. Figure 5-18 depicts Safranin-O stained HBMSCs (A) and HDF cells (B) both treated with chondrogenic differentiation induction medium for three weeks.

While HBMSCs show chondrogenic differentiation, no changes are seen in HDF cells toward chondrogenesis (Figure 5-18).

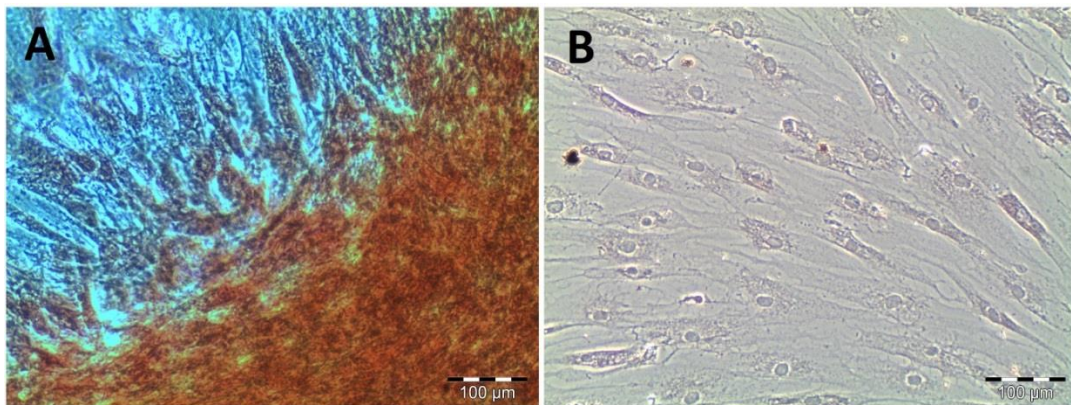


Figure 5-18: Safranin-O staining of A) HBMSCs at P8 treated with chondrogenic differentiation induction medium for 3 weeks, and B) HDF cells at P6 with the same treatment.

The results of the tri-lineage differentiation test show that although HDF cells at low passages may show some weak evidences of lineage differentiation, which is due to the contamination with other cells, at higher proper passages they get more and more purified and do not show any evidence of lineage differentiation.

5.3.6 Immunostaining

5.3.6.1 FlowCytometry

Flowcytometry graphs of HDF cells at passage 6 show a single cell population stained for CD90 as the fibroblast-specific marker. Non-stained cells were used as negative control, taking place in the 3rd quarter indicating that cells did not show any signal for CD90 marker (Figure 5-19-A). Cells positive for CD90 only were located in the Q4 quarter (Figure 5-19-B). Figure 5-19-C also shows the histogram of cells stained with mouse monoclonal antibody to CD90. The X-axis of the histogram represents the signal value in channel numbers, while the Y-axis shows the number of events per channel number. Signals with identical intensities accumulate in the same channel. Therefore,

this histogram shows that the majority of events accumulated in the Cy5 channel and were positive for CD90.

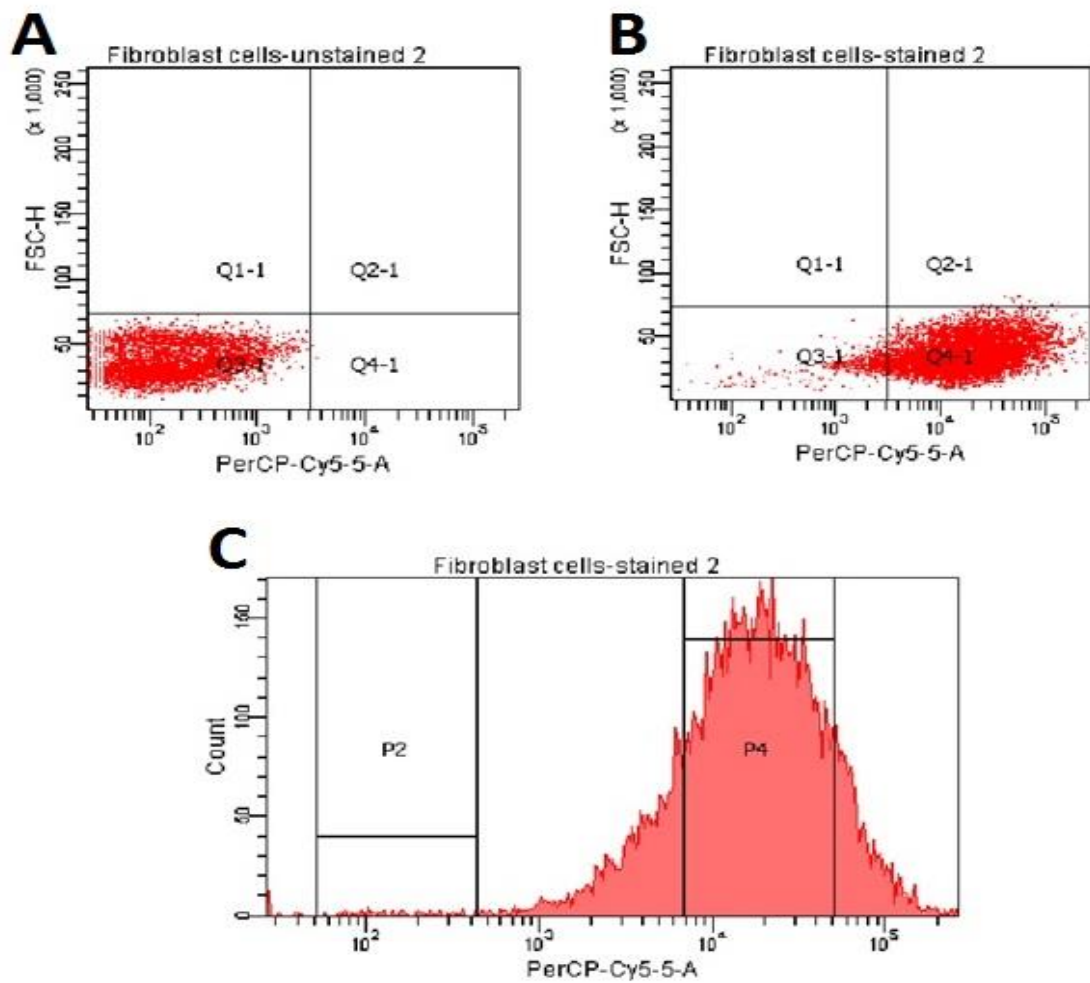


Figure 5-19: Flowcytometry scatter plots of HDF cells at P6 stained with Cy5 for CD90. A) unstained HDF cells as control were placed in 3rd quarter, B) pure population of Cy5 stained HDFs for CD90 as the fibroblast-specific marker, C) Histogram of Cy5 as a single parameter. X axis represents the intensity of the signal in channel numbers while Y axis shows the quantity of the events per channel number.

5.3.7 Gene expression

Results of gene expression profile of HDF cells are shown in Figure 5-20. The THY1 gene, which contains information for production of fibroblast specific antigen (FSA) was expressed twice much in HDF cells at P5 compared to HBMSCs (P8) and HADSCs (P0). The S100A4 gene encoding the data for fibroblast-specific protein 1 showed the same expression value in HBMSCs as in HDF cells but a much lower expression in HADSCs.

Desmin expression in fibroblasts was much higher than HBMSCs, but almost the same in HADSCs.

All four stemness markers (REX1, SOX2, NANOG, and OCT4) showed much higher expression values in both HBMSCs and HADSCs compared to HDF cells.

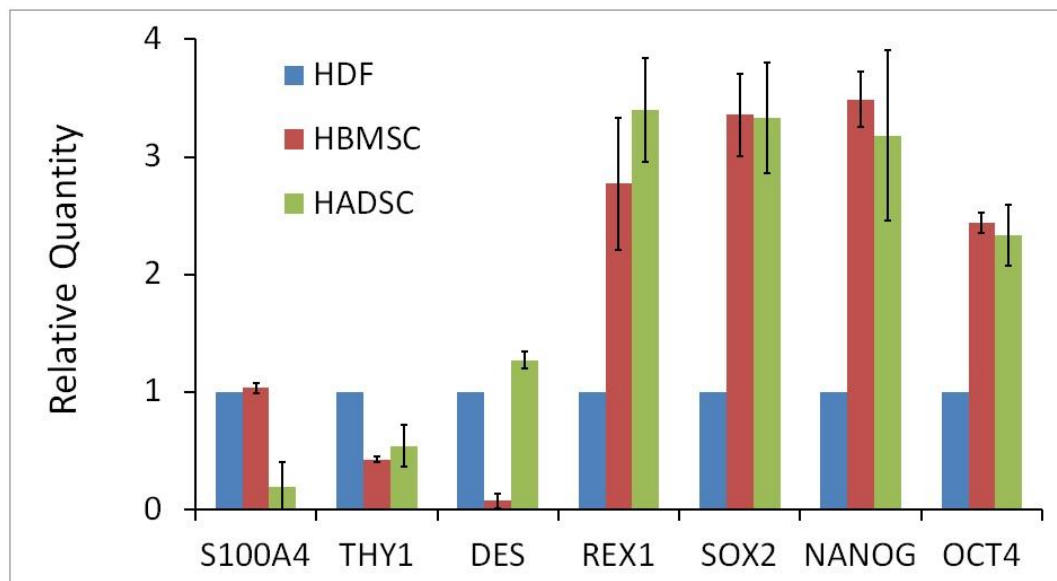


Figure 5-20: Relative quantification of expression of fibroblast-specific marker and stemness genes in primary human dermal fibroblasts (HDF) at passage 5. Human bone marrow stem cells (HBMSC) at P8 and human adipose derived stem cells (HADSC) at P0 were used as controls. GAPDH has been used as the housekeeping gene.

Fibroblastic contamination in HADSCs used at P0 can be the reason for equal expression of Desmin in these cells with HDFs. On the other hand the expression of stemness genes in fibroblast populations is not supposed to be zero (Page et al., 2009).

5.4 Discussion

In this study we used the outgrowth technique for the isolation of HDF cell. Although the outgrowth method might seem a slower method, and it yields a lower recovery of cells compared to the enzymatic digestion methods, yet this provides the opportunity of multiple reuses of the skin explants for cell isolation. As compared to the enzymatic digestion method of cell isolation, the outgrowth method tends to isolate cells with a higher motility. When cell motility is a concern, especially when the cells are meant to be seeded on porous materials and the ability of cells to penetrate deep into the inner layers of the scaffolds is a matter of importance, the outgrowth method is the technique of choice for selecting the migrating cells (Rittié & Fisher, 2005). Moreover, even though the first isolation from freshly cut skin might take 2-3 weeks, the same skin pieces can be shifted to new culture dishes for the next course of isolation which will yield cells much faster (within 3-7 days). This process can be repeated several times, resulting in a high total cell yield.

HDF morphology was confirmed through the use of inverted phase, confocal and scanning electron microscopes. Application of tri-lineage differentiation induction media proved the purity of HDF cell populations at proper passage ($\geq 5^{\text{th}}$) and being free from stem cells.

As an immunophenotyping test flowcytometry of HDF cells stained with Cy5 for CD90 (THY1) as a fibroblast-specific cell surface protein confirmed the identity of the HDF cells.

The gene expression profile of HDF cells was also compared with that of two types of stem cells, which revealed that our HDF cell population is significantly different from stem cells.

In conclusion, we managed to isolate a high motility pure population of human dermal fibroblasts which is perfectly suitable for tissue engineering application.

CHAPTER 6: CHONDROGENIC EFFECTS OF CMD SCAFFOLDS ON HDFs

6.1 Introduction

Cell-based therapies in cartilage tissue engineering take advantage of highly interconnected porous scaffolds capable of providing enough surface area and space for cell attachment, proliferation, nutrient and waste exchange as well as extracellular matrix production and deposition. The material from which the scaffold is fabricated plays a key role in chondroinduction. Various types of hydrogels, polymers, and composites of different materials that can support cartilage matrix production have been tried. (Hutmacher, 2000; Lu et al., 2001; Moradi et al., 2013; Moutos & Guilak, 2008). It has been suggested that modified native extracellular matrix (ECM) may contain bioactive factors that can contribute to cell growth, migration, and chondrogenic differentiation (Badylak, 2002; Benders et al., 2013; Izadifar et al., 2012). Human (Q. Yang, Peng, Guo, Huang, Zhang, Yao, et al., 2008) and porcine (Cheng et al., 2009) articular cartilage ECM derived scaffolds have shown promising results with the use of human adipose derived adult stem cells and canine bone marrow stem cells respectively, supporting the hypothesis that a scaffold derived absolutely from cartilage ECM can induce chondrogenesis. The source from which the matrix is derived is a big concern. Human sources cannot be practically reliable on a high throughput route due to lack of abundance. Porcine derived products also have limitations due to religious and ethical considerations. Animal sources with high abundance but without ethical issues can be the solutions of choice. Preserving the integrity of native cartilage ECM components is a key factor in ensuring that the total capacity of bioactive factors responsible for chondrogenesis. For cartilage tissue engineering purposes, the scaffold is supposed to support the maintenance of chondrocytes or differentiation of other cells with chondrogenic potential.

In chapter 3 we presented the detailed process of fabrication, characterization and optimization of bovine articular cartilage matrix derived porous scaffolds for cartilage tissue engineering applications. We showed that UV and UVDHT treated 15% CMD scaffolds possessed optimal geometry and architecture. In this chapter we present the detailed methods of assessment for the chondrogenic effects of bovine articular cartilage matrix derived porous scaffolds on human dermal fibroblast cells. To assess the biocompatibility of the optimized CMD scaffolds HDF cell viability and proliferation were qualitatively and quantitatively assessed through serial Resazurin reduction, DNA quantification, and confocal laser scanning and field emission scanning electron microscopy images. The chondroinductive potential of the CMD scaffolds was assessed through serial relative quantification of the expression of the chondrogenic genes as well as the production of sulphated glycosaminoglycans. Also, changes in scaffold size and shape were quantified and the correlation between scaffold shrinkage and cell proliferation and chondrogenic differentiation was described.

6.2 Materials and Methods

6.2.1 Cell Seeding

HDF cells at passage 4 were resuspended in Chondrogenic medium at a final density of $10 \times 10^6 \text{ ml}^{-1}$. The Chondrogenic medium consisted of DMEM-HG supplemented with 20% (v/v) FBS, 1% Penicillin-Streptomycin, 1% HEPES, 1% non-essential amino-acids, 1% ITS+Premix, 50 $\mu\text{g/ml}$ L-ascorbic acid, 40 $\mu\text{g/ml}$ L-Proline, 10 nM Dexamethasone, 10 nM TGF- β 3 (Cheng et al., 2009; Cheng et al., 2011; Q. Yang, Peng, Guo, Huang, Zhang, Yang, et al., 2008; Zheng et al., 2011). UV and UVDHT treated CMD scaffolds (n=17 for each group at every time point) were pre-wetted with 50 μl of chondrogenic medium and incubated in a 37°C humidified 5% CO₂ incubator for 15 minutes. 50 μl of HDF cell suspension (5×10^5 cells) was gently seeded on each scaffold. The scaffolds were incubated in a 37°C humidified 5% CO₂ incubator for 3

hours, then topped up very gently with 1 ml of pre-warmed fresh chondrogenic medium. Chondrogenic medium was changed every two days. Cell viability tests, scanning electron microscopy for cell-matrix interaction study, and biochemical and molecular analyses were performed at Day 2, 8, 15, 22, 29, 35, and 42 time points.

6.2.2 Cell Growth and Viability

Cell viability was determined using LIVE/DEAD[®] Viability/ Cytotoxicity Kit (Invitrogen, UK). 1 μ l of Calcein AM (4mM in anhydrous DMSO) added to 2.5 μ l of Ethidium homodimer (2mM in DMSO/H₂O 1:4 (V/V) (Molecular probes[®] - Lifetechnologies[™], USA) were diluted in 1 ml pre-warmed 37°C PBS. At every weekly time point one out of each seeded scaffold groups (UV and UVDHT) underwent staining through incubation with 500 μ l of the diluted dye solution at 37°C, 5% CO₂ for 45-60 mins prior to imaging.

Imaging was performed with green fluorescence at ex/em ~495 nm/~515 nm for live cells and red fluorescence at ex/em ~495 nm/~635 nm for dead cells using a confocal laser scanning microscope (Leica TCS SP5 II, Germany).

6.2.3 Cell Proliferation

Cell proliferation was assessed via the Resazurin reduction assay (Dienstknecht et al., 2010; Voytik-Harbin et al., 1998; Yu et al., 2003). At days 2, 8, 15, 22, 29, 35, and 42 the seeded and non-seeded CMD scaffolds (n=16 for each group including the unseeded control sample) were incubated (37°C, 5% CO₂) with 1 ml of pre-warmed 10% Resazurin in PBS for four hours. The absorbance was measured by a plate reader (FLUOstar OPTIMA BMG LABTECH, Germany) at 570 nm and 595 nm. Percentage reduction in Resazurin was calculated using the manufacturer defined formula (Gang et al., 2004).

6.2.4 Cell-scaffold Interaction Studies

The seeded scaffolds were preserved in 2.5% Glutaraldehyde and underwent dehydration in a graded ethanol series (25%, 40%, 60%, 80%, 95% and 100%, each for 30 min), followed by freeze-drying overnight. The freeze-dried samples were then coated with gold-palladium (Quorum, Q150R s) and scanned using a Quanta™ 250 FEG – FEI microscope for cell-scaffold interaction studies.

6.2.5 DNA Quantification

Scaffolds ($n \geq 5$) were subjected to Papain digestion as described elsewhere (Caroline D. Hoemann, 2004; Moradi, Pramanik, Ataollahi, Abdul-Khalil, et al., 2014). Briefly, scaffolds were digested by incubating in 1 ml of Papain digest buffer (0.01 M L-cysteine, 0.01M Na₂EDTA, and 0.125 mg/mL papain in 0.1M sodium phosphate buffer) for overnight at 65°C with intermittent agitations. After precipitating the remaining debris, the digest solution was analysed for DNA content using Hoechst 33258 dye ($0.1 \mu\text{l.ml}^{-1}$ in TEN buffer) with calf thymus DNA (*Sigma D1501*) as standard. Plate reading was performed at (ex/em ~355 nm/~460 nm) in a microplate reader (FLUOstar OPTIMA BMG LABTECH, Germany).

6.2.6 Construct Shrinkage and Contraction

A separate 48 well plate with seeded and non-seeded UV and UVDHT treated scaffolds ($n=7$ for seeded and $n=5$ for non-seeded) was used for shrinkage test. Sterile plastic discs with known constant diameter of 9 mm were used as the scales (Figure 6-1). All scaffolds were treated with the same media exactly like the other plates. The media were removed every other day for quantification of sulfated glycosaminoglycan (GAGs) production using a 1,9-dimethylmethylene blue (DMMB) assay (Sigma, USA). Digital images of top views of the plate were captured after discarding the medium and were

analysed the by ImageJ® software for cross-sectional surface area changes. The plastic discs were used for setting the scales in each picture in ImageJ®.

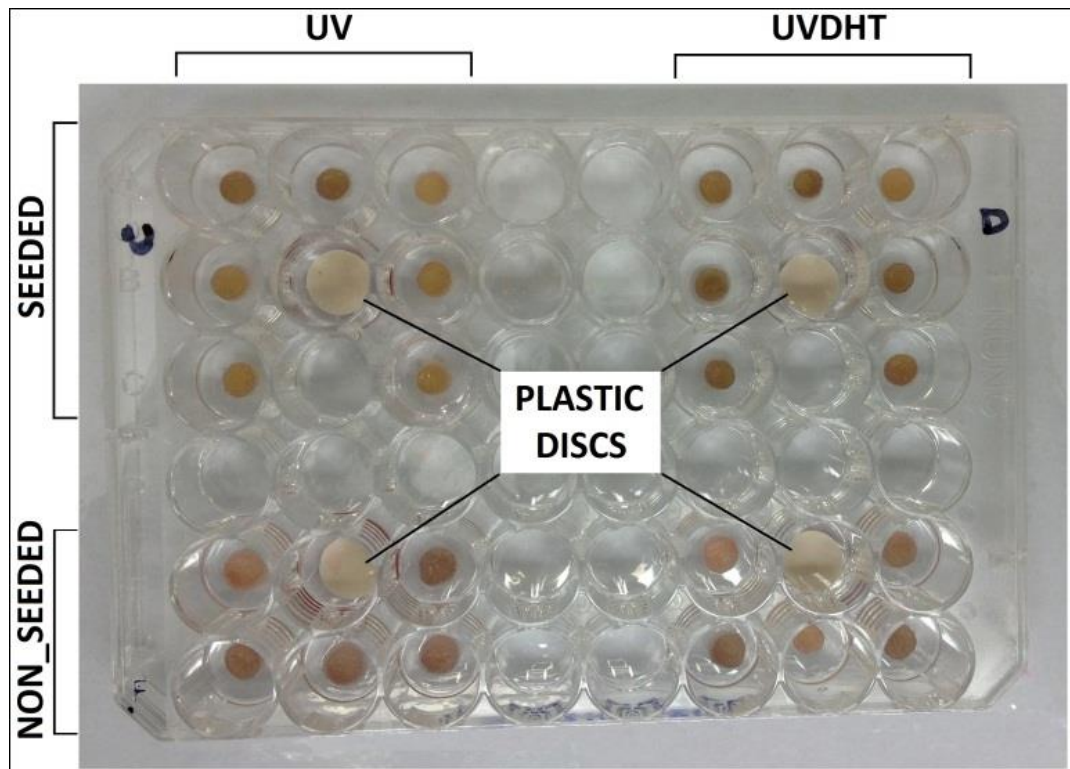


Figure 6-1: Scaffold shrinkage test after HDF cell seeding at different time points was tested by measuring the cross-sectional surface area of the scaffolds. Plastic white discs with known constant diameter were used for setting the scale in each picture.

Total shrinkage was calculated by dividing the cross-sectional surface area at each time point to that of the original scaffold:

$$Total\ Shrinkage\ (\%) = 100 - \left(\frac{cross\ sectional\ surface\ area}{original\ cross\ sectional\ surface\ area} * 100 \right)$$

To determine the cell-mediated contraction (CMC) the contraction of seeded scaffolds was minused from that of non-seeded controls (C. Lee et al., 2001; Schulz Torres, M Freyman, Yannas, & Spector, 2000).

$$CMC = \left(\frac{\text{original top surface area} - \text{top surface area}}{\text{original top surface area}} \right)_{Seeded} - \left(\frac{\text{original top surface area} - \text{top surface area}}{\text{original top surface area}} \right)_{Non-seeded}$$

6.2.7 GAGs Quantification

The sulfated glycosaminoglycan (GAGs) content in medium (n≥15) and the papain digested samples (n≥5) was assessed using a *Dimethyl-methylene blue* (16mg.ml⁻¹) assay with a chondroitin-4-sulfate standard as described elsewhere (Caroline D Hoemann, 2004). Absorbance reading was performed at ex~595 nm in a microplate reader.

6.2.8 Gene Expression

6.2.8.1 RNA Isolation

RNA isolation from seeded scaffolds was done using Tri-Reagent[®] solution (Lifetechnologies[™] #AM9738) and according to the instructions from the manufacturer (Biosystems, 2008). The scaffolds were gently washed with PBS and transferred to 1.5 ml microcentrifuge labelled tubes. Mechanical shredding and homogenization of the scaffolds were done using pestles in 1.5 ml micro-centrifuge tubes. 500 ul Chloroform (Fisher # BP 1145-1) was added to each tube, vortex-mixed, and incubated at room temperature for 15minutes, followed by centrifugation at 12000 RCF, 4°C, 15 min. The upper clear layer containing RNA (250 ul) was transferred to a new tube and the two remaining lower layers containing DNA were frozen @ -80 in the same tube for further DNA quantification through Hoechst assays. 500 ul Isopropanol (Sigma # I9516) was added to the RNA and vortex mixed, and then incubated at room temperature for 5minutes. Centrifugation was performed at 12000 RCF, 4°C, for 10 min. The supernatant was discarded. 1 ml of 75% Ethanol (prepared from absolute Ethanol and Ultra-Pure distilled RNase/DNase-free water) was added to each RNA

pellet, vortex-mixed, and incubated at room temperature for 5 minutes. Centrifugation at 7500 RCF, 4°C, for 5 min was followed by removal of supernatant Ethanol. The RNA pellet was re-suspended in 20 µl Ultra-Pure distilled RNase/DNase-free water (Invitrogen # 10977), vortex-mixed and subjected to RNA quantification using the Nanodrop ND2000 (Thermo Scientific).

6.2.8.2 cDNA Synthesis

cDNA synthesis was done using the High-Capacity RNA-to-cDNA™ Kit (Applied Biosystems # 4387406). Up to 2000 ng of RNA from each sample plus Ultra-Pure distilled RNase/DNase-free water, collectively to a total volume of 9 µl was transferred to a 0.2 ml PCR tube, and topped up with 10 µl of 2X RT Buffer Mix (includes dNTPs, random octamers, and oligo dT-16) and finally 1 µl of 20X Enzyme mix (MuLV and RNase inhibitor protein). RT-PCR was performed using a MyGene Series Peltier Thermal Cycler Model MG96G.

6.2.8.3 TaqMan® Gene Assays

Collagen, type 1, alpha 1, provides genetic information for the construction of the type 1 collagen macromolecule that is the most abundant form of collagen in the human body and acts as the supporting and strengthening of tissues like bone, tendon, cartilage and skin. Molecular location of this gene is on the long arm of chromosome 17 (National Library of Medicine, 2014b).

Triple-stranded rope-like procollagen macromolecules are composed of two pro-alpha 1(I) and one pro-alpha 2(II) (encoded by COL1A2 gene) chains that twist together. Processed procollagens make mature collagen molecules which auto-arrange and form long thin collagen fibrils. Cross-linkage of these thin fibrils results in formation of extracellular strong collagen I fibrils (National Library of Medicine, 2014c).

Located on chromosome 12, “collagen, Type 2, alpha 1” gene, also known as COL2A1 is responsible for encoding the production of pro-alpha 1(II) chain, a subcomponent of collagen type II which is primarily found in cartilage tissue. It is also found in the vitreous (eyeball gel), the inner ear and the nucleus pulposus (the central part of the inter-vertebrate disc). Mutations in COL2A1 gene have been shown to cause defective collagen type II and end up with several disorders (National Library of Medicine, 2014d).

Aggrecan, the most abundant proteoglycan in the cartilage, is a protein with several adjunct sugar molecules. Attaching to the other components of cartilage, Aggrecan organizes and reinforces molecular network within the cartilage. The gel-like structure of cartilage comes from the water molecules attached to the sugar part of Aggrecan. The gene that contains the information for production of Aggrecan is called ACAN, a member of PG family of genes (National Library of Medicine, 2014a).

Proteoglycan 4 is a large protein synthesised specifically by the superficial chondrocytes of the articular cartilage acting as a boundary lubricant at the cartilage surface. The protein is encoded by PRG4 gene located on the long arm of chromosome 1 (National Library of Medicine, 2014e).

SOX9 is the official symbol for SRY (sex determining region Y)-box 9 gene which provides instructions for production of SOX9 protein that plays a critical role in development of the skeleton and reproductive system during the embryonic term. The protein acts as a transcription factor binding to specific regions of DNA and regulating the activity of other genes. It acts as a transcription factor for the HMG (high mobility group) domain expressed in cartilage cells. SOX9 gene is expressed in cartilage coincidentally with COL2A1 gene (Bell et al., 1997). SOX9 protein binds to and activates the essential chondrocyte-specific enhancer sequences in non-chondrocytic cells (Veronique Lefebvre, Huang, Harley, Goodfellow, & de Crombrughe, 1997; Ng et

al., 1997; Wright et al., 1995; Zhao, Eberspaecher, Lefebvre, & de Crombrughe, 1997).

Cartilage oligomeric matrix protein encoded by COMP gene on chromosome 19 is one of the calcium-binding proteins found in the ECM spaces surrounding chondrocytes. It has been shown that COMP enhances matrix assembly during chondrogenesis of human mesenchymal stem cells (Haleem-Smith, Calderon, Song, Tuan, & Chen, 2012; Kipnes et al., 2003).

Table 6-1: TaqMan® Assay Probes Used in QPCR.

Gene name	Abbrev.	Transcript Variant	NCBI Ref. Seq.	Assay No.
Collagen I	Col1A1		NM_000088.3	Hs00164004_m1
	Col1A2		NM_000089.3	Hs00164099_m1
Collagen II	Col2A1	1	NM_001844.4	Hs00264051_m1
		2	NM_033150.2	
Cartilage Oligomeric Matrix Protein	COMP		NM_000095.2	Hs00164359_m1
Sex Determining Region Y-Box 9	SOX9		NM_000346.3	Hs01001343_g1
Aggrecan	ACAN	1	NM_001135.3	Hs00153936_m1
		2	NM_013227.3	
Proteoglycan 4	PRG4	A	NM_005807.3	Hs00981633_m1
		B	NM_001127708.1	
		C	NM_001127709.1	
		D	NM_001127710.1	
Glyceraldehyde 6-Phosphate Dehydrogenase	GAPDH	1	NM_002046.4	Hs02758991_g1
		2	NM_001256799.1	

6.2.9 Gene Expression

To assess the quantitative expression of each of the genes listed in table 1, triplicates of 1 µl of cDNA sample were transferred to a 96 well PCR plate (MicroAmp® InduraPlate™, Applied Biosystems®), topped up with 10 µl of TaqMan® master mix, 8 µl of Nuclease-free water, and 1 µl of the target/housekeeping gene (TaqMan® Assay).

The plate was sealed with adhesive film (MicroAmp®, Applied Biosystems®). QPCR was performed using a *StepOnePlus*™ Real-Time PCR System - Life Technologies.

Relative quantification (RQ) of expressed genes was calculated from threshold cycle (Ct) values using the following formula:

$$RQ = 2^{-(\Delta Ct_{Target} - \Delta Ct_{Reference})}$$

Where:

$$\Delta Ct_{Target} = Ct_{Target_{Target\ Gene}} - Ct_{Target_{Housekeeping\ Gene}}$$

And:

$$\Delta Ct_{Reference} = Ct_{Reference_{Target\ Gene}} - Ct_{Reference_{Housekeeping\ Gene}}$$

6.2.10 FESEM

The same samples used for confocal laser scanning microscopy were preserved after the scanning session in 2.5% Glutaraldehyde and underwent dehydration process in graded ethanol series (25%, 40%, 60%, 80% and 100%, each for 30 min), followed by freeze-drying. The dry samples were then coated with gold-palladium (Quorum, Q150R s) and scanned using a Quanta™ 250 FEG – FEI microscope for cell-scaffold interaction studies.

6.3 Results

6.3.1 Resazurin Reduction

Figure 6-2 depicts the results of percentage reduction in Resazurin absorption in HDF seeded UV and UVDHT treated CMD scaffolds. A steep increase was seen in Resazurin reduction in UV treated scaffolds during the first three weeks after cell seeding,

indicating of cell proliferation within the porous spaces of the scaffolds. This rapid rise was followed by a mild drop and the subsequent monotonic plateau resulting from the retardation in cell growth due to lack of space and cell-cell contact inhibition.

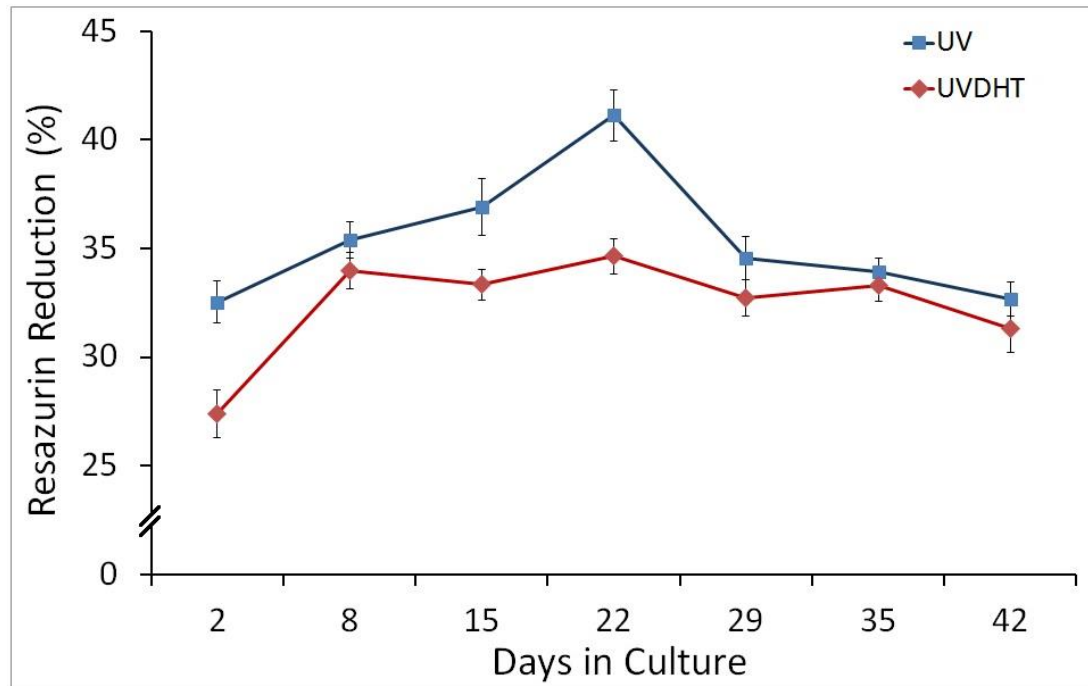


Figure 6-2: Percentage reduction in Resazurin absorption in HDF seeded UV and UVDHT treated CMD scaffolds at different weekly time-points.

Significant increases in Resazurin reduction ($P < 0.05$) in UV group during the first three weeks of culture was indicating the cell proliferation which was followed by a drop in the fourth week followed by an almost constant trend up to the 6th week. Resazurin reduction showed a milder steep during the first three weeks but the same steady trend during the rest of time points.

6.3.2 Confocal laser scanning microscopy (CLSM)

Serial CLSM graphs of HDF cells seeded on both groups of CMD scaffolds clearly illustrated the cell attachment and progressive proliferation and infiltration of the growing cells into and filling the pores of the porous scaffolds. Although cells seeded on UVDHT scaffolds showed a slower growth during the first 2 weeks, they reached the

same confluent state at third week as those seeded on UV treated CMD scaffolds. Both groups keep showing the same constant dense features in confocal images after the third week of culture. Cell morphology in both groups remained fibroblastic during the culture period (Figure 6-3&4).

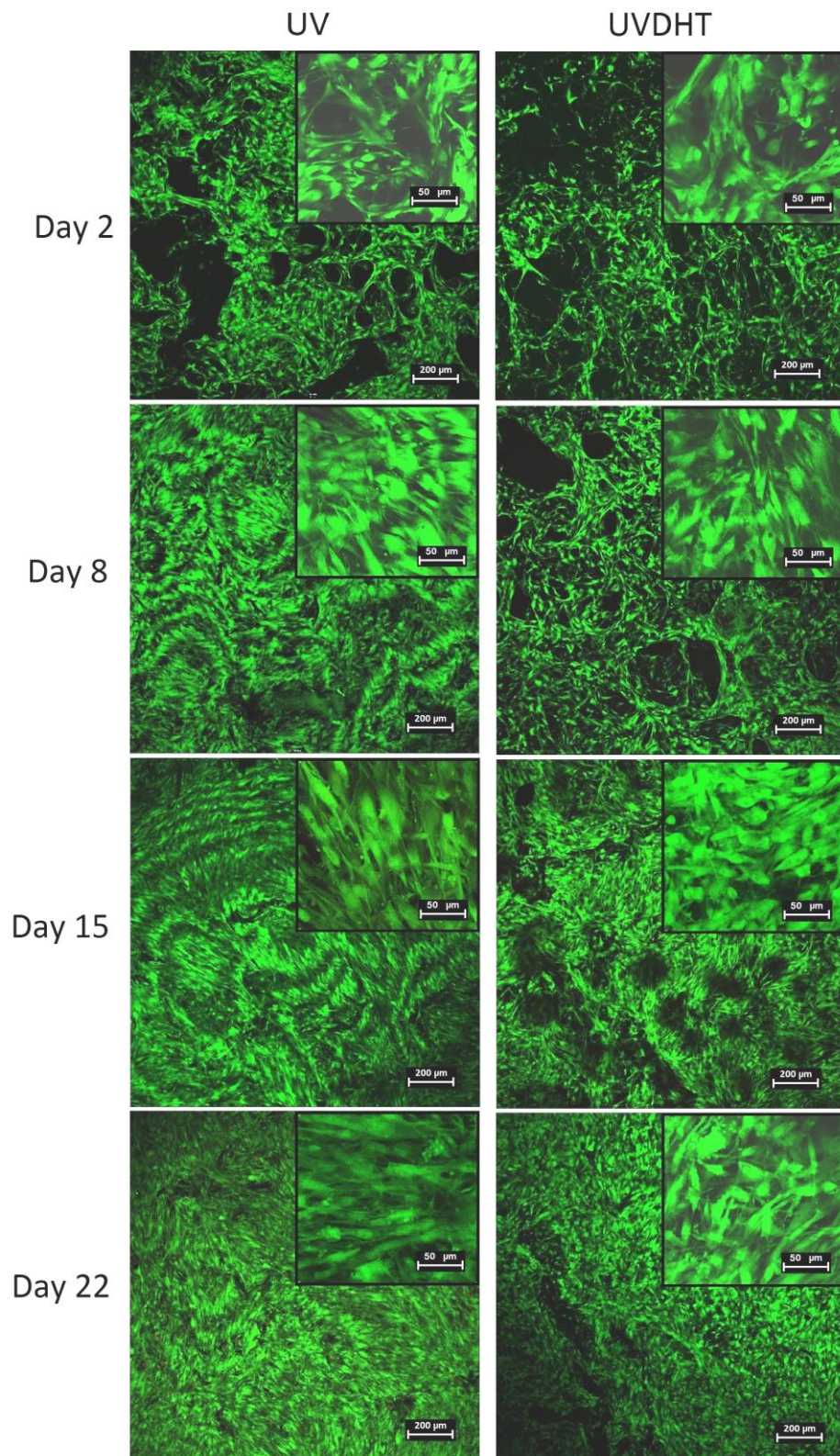


Figure 6-3: Confocal laser scanning micrographs of HDF cells seeded on UV and UVDHT treated CMD scaffolds at different weekly time points. All images have been captured after staining with LIVE/DEAD® Viability/Cytotoxicity Kit (green for Calcein and red for Ethidium homodimer). (The scale bars in main and inset images represent for 200μm and 50 μm respectively).

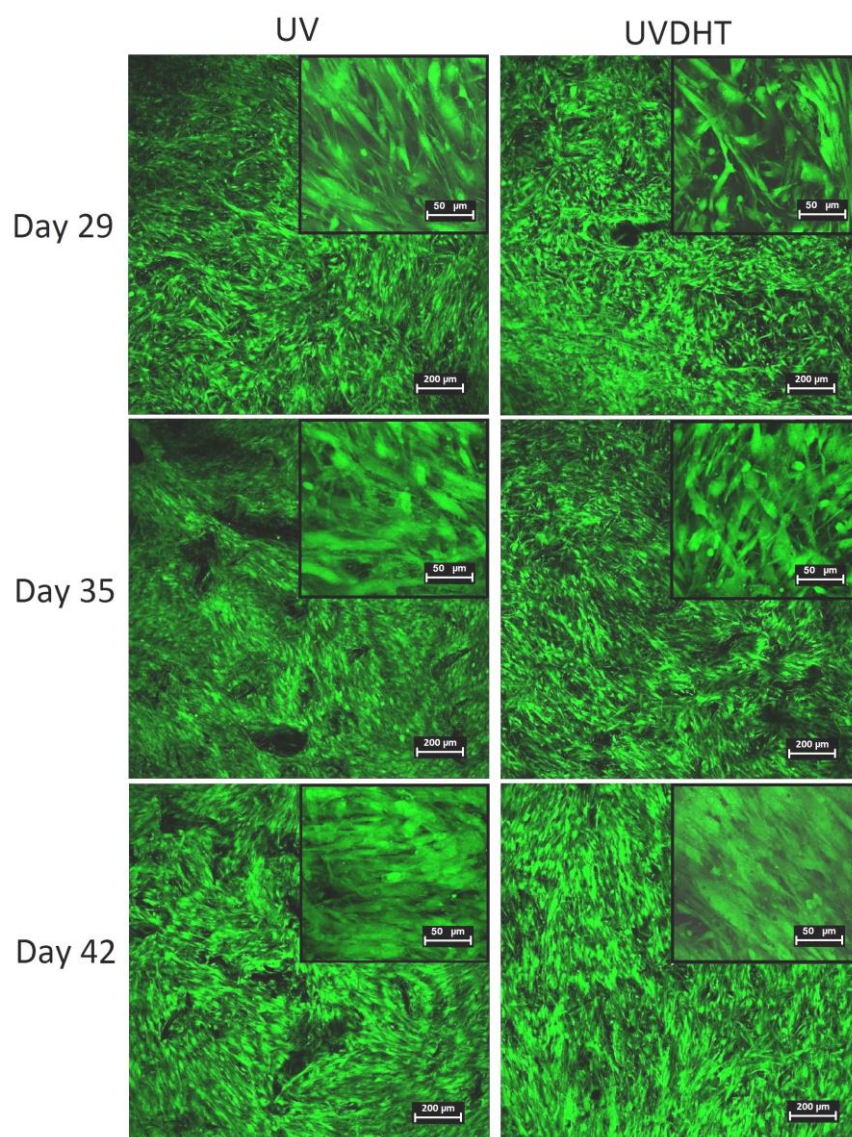


Figure 6-4: Continued form Figure 6-3.

6.3.3 DNA Quantification

DNA quantification of papain digested scaffolds shows a sharp upward trend in the DNA content during the first three weeks after culture indicating an increasing proliferation of cells on both UV and UVDHT treated CMD scaffolds. The steep slope collapses after the third week to a mild decreasing trend. Shrinkage and contraction of the scaffolds diminishes the growth area and attenuates the cell proliferation.

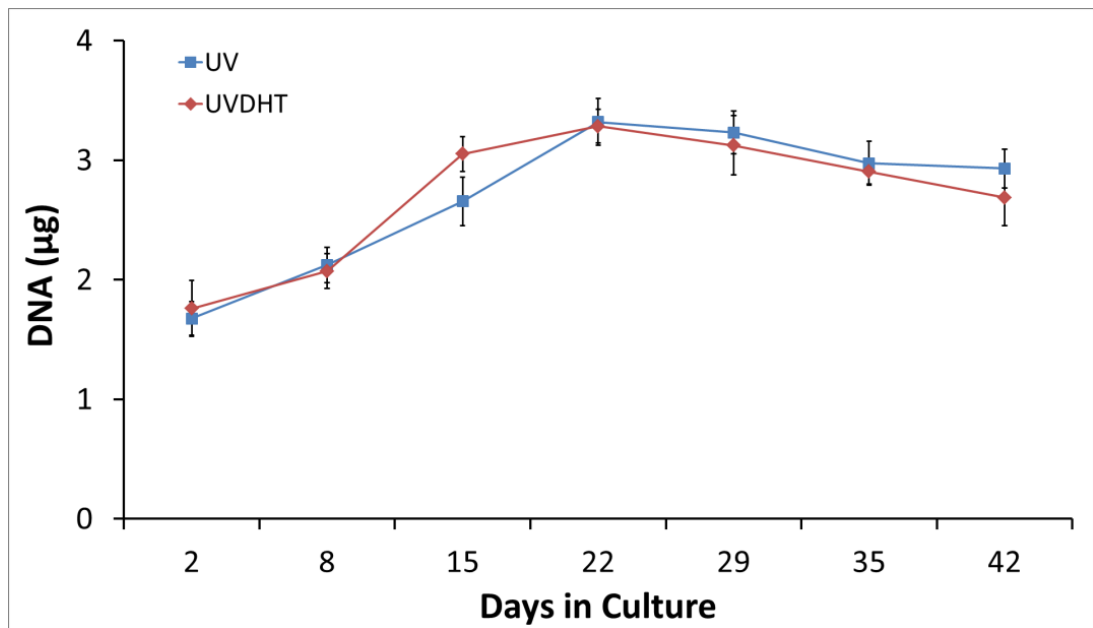


Figure 6-5: Total DNA by Hoechst method in papain digested cell seeded UV and UVDHT treated CMD scaffolds (n=5 for each group) at different weekly time-points after subtraction of average DNA in unseeded (blank) samples.

A two-way between-groups analysis of variances was conducted to determine the differences in Total DNA concentration between the two groups (cell seeded UV and UVDHT treated CMD scaffolds) at different time points. The significance value for Levene's test of homogeneity of variances was 0.066 (greater than 0.05), indicating that the assumption of homogeneity of variance has not been violated.

Post-hoc comparisons using the Tukey HSD test indicated that although the DNA content was not significantly higher at Day8 compared to Day2, however, a significant increase in the DNA content happened at the 2nd and 3rd weeks of culture, which was followed by a drop at the 4th week which remained constant until the Day42 with another significant decrease. No significant difference was seen in the DNA content between the UV and UVDHT groups at different time points ($P \geq 0.05$).

6.3.4 FESEM

Serial FESEM micrographs of HDF seeded UV and UVDHT treated CMD scaffolds at weekly time points are shown in Figure 6-6&7. The first couple of images (A and A')

are representative for the unseeded UV and UVDHT treated scaffolds, showing the wrinkled morphology of surfaces and filamentous structures of interconnected pores. Cell attachment and proliferation on all over the surfaces and inside the pores of both types of CMD scaffolds clearly shows the gradual growth and spreading of the cells, progressively filling all the spaces and covering the surfaces, resulting in entirely consistent cell-coated surfaces all over the constructs at Day22. FESEM images of the samples at any time point after Day22 show surfaces covered with intertwined visually inseparable cells.

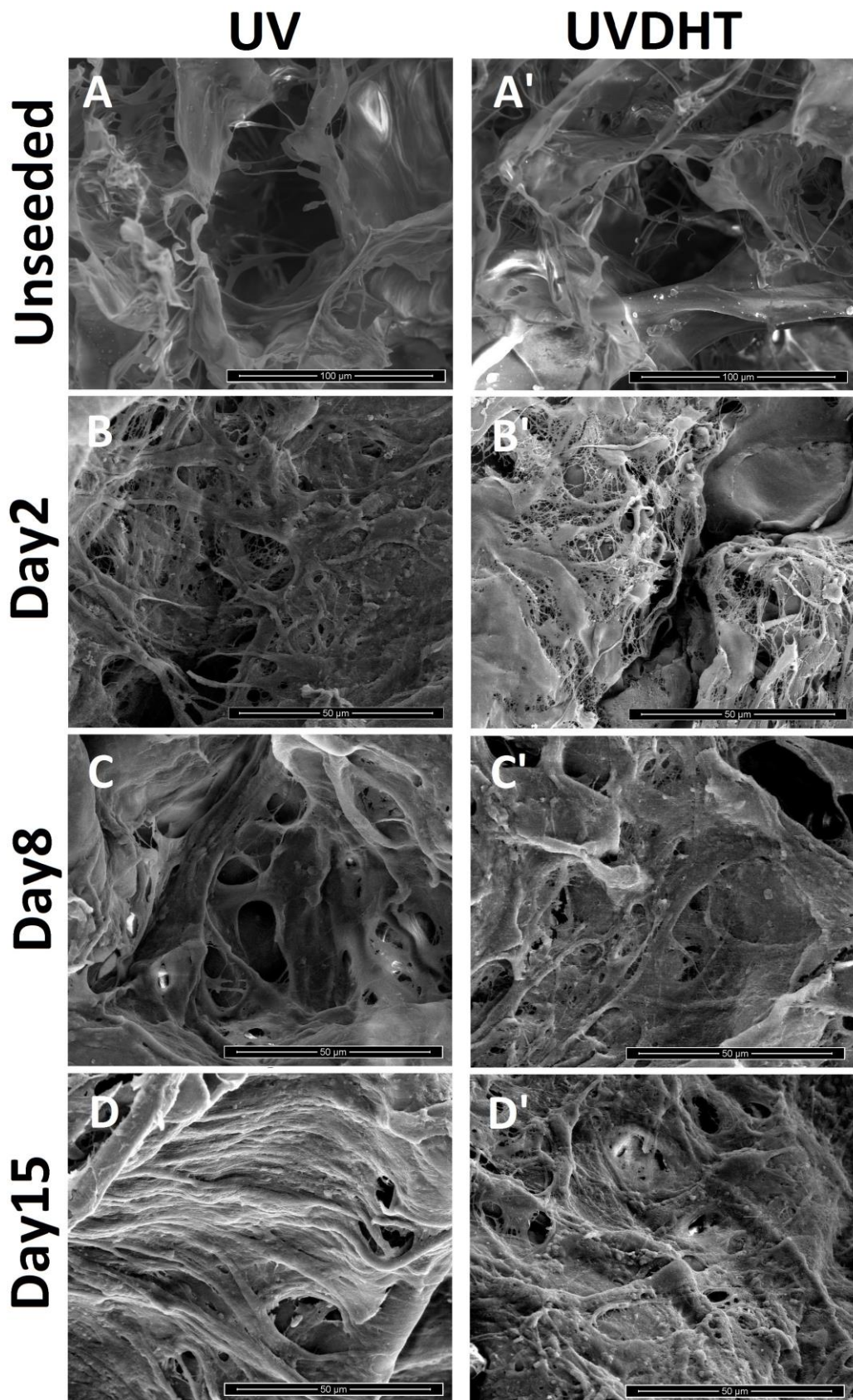


Figure 6-6: FESEM micrographs of unseeded (A&A') and cell seeded UV and UVDHT treated CMD scaffolds at weekly time points from Day 2 (B&B') to Day 42 (H&H'). The scale-bar for image A is 100 μm while for the rest of the images they represent for 50 μm .

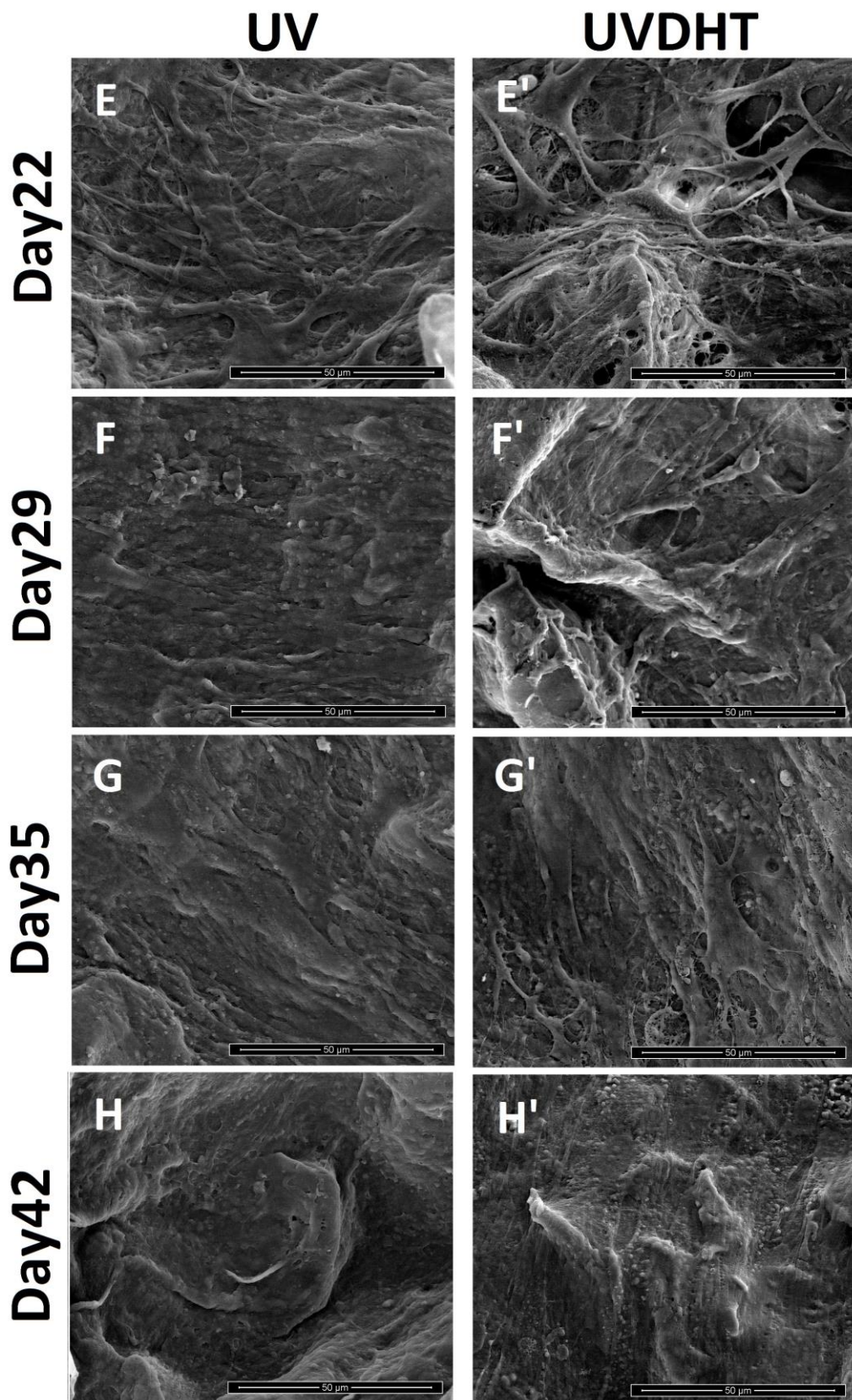


Figure 6-7: Continued for Figure 6-6.

6.3.5 Scaffold Shrinkage/Contraction

Serial digital top images of representative scaffolds captured at weekly time points are shown in Figure 6-8. Decreases in the size of scaffolds, especially the seeded ones are clearly visible. Surface area measurements using ImageJ[®] was applied to conduct a quantitative study.

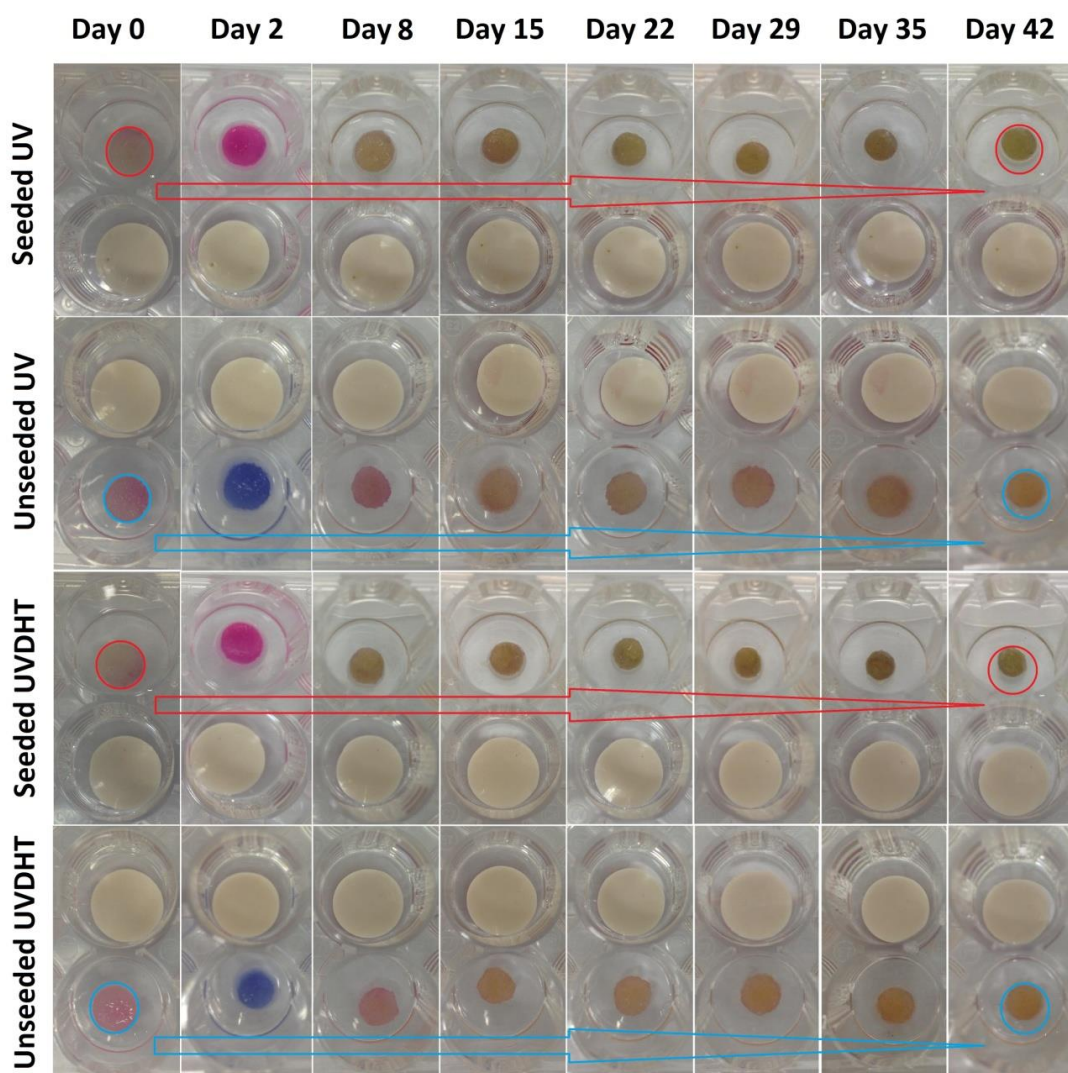


Figure 6-8: Serial digital images of top view of representative blank (unseeded) and HDF seeded UV and UVDHT treated CMD scaffolds at seeding time and consecutive weekly time points. The white circular plastic discs were used as the constant fixed-dimension scales.

Figure 6-10 shows the average cross-sectional (top) surface area of dry, unseeded and seeded wet UV and UVDHT treated 15% CMD scaffolds (n=7 for seeded and n=5 for

unseeded scaffolds) at seeding time and different weekly time points. All wetted scaffolds either with cell suspension or equivalent volume of culture medium showed a slight non-significant ($P>0.05$) increase in the cross-sectional surface area immediately after wetting, which is expected due to the spongy nature of the scaffolds and the surface tension of the medium as demonstrated in Figure 6-9.

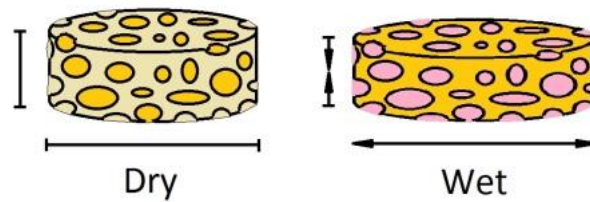


Figure 6-9: Effect of wetting on the dimensions of porous spongy scaffolds.

A two-way (between-groups) analysis of variances was conducted to determine the differences in cross-sectional surface area between the four groups (Seeded and Unseeded UV and UVDHT treated 15% CMD scaffolds) at different time points. Post-hoc comparisons using the Tukey HSD test was used to find the differences between the different groups at different time points. A value of $P\geq 0.05$ was assumed as non-significant.

As the cells attached on the surfaces and inside the pores of the scaffolds, shrinkage started and the top surface area showed a rapid fall during the first three weeks concurrently with increasing proliferation of the cells as previously shown and confirmed in Resazurin reduction, DNA content, confocal laser microscopy and FESEM images. However, the sharp decrease in the surface area got tapered down after Day22 of culture. Even unseeded scaffolds showed a downward trend of surface area, which slowed down and showed a mild slope after the Day8. This suggests that not all the shrinkage is cell induced and at least part of scaffold shrinkage results from scaffold contraction and degradation processes. Although the difference in cross-sectional

surface area of cell seeded UV and UVDHT treated 15% CMD scaffolds is not significant at different time points ($P>0.05$), however the significant difference between Unseeded UV and UVDHT treated 15% CMD scaffolds started from Day22 and onwards, showing a significantly bigger drop in the cross-sectional surface area of Unseeded UVDHT scaffolds compared to Unseeded UV treated scaffolds, reconfirming the higher stiffness of UV treated scaffolds. Although 15% UV and UVDHT treated CMD scaffolds have been shown to possess higher cross-linking among other CMD scaffolds, apart from the degradation effect, cell mediated contraction of the scaffolds is still shrinking the scaffolds in a significant scale.

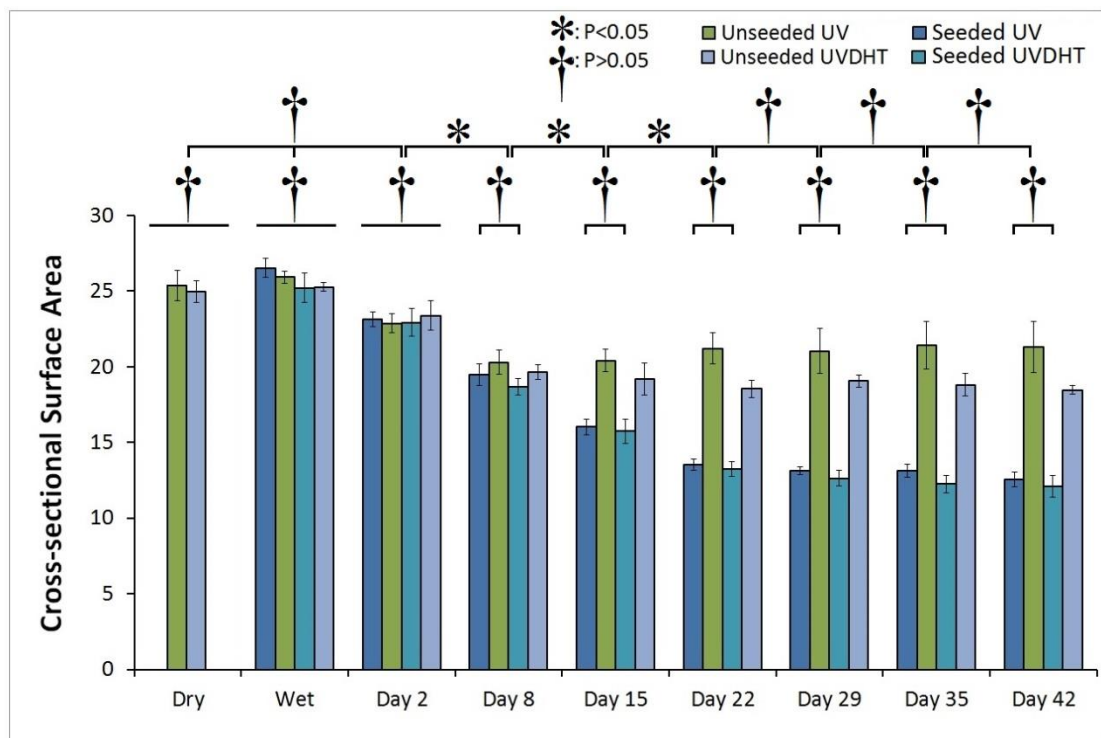


Figure 6-10: Measurements of cross-sectional surface area (top view) of the seeded and unseeded UV and UVDHT treated 15% CMD scaffolds (n=7 for seeded and n=5 for unseeded scaffolds. Significant and non-significant differences are shown by (*: $P<0.05$) and (†: $P>0.05$).

Results of total shrinkage (%) and cell-mediated contraction (%) at different weekly time points are shown in Figure 6-11. A two-way between-groups analysis of variances was conducted to determine the differences in percentage shrinkage between the UV

and UVDHT treated 15% CMD scaffolds at different time points. Post-hoc comparisons using the Tukey HSD test was used to find the differences between the two groups at different time points. A value of $P \geq 0.05$ was assumed as non-significant.

As it can be clearly seen HDF seeded UV treated CMD constructs show a sharp decrease in the size during the first three weeks after seeding but then reach a steady state with a gentle increase in shrinkage and contraction during the next four weeks. UVDHT treated CMD scaffolds continue their sharp rise in shrinkage until the fourth week of seeding and while cell-mediated contraction has a considerably weaker effect on UVDHT treated scaffolds they exert the same degree of total shrinkage in the size as UV treated scaffolds.

Also, having considered the equal porosity among both group of scaffolds, although cell mediated contraction (CMC) in UV group is significantly higher due to a higher rate of cell proliferation compared to the UVDHT group in almost all time points, there is no significant difference in total shrinkage between the UV and UVDHT groups. The higher CMC in UV group is contemporaneous and legitimizable with the higher cell growth and proliferation in UV group shown in Resazurin reduction test results. The bigger CMC in UV group due to higher cell proliferation has been compensated by the higher stiffness, resulting in a total shrinkage rate similar to the UVDHT group with a proportionally lower cell proliferation as well as lower stiffness.

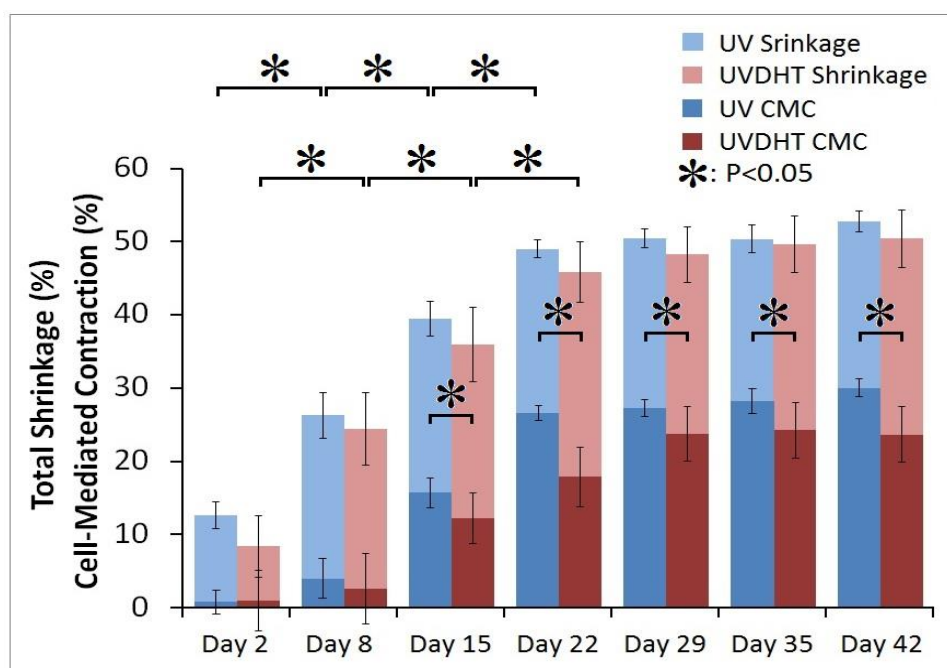


Figure 6-11: Percentage of total shrinkage in HDF seeded UV and UVDHT treated CMD scaffolds (n=7 for seeded scaffolds and n=5 for unseeded scaffolds) at different weekly time-points. Part of this shrinkage is due to cell mediated contraction (CMC). Asterix stands for P<0.05.

6.4 Chondrogenic Differentiation

6.4.1 GAGs Content

Attempts to measure GAGs through DMMB method failed to show any GAGs in the medium up to Day42. This means that no significant amounts of GAGs either released from the scaffolds as a result of biodegradation or from the HDF cells seeded on the CMD scaffolds as their extracellular matrix production could be detected by DMMB method.

Unlike the medium, Papain digested constructs at different weekly time points showed a good trend of GAGs accumulation within the cells. Figure 6-12 displays the GAGs content of papain digested cell seeded UV and UVDHT scaffolds after subtraction of average GAGs content in papain-digested unseeded samples (blanks). A peak in GAGs production in both groups is achieved within two weeks after cell seeding, followed by

a reduction in the third week and then a plateau, but always higher compared to the Day2.

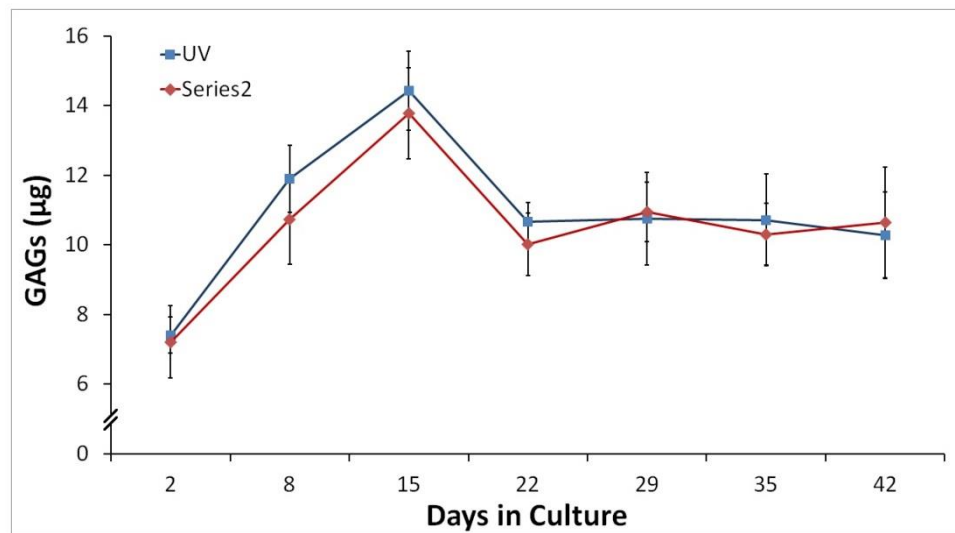


Figure 6-12: Sulfated Glycosaminoglycan content in cell seeded UV and UVDHT treated CMD scaffolds (n=5 in each group) at different weekly time points after subtraction of the average GAGs in unseeded samples, measured through DMMB method.

When the GAGs production is plotted against shrinkage rate (Figure 6-13), the effect of available surface area and space for the cells to grow and deposit ECM molecules like GAGs is revealed more clearer. These results clearly demonstrate the HDF cells tendency to produce GAGs when they are seeded on CMD scaffolds, however, GAGs production slowed down coincidentally with the scaffold shrinkage. This trend suggests that scaffold shrinkage and contraction is a potential cause of the reduction in GAGs production. As demonstrated previously (Buckley et al., 2009; C-Y Charles Huang, Paul M Reuben, Gianluca D'Ippolito, Paul C Schiller, & Herman S Cheung, 2004; R. Mauck, C. Wang, E. Oswald, G. Ateshian, & C. Hung, 2003b), increasing the proportional cell density favors chondrogenesis in terms of cartilage matrix production, but at a certain critical point when cells lack physical space, their growth and ECM producibility diminishes.

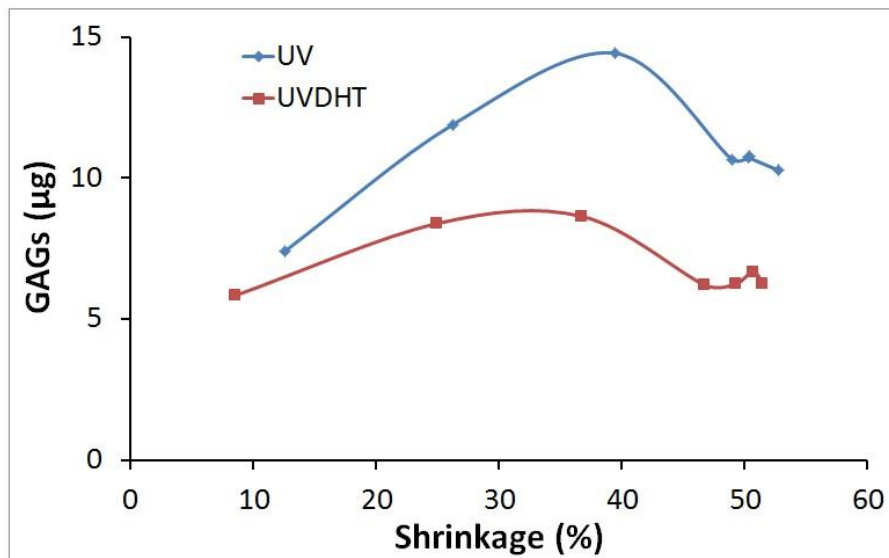
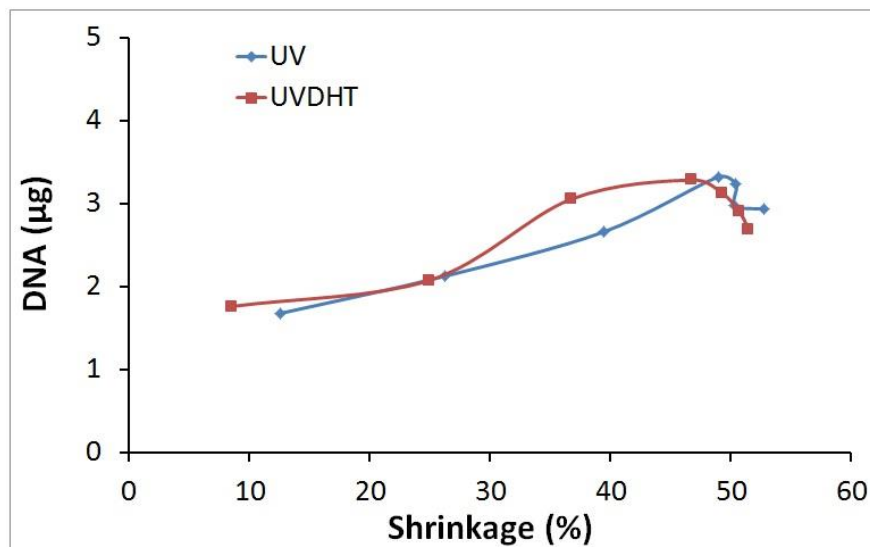


Figure 6-13: Correlation between sulfated glycosaminoglycan production and shrinkage rate in cells seeded on UV and UVDHT treated 15% CMD scaffolds.

A similar correlation exists between the DNA content and the shrinkage rate of cell seeded UV and UVDHT treated CMD constructs (Figure 6-14), reconfirming the effect of scaffold shrinkage on proliferation pattern of cells seeded on these porous scaffolds.



6-14: Correlation between total DNA and shrinkage rate in HDF-seeded UV and UVDHT treated 15% CMD scaffolds.

6.4.2 QPCR

Although an initial down regulation of COL1A1 gene was seen in Day 2 compared to the negative control HDF cells, the overall trend was increasing in both UV and UVDHT groups during the culture period with a significant higher expression ($P<0.05$) in UV group and up to 3-4 folds compared to the negative control. (Figure 6-15, A).

COL1A2 gene showed an upward trend in both UV and UVDHT groups during the first 3 weeks of culture, followed by a drop and the consequent plateau in both groups during the rest of the culture period (Figure 6-15, B). The expression of Col1A2 was significantly higher ($P<0.05$) in UVDHT group in all time points ($P<0.05$).

COL2A1 as the cartilage specific gene clearly showed two phases of expression: an almost constant expression with even some mild down regulation during the first 2-3 weeks, followed by the second phase with a sharp upregulation in both groups, with a significantly higher trend in UVDHT group ($P<0.05$). An overall increase up to over three and four folds in expression of COL2A1 was seen during the 7 weeks of culture in both UV and UVDHT groups (Figure 6-15, C).

The expression of ACAN, the gene encoding the cartilage proteoglycan molecule, Aggrecan, clearly showed a drastically increasing trend in both groups with a significantly higher trend in UVDHT group compared to the negative control (Figure 6-15, D).

SOX9, the gene containing the data for production of the transcription factor for the high mobility group domain expressed in cartilage cells, and COMP gene which is in charge of matrix assembly enhancement during chondrogenesis, both showed sharp upward steps during the first three weeks of culture, followed by a sharp drop in SOX9 to a level even lower than negative control, while an almost steady state for COMP but still much higher than the negative control (Figure 6-15, E and F).

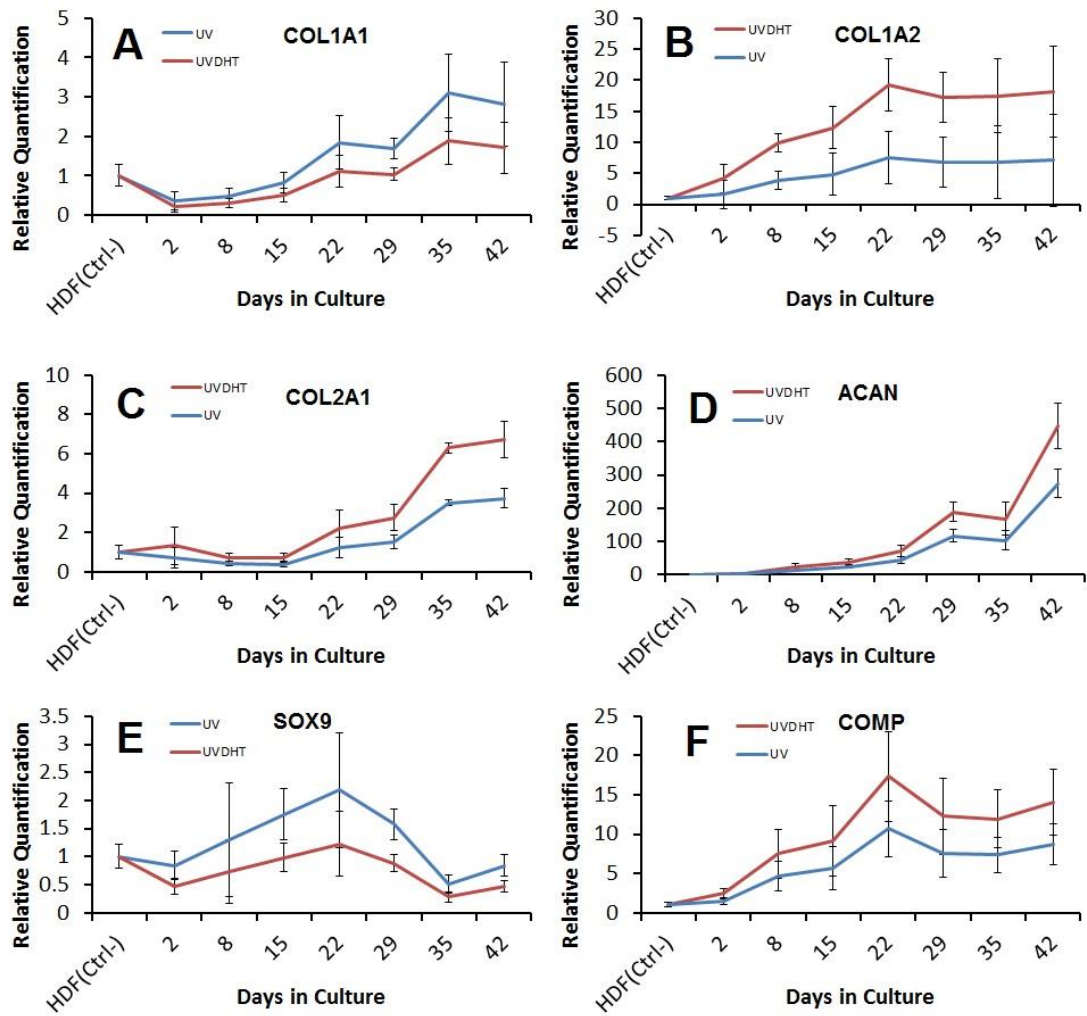


Figure 6-15: Quantitative gene expression of COL1A1 in HDFs seeded on UV and UVDHT treated CMD scaffolds (n=7 in each group) at weekly time points. The data have been normalized to GAPDH. HDF cells were used as Ctrl .

6.4.2.1 Scaffold Shrinkage/Contraction

Serial digital top images of representative scaffolds captured at weekly time points are shown in Figure 6-16, A. Decreases in the scaffold sizes during the time, especially in the seeded ones are clearly visible. Surface area measurements using ImageJ[®] was applied to conduct a quantitative study.

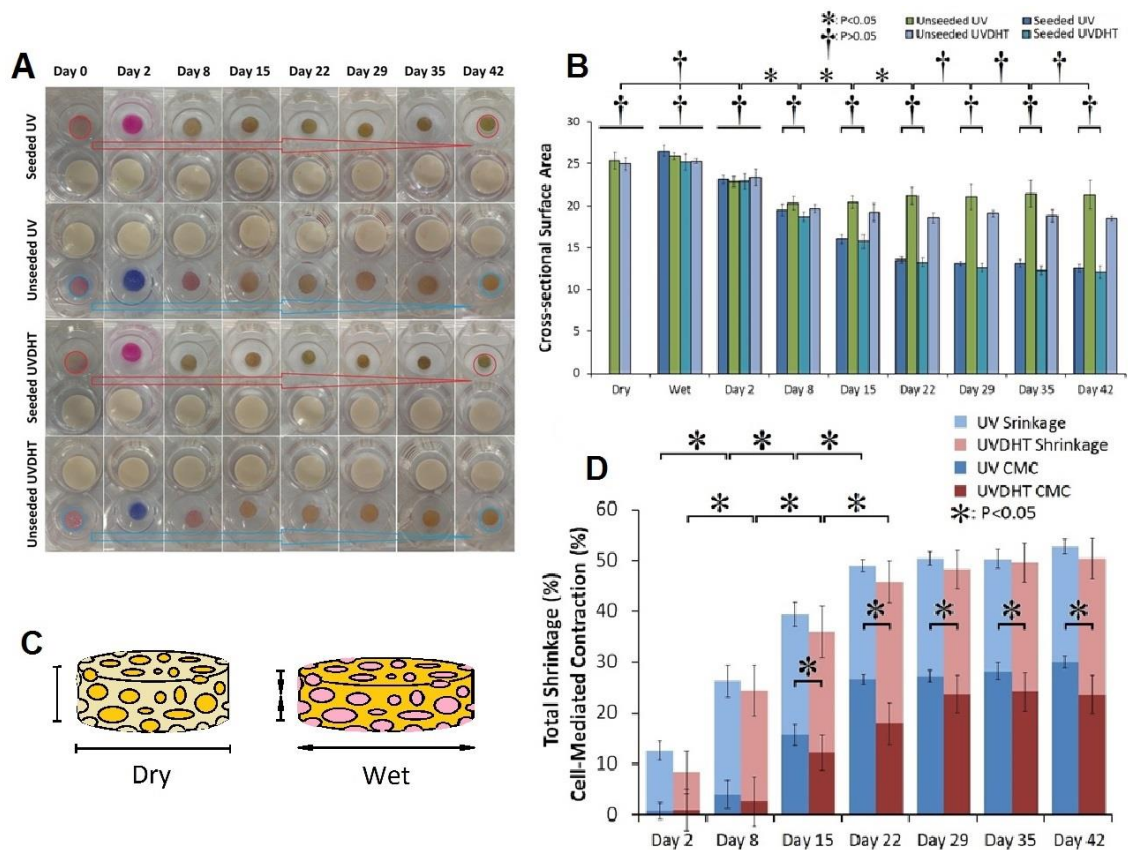


Figure 6-16: A) Serial digital images of top view of representative blank (unseeded) and HDF seeded UV and UVDHT treated CMD scaffolds at seeding time and consecutive weekly time points. The white circular plastic discs were used as the constant fixed-dimension scales.

B) Measurements of cross-sectional surface area (top view) of the seeded and unseeded UV and UVDHT treated CMD scaffolds (n=7 for seeded and n=5 for unseeded scaffolds). Significant and non-significant differences are shown by (*: P<0.05) and (†: P>0.0).

C) The initial effect of wetting on the dimensions of porous spongy scaffolds.

D) Percentage of total shrinkage in HDF seeded UV and UVDHT treated CMD scaffolds (n=7 for seeded scaffolds and n=5 for unseeded scaffolds) at different weekly time-points. Part of this shrinkage is due to cell mediated contraction (CMC). Asterix stands for P<0.05.

Figure 6-16, B shows the average cross-sectional (top) surface area of dry, unseeded and seeded wet UV and UVDHT treated 15% CMD scaffolds (n=7 for seeded and n=5 for unseeded scaffolds) at seeding time and sequential weekly time points. Wetted scaffolds, either with cell suspension or equivalent volume of culture medium, showed a non-significant ($P>0.05$) increase in the cross-sectional surface area immediately after wetting. This may be due to the hydrophilic spongy nature of the scaffolds and the surface tension of the medium compressing the scaffold, resulting in a light decrease in the height and a simultaneous slight increase in the top surface area as demonstrated in Figure 6-16, C.

As the cells attached on the surfaces and inside the pores of the scaffolds, shrinkage increased and the top surface area showed a rapid fall during the first three weeks concurrently with increasing proliferation of the cells as previously shown and confirmed in DNA content, confocal laser microscopy and FESEM images. However the sharp decrease in the surface area got tapered down after Day22 of culture. Unseeded scaffolds showed a downward trend of surface area during the first week of immersion in the culture medium, which slowed down and showed a mild slope after Day8. This suggests that not all the shrinkage is cell induced and at least part of scaffold shrinkage results from scaffold contraction and degradation processes. Although the difference between the cross-sectional surface area of seeded UV and UVDHT scaffolds was not significant at different time points ($P>0.05$), however a significant difference between Unseeded UV and UVDHT scaffolds started from Day22 and onwards, showing a significantly bigger drop in the cross-sectional surface area of Unseeded UVDHT scaffolds compared to Unseeded UV treated scaffolds, reconfirming the higher stiffness of UV treated scaffolds. Although 15% UV and UVDHT treated CMD scaffolds have been shown to possess higher cross-linking among other CMD scaffolds

(Moradi, Pramanik, Ataollahi, Abdul-Khalil, et al., 2014), cell mediated contraction of the scaffolds is still shrinking the scaffolds in a significant scale.

Results of total shrinkage (%) and cell-mediated contraction (%) at different weekly time points are shown in Figure 6-16, D. As it can be clearly seen HDF seeded UV treated CMD constructs show a sharp decrease in the size during the first three weeks after seeding but then reach a steady state with a gentle increase in shrinkage and contraction during the next four weeks. UVDHT treated CMD scaffolds continue their sharp rise in shrinkage until the fourth week of seeding. While cell-mediated contraction has a considerably weaker effect on UVDHT treated scaffolds they exert the same degree of total shrinkage in the size as UV treated scaffolds.

Also, having considered the equal porosity among both groups of scaffolds, there was no significant difference in total shrinkage between the UV and UVDHT groups.

6.4.2.2 The correlation between the Shrinkage, Cell Proliferation and Chondrogenesis

The correlation between COL2A1 and ACAN gene expression and the DNA content (Figure 6-17, A&B) clearly showed two distinct phases of gene expression during the 42 days of cell culture. The first phase was determined by an increase in the DNA content with a plateau state of COL2A1 and ACAN genes expression within the first 2-3 weeks of culture. The second phase was defined by a cessation in the DNA content and a simultaneous increase in the expression of COL2A1 and ACAN genes. The asynchronicity of cell proliferation with differentiation has already been addressed in other works (Strehl, Schumacher, de Vries, & Minuth, 2002; Topisirovic & Sonenberg, 2014). Also, chondrogenic differentiation has been shown to be dependent on high cell density (Buckley et al., 2009; C-Y Charles Huang et al., 2004; Mauck et al., 2003b).

During the first phase, cell proliferation provides the high density as a prerequisite for the second phase of differentiation.

Plotting the DNA content as a function of cell proliferation against the shrinkage rate also showed a biphasic trend indicating that as the cells proliferate progressively, they contract and shrink the scaffolds accordingly until a certain critical point when a scarcity in the surface area and space leaves no sufficient room for cell proliferation (Figure 6-17, C). Beyond this critical point any further increases in the shrinkage was contemporaneous with a slump in cell proliferation. This finding was in agreement with the previous studies (C. Lee et al., 2001; Schulz Torres et al., 2000).

The correlation between GAGs production and the shrinkage rate is presented in Figure 6-17, D. The HDF cells clearly showed a tendency to produce GAGs when seeded on CMD scaffolds. GAGs production was drowsed off coincidentally with the scaffold shrinkage and contraction pattern. This trend suggests that scaffold shrinkage and contraction is a potential cause of the reduction in GAGs production. As addressed in other works increasing the proportional cell density favours chondrogenesis in terms of cartilage matrix production, but at a certain critical point when the cells face lack of enough space, their growth and ECM producibility diminishes (C-Y Charles Huang et al., 2004; Mauck et al., 2003a).

The correlation between the expression of COL2A1 and ACAN genes and the scaffold shrinkage (Figure 6-17, E & F) reconfirmed the biphasic trend of cell proliferation-differentiation and revealed that the cell proliferation phase and the increasing shrinkage were concurrent with steady state of slow chondrogenic gene expression, but during the second phase the fast increasing expression of COL2A1 and ACAN genes was simultaneous with an invariant shrinkage.

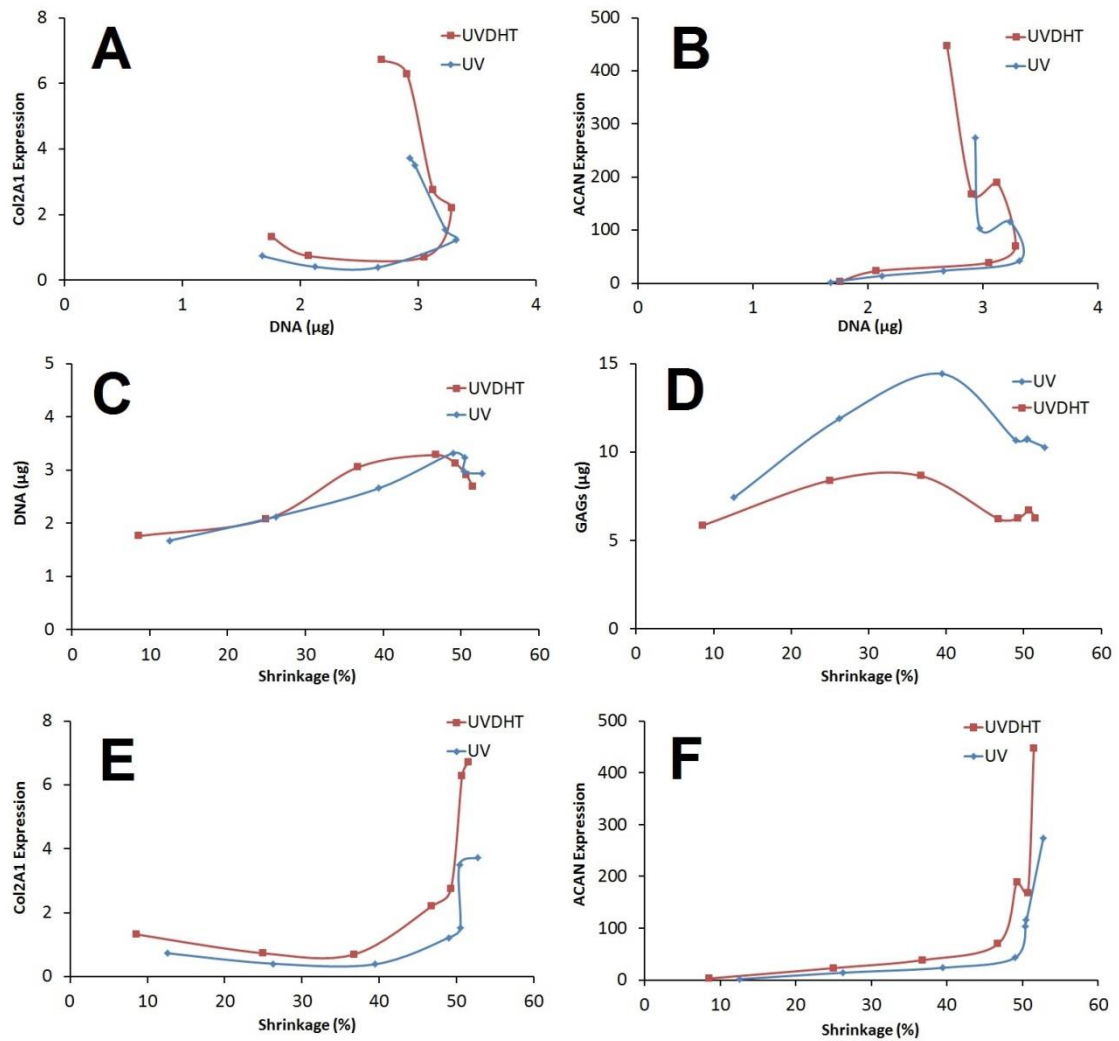


Figure 6-17: Correlation between A) COL2A1 and B) ACAN gene expression, and DNA content, C) the DNA and D) GAGs content, and E) COL2A1 and F) ACAN expression all against shrinkage rate.

6.5 Discussion

Chondrogenic potential of porcine(Cheng et al., 2009) and human(Q. Yang, Peng, Guo, Huang, Zhang, Yao, et al., 2008) CMD constructs on various stem cells has been previously investigated. It is also apparent, cell mediated contraction and shrinkage of non-treated and structurally enhanced matrix derived scaffolds and their effects on chondrogenesis have been studied in previous studies(Zaleskas et al., 2004). In this chapter we discussed the methods of evaluating the chondrogenic potential of structurally tailored and optimized bovine articular CMD porous scaffolds on cultured

primary human dermal fibroblasts as semi-differentiated cells of mesenchymal origin. The probability of cell mediated contraction and scaffold shrinkage in physically treated CMD scaffolds and their effects on chondrogenic differentiation of HDF cells were also investigated.

Serial measurements of DNA content and Resazurin reduction as well as imaging techniques (CLSM and FESEM) demonstrated that physically treated bovine CMD scaffolds are suitable biocompatible constructs for HDF cell attachment and proliferation. This was a completely expected outcome as the main component of CMD scaffolds is collagen which has been shown to be a perfect biomaterial for different types of cells (Chevallay & Herbage, 2000; Julie Glowacki & Mizuno, 2008; Parenteau-Bareil, Gauvin, & Berthod, 2010).

Chondrogenic potential of bovine CMD scaffolds was also studied through quantification of their sulphated glycosaminoglycan content and also the expression of chondrogenic genes at sequential time points. Our findings showed that primary human dermal fibroblast cells are capable of GAGs production provided that they are placed in a proper chondrogenic environment.

Upregulation of cartilage tissue specific genes like collagen type II, aggrecan, SOX9 and COMP confirmed the differentiation of dermal fibroblasts to chondrocytes under proper chondrogenic 3D culture conditions. Some of the signalling mechanisms involved in chondrogenesis have already been described. It has been reported that Sox9 is one of the earliest markers expressed in the mesenchymal condensations (Véronique Lefebvre, Li, & de Crombrughe, 1998). As a key transcription factor in chondrogenesis, Sox9 is known for its role in activation of the expression of several cartilage-specific genes, including Col2a1, ACAN and COMP (Taipaleenmäki,

2010). During chondrogenesis, the expression of SOX-9 is up-regulated by TGF- β signalling (Shanmugarajan, Kim, Lee, & Im, 2011).

We showed that scaffold shrinkage have inconsistent effects on cell chondrogenesis. Our findings revealed two distinct phases during the 6-week culture period. The simultaneous cell proliferations and scaffold shrinkage during the proliferation phase speeds up and facilitates the cell condensation which has been reported to be critically essential for chondrogenesis (Kavalkovich, 2000). This phase was synchronous with sharp increases in SOX9 gene expression as a chondrogenesis enhancer (Ng et al., 1997; Wright et al., 1995; Zhao et al., 1997). This suggests that the cell condensation at least partly triggers the up-regulation of the SOX9 expression which in turn activates the expression of COMP, COL2A1 and ACAN.

The second phase starts at the peak point of cell proliferation and scaffold shrinkage with a suspension in cell proliferation, increases in expression of Col2A1 and ACAN genes as major chondrogenic differentiation markers. The biphasic trend suggests the presence of a critical state of cell density and cell-scaffold interaction in which the chondrogenic mechanisms are triggered. This compulsory critical state was shown to be achievable partially through scaffold shrinkage which has so far been thought to have only limitative effects on chondrogenesis.

Although our previous results showed a higher degree of cross linkage and hence improved mechanical properties in UV treated compared to UVDHT treated CMD scaffolds, UVDHT group showed significantly higher levels of Col2A1 and ACAN genes expression.

In conclusion, physically treated bovine articular cartilage matrix derived scaffolds are capable of inducing chondrogenic differentiation in human dermal fibroblasts. Although this chondroinductive effect can be traced back to SOX9 level, however the precise

mechanism/s through which the cartilage matrix up-regulates SOX9 expression remain to be explored in other studies.

CHAPTER 7: DISCUSSION AND CONCLUSION

It has been shown that extracellular matrix derived scaffolds from different sources have the potential to promote cartilage regeneration using tissue engineering applications. The source of biomaterial, the method of fabrication and the efficacy of chondrogenic differentiation have always been the main concerns related to engineering cartilage tissue oriented matrix derived scaffolds. Apart from the abundance of the source and ease of harvesting, the fabrication method has always been a major concern to retrieve the maximal bioactive chondroinductive ingredients of CMD scaffolds. Moreover, matrix derived scaffolds have poor mechanical properties and therefore, non-invasive treatments are necessary to increase their cross-linking and enhance the physical and structural properties of such scaffolds. The development of cartilage matrix derived scaffolds that possess suitable mechanical properties and chondroinductive abilities provide substantial advantage to the efforts of cartilage tissue engineering. Hence, the studies in this thesis were conducted to assess the chondroinductive potential of architecturally optimized CMD scaffolds.

The first aim of the current study was to fabricate optimized CMD scaffolds by conducting a quantitative assessment of the changes in the architectural and the mechanical properties of physically cross-linked CMD scaffolds. We have reported the detailed processes of fabrication, physical treatment and methods of optimization of CMD scaffolds with bovine origin (Moradi, Pramanik, Ataollahi, Abdul-Khalil, et al., 2014). A simple, restorative and non-invasive method of freeze-drying was used to fabricate scaffolds with different concentrations of CMD material. The scaffolds were treated with one of the five conditions to create cross-linking (Non-treated, UV, DHT, UVDHT, and DHTUV). In order to optimize the scaffold architecture, physical characterization was performed using FTIR, TGA, DSC, FESEM, porosimetry, mechanical tests and post-treatment shrinkage measurement.

A simple, highly accurate and precise method was developed to measure the porosity of highly porous ultra-light materials such as the CMD scaffolds in one of our experiments. We demonstrated that at 15% concentration of cartilage matrix material, the fabrication of CMD porous scaffolds was optimal, beyond which the architecture of the scaffolds can drastically change to become unfavourable. We also demonstrated that UV and UVDHT treatment of 15% CMD scaffolds yielded optimized and properly tailored scaffolds for cartilage tissue engineering applications.

The isolation, culture and characterization of primary human dermal fibroblast cells were discussed in chapter five. The cells were later used to assess the chondroinductive potential of UV and UVDHT treated 15% CMD scaffolds. Seeding the HDF cells on UV and UVDHT treated 15% bovine CMD scaffolds demonstrated that the materials were biocompatible constructs that allow HDF cells to attach, proliferate and produce cartilage matrix proteins e.g. GAGs. In addition, this results in the triggering of the mechanisms that upregulate the expression of cartilage specific genes including collagen type II, Aggrecan, SOX9, and COMP.

Although UV and UVDHT treated 15% CMD scaffolds have demonstrated higher mechanical properties, the 3D culture of primary HDF cells on these scaffolds led to substantial shrinkage, part of which was found to be due to cell mediated contractions. Of interest was also the fact that we demonstrated a biphasic process of proliferation-chondroinduction during the cell culture. The synchronous trend of cell proliferation with the shrinkage of constructs clearly revealed that the cessation and subsequent drop in cell proliferation was a consequence of the reduction in construct size. While scaffold shrinkage has been reported to have inhibitory effects on chondrogenesis, our findings revealed that it may have contradictory effects. The initial period of upward slope in cell proliferation provided a high-density population of cells, resulting in a higher magnitude of cell-mediated contraction of the scaffold. These augmented cell condensations

appeared to have ambivalent effects on chondrogenesis: preventing the cells to deposit more extracellular matrix due to the space scarcity, and simultaneous up-regulation of SOX9 gene expression; resulting in an increased expression of COMP, COL2A1 and ACAN as cartilage specific genes. Upregulation of SOX9 gene during the cell condensation phase resulting in an increased expression of COL2A1 and ACAN genes during the chondroinductive phase suggest that TGF β signalling pathway might be involved in the chondroinduction of HDF cells using CMD scaffolds.

In conclusion, the present thesis suggests that bovine articular CMD porous scaffolds have the potential to induce chondrogenic differentiation in human dermal fibroblasts, thus making it a potential biomaterial with likely future clinical applications. However, the present thesis lacks study that identifies the precise underlying mechanisms of which chondroinduction by CMD scaffolds was controlled. Hence, this remains to be studied in future studies. Of note, although scaffold shrinkage has an opposite effect on the chondrogenic properties of CMD scaffolds, improving the mechanical properties of CMD scaffolds may minimize the shrinkage and increase matrix deposition. This too will need to be looked at more deeply in future research undertakings.

REFERENCES

- Aichroth, P., Burwell, R., & Laurence, M. (1972). Transplantation of synovial joint surfaces: An experimental study. *J. Bone Joint Surg.* 54B, 747.
- Al-Nasiry, S., Geusens, N., Hanssens, M., Luyten, C., & Pijnenborg, R. (2007). The use of Alamar Blue assay for quantitative analysis of viability, migration and invasion of choriocarcinoma cells. *Human reproduction*, 22(5), 1304-1309. doi: 10.1093/humrep/dem011
- Altman, D. G., & Bland, J. M. (1983). Measurement in medicine: the analysis of method comparison studies. *The statistician*, 307-317. doi: 10.2307/2987937
- Badylak, S. F. (2002). *The extracellular matrix as a scaffold for tissue reconstruction*. Paper presented at the Seminars in Cell & Developmental Biology.
- Bell, D. M., Leung, K. K., Wheatley, S. C., Ng, L. J., Zhou, S., Ling, K. W., . . . Cheah, K. S. (1997). SOX9 directly regulates the type-II collagen gene. *Nature Genetics*, 16(2), 174-178. doi: 10.1038/ng0697-174
- Bellamkonda, R., Ranieri, J. P., Bouche, N., & Aebischer, P. (1995). Hydrogel-based three-dimensional matrix for neural cells. *Journal of Biomedical Materials Research*, 29(5), 663-671. doi: 10.1002/jbm.820290514
- Bellincampi, L. D., & Dunn, M. G. (1997). Effect of crosslinking method on collagen fiber-fibroblast interactions. *Journal of Applied Polymer Science*, 63(11), 1493-1498. doi: 10.1002/(SICI)1097-4628(19970314)63:11<1493::AID-APP11>3.0.CO;2-3
- Benders, K. E., Weeren, P., Badylak, S. F., Saris, D. B., Dhert, W. J., & Malda, J. (2013). Extracellular matrix scaffolds for cartilage and bone regeneration. *TRENDS in Biotechnology*, 31(3), 169-176. doi: 10.1016/j.tibtech.2012.12.004
- Bertoldi, S., Farè, S., & Tanzi, M. C. (2011). Assessment of scaffold porosity: the new route of micro-CT. *Journal of Applied Biomaterials & Biomechanics*, 9(3). doi: 10.5301/JABB.2011.8863
- Bhosale, A., & Richardson, J. (2008). Articular cartilage: structure, injuries and review of management. *British medical bulletin*, 87(1), 77.
- Biosystems, A. (2008). TRI Reagent® Solution. In A. Biosystems (Ed.): Ambion.
- Bland, J. M., & Altman, D. G. (1986). Statistical methods for assessing agreement between two methods of clinical measurement. *The Lancet*, 327(8476), 307-310. doi: 10.1016/S0140-6736(86)90837-8
- Bradham, R. R. (1960). The importance of porosity in vascular prostheses. *The American Journal of Surgery*, 100(4), 557-560. doi: 10.1016/0002-9610(60)90321-4
- Bryant, S. J., & Anseth, K. S. (2002). Hydrogel properties influence ECM production by chondrocytes photoencapsulated in poly (ethylene glycol) hydrogels. *Journal of Biomedical Materials Research*, 59(1), 63-72. doi: 10.1002/jbm.1217

- Buckley, C. T., Thorpe, S. D., O'Brien, F. J., Robinson, A. J., & Kelly, D. J. (2009). The effect of concentration, thermal history and cell seeding density on the initial mechanical properties of agarose hydrogels. *Journal of the Mechanical Behavior of Biomedical Materials*, 2(5), 512-521. doi: 10.1016/j.jmbbm.2008.12.007
- Buckwalter, J., & Mankin, H. (1997). Instructional Course Lectures, The American Academy of Orthopaedic Surgeons-Articular Cartilage. Part I: Tissue Design and Chondrocyte-Matrix Interactions*~~{}~~. *The Journal of Bone and Joint Surgery*, 79(4), 600.
- Calvo, J. I., Bottino, A., Capannelli, G., & Hernández, A. (2008). Pore size distribution of ceramic UF membranes by liquid-liquid displacement porosimetry. *Journal of Membrane Science*, 310(1), 531-538. doi: 10.1016/j.memsci.2007.11.035
- Camacho, N. P., West, P., Torzilli, P. A., & Mendelsohn, R. (2001). FTIR microscopic imaging of collagen and proteoglycan in bovine cartilage. *Biopolymers*, 62(1), 1-8. doi: 10.1002/1097-0282(2001)62:1<1::AID-BIP10>3.0.CO;2-O
- Charlebois, M., McKee, M. D., & Buschmann, M. D. (2004). Nonlinear tensile properties of bovine articular cartilage and their variation with age and depth. *Journal of Biomechanical Engineering*, 126(2), 129-137. doi: 10.1115/1.1688771
- Charles Huang, C. Y., Reuben, P. M., D'Ippolito, G., Schiller, P. C., & Cheung, H. S. (2004). Chondrogenesis of human bone marrow-derived mesenchymal stem cells in agarose culture. *The Anatomical Record Part A: Discoveries in Molecular, Cellular, and Evolutionary Biology*, 278(1), 428-436. doi: 10.1002/ar.a.20010
- Charles Huang, C. Y., Reuben, P. M., D'Ippolito, G., Schiller, P. C., & Cheung, H. S. (2004). Chondrogenesis of human bone marrow derived mesenchymal stem cells in agarose culture. *The Anatomical Record Part A: Discoveries in Molecular, Cellular, and Evolutionary Biology*, 278(1), 428-436.
- Charulatha, V., & Rajaram, A. (2003). Influence of different crosslinking treatments on the physical properties of collagen membranes. *Biomaterials*, 24(5), 759-767. doi: 10.1016/S0142-9612(02)00412-X
- Chen, F. G., Zhang, W. J., Bi, D., Liu, W., Wei, X., Chen, F. F., . . . Cao, Y. (2007). Clonal analysis of nestin-vimentin+ multipotent fibroblasts isolated from human dermis. *Journal of Cell Science*, 120(16), 2875.
- Cheng, N.-C., Estes, B. T., Awad, H. A., & Guilak, F. (2008). Chondrogenic differentiation of adipose-derived adult stem cells by a porous scaffold derived from native articular cartilage extracellular matrix. *Tissue Engineering Part A*, 15(2), 231-241. doi: doi:10.1089/ten.tea.2008.0253.
- Cheng, N.-C., Estes, B. T., Awad, H. A., & Guilak, F. (2009). Chondrogenic Differentiation of Adipose-Derived Adult Stem Cells by a Porous Scaffold Derived from Native Articular Cartilage Extracellular Matrix. *ITissue Engineering: Part A*, 15(2), 231-241. doi: 10.1089/ten.tea.2008.0253

- Cheng, N.-C., Estes, B. T., Young, T.-H., & Guilak, F. (2011). Engineered cartilage using primary chondrocytes cultured in a porous cartilage-derived matrix. *Regenerative Medicine*, 6(1), 81-93. doi: 10.2217/rme.10.87.
- Chevallay, B., & Herbage, D. (2000). Collagen-based biomaterials as 3D scaffold for cell cultures: applications for tissue engineering and gene therapy. *Medical and Biological Engineering and Computing*, 38(2), 211-218.
- Chiou, M., Xu, Y., & Longaker, M. T. (2006). Mitogenic and chondrogenic effects of fibroblast growth factor-2 in adipose-derived mesenchymal cells. *Biochemical and biophysical research communications*, 343(2), 644-652. doi: 10.1016/j.bbrc.2006.02.171
- Curl, W. W., Krome, J., Gordon, E. S., Rushing, J., Smith, B. P., & Poehling, G. G. (1997). Cartilage Injuries: A Review of 31,516 Knee Arthroscopies. *Arthroscopy: The Journal of Arthroscopic and Related Surgery*, 13(4), 456-460.
- Damink, L., Dijkstra, P., Van Luyn, M., Van Wachem, P., Nieuwenhuis, P., & Feijen, J. (1995). Changes in the mechanical properties of dermal sheep collagen during in vitro degradation. *Journal of Biomedical Materials Research*, 29(2), 139-147. doi: 10.1002/jbm.820290202
- Damink, L. O., Dijkstra, P., Van Luyn, M., Van Wachem, P., Nieuwenhuis, P., & Feijen, J. (1995). Glutaraldehyde as a crosslinking agent for collagen-based biomaterials. *Journal of Materials Science: Materials in Medicine*, 6(8), 460-472. doi: 10.1007/BF00123371
- Deng, Y., Hu, J. C., & Athanasiou, K. A. (2007). Isolation and chondroinduction of a dermis-isolated, aggrecan-sensitive subpopulation with high chondrogenic potential. *Arthritis & Rheumatism*, 56(1), 168-176. doi: 10.1002/art.22300
- Diekman, B. O., Rowland, C. R., Lennon, D. P., Caplan, A. I., & Guilak, F. (2009). Chondrogenesis of adult stem cells from adipose tissue and bone marrow: induction by growth factors and cartilage-derived matrix. *Tissue Engineering Part A*, 16(2), 523-533. doi: 10.1089/ten.tea.2009.0398
- Dienstknecht, T., Eehalt, K., Jenei-Lanzl, Z., Zellner, J., Müller, M., Berner, A., . . . Angele, P. (2010). Resazurin dye as a reliable tool for determination of cell number and viability in mesenchymal stem cell culture. *Bulletin of experimental biology and medicine*, 150(1), 157-159.
- Erickson, G., Gimble, J., Franklin, D., Rice, H., Awad, H., & Guilak, F. (2002). Chondrogenic potential of adipose tissue-derived stromal cells in vitro and in vivo. *Biochemical and biophysical research communications*, 290(2), 763-769.
- Finkelstein, H., & Mayer, L. (1931). The arthroscope: A new method of examining joints. *The Journal of Bone and Joint Surgery*, 13(3), 583.
- French, M., Liu, E., & Athanasiou, K. (2002). *In vitro differentiation of neonatal foreskin fibroblasts to chondrocytes*.
- French, M., Rose, S., Canseco, J., & Athanasiou, K. (2004). Chondrogenic differentiation of adult dermal fibroblasts. *Annals of biomedical engineering*, 32(1), 50-56.

- French, M., Smith, S., Akanbi, K., Sanford, T., Hecht, J., Farach-Carson, M., & Carson, D. (1999). Expression of the heparan sulfate proteoglycan, perlecan, during mouse embryogenesis and perlecan chondrogenic activity in vitro. *The Journal of cell biology*, 145(5), 1103. doi: 10.1083/jcb.145.5.1103
- Froget, S., Barthelemy, E., Guillot, F., Soler, C., Coudert, M. C., Benbunan, M., & Dosquet, C. (2003). Wound healing mediator production by human dermal fibroblasts grown within a collagen-GAG matrix for skin repair in humans. *European Cytokine Network*, 14(1), 60-64.
- Fry, W., DeWeese, M., Kraft, R., & Ernst, C. (1964). Importance of porosity in arterial prostheses. *Archives of Surgery*, 88(5), 836. doi: 10.1001/archsurg.1964.01310230112022.
- Fulcher, G. R., Hukins, D. W., & Shepherd, D. E. (2009). Viscoelastic properties of bovine articular cartilage attached to subchondral bone at high frequencies. *BMC Musculoskeletal Disorders*, 10(1), 61. doi: 10.1186/1471-2474-10-61
- Furneaux, R., Rigby, W., & Davidson, A. (1989). The formation of controlled-porosity membranes from anodically oxidized aluminium. *Nature*, 337(6203), 147-149. doi: 10.1038/337147a0
- Gago, N., Pérez-López, V., Sanz-Jaka, J. P., Cormenzana, P., Eizaguirre, I., Bernad, A., & Izeta, A. (2009). Age-Dependent Depletion of Human Skin-Derived Progenitor Cells. *Stem Cells*, 27(5), 1164-1172.
- Gang, E. J., Hong, S. H., Jeong, J. A., Hwang, S. H., Kim, S. W., Yang, I., . . . Kim, H. (2004). In vitro mesengenic potential of human umbilical cord blood-derived mesenchymal stem cells. *Biochemical and biophysical research communications*, 321(1), 102-108.
- Gilbert, D. L. (1988). *Collagen macromolecular drug delivery systems*. The University of Utah, Utah, USA.
- Glowacki, J. (1996). Cellular reactions to bone-derived material. *Clinical Orthopaedics and Related Research*, 324, 47.
- Glowacki, J. (2000). In vitro engineering of cartilage. *In vitro*, 37(2), 171-178.
- Glowacki, J., & Mizuno, S. (1997). Cell induction device: Google Patents.
- Glowacki, J., & Mizuno, S. (2008). Collagen scaffolds for tissue engineering. *Biopolymers*, 89(5), 338-344. doi: 10.1002/bip.20871
- Glowacki, J., & Mulliken, J. (1985). Demineralized bone implants. *Clinics in plastic surgery*, 12(2), 233.
- Glowacki, J., Yates, K., Little, G., & Mizuno, S. (1998). Induced chondroblastic differentiation of human fibroblasts by three-dimensional culture with demineralized bone matrix. *Materials Science and Engineering: C*, 6(4), 199-203.

- Glowacki, J., Zhou, S., & Mizuno, S. (2009). Mechanisms of Osteoinduction/Chondroinduction by Demineralized Bone. *Journal of Craniofacial Surgery*, 20, 634.
- Haleem-Smith, H., Calderon, R., Song, Y., Tuan, R. S., & Chen, F. H. (2012). Cartilage oligomeric matrix protein enhances matrix assembly during chondrogenesis of human mesenchymal stem cells. *Journal of cellular biochemistry*, 113(4), 1245-1252. doi: 10.1002/jcb.23455
- Hangody, L., & Fules, P. (2003). Autologous osteochondral mosaicplasty for the treatment of full-thickness defects of weight-bearing joints: ten years of experimental and clinical experience. *The Journal of Bone and Joint Surgery*, 85(Supplement 2), 25.
- Hangody, L., Kish, G., Karpati, Z., Szerb, I., & Udvarhelyi, I. (1997). Arthroscopic autogenous osteochondral mosaicplasty for the treatment of femoral condylar articular defects A preliminary report. *Knee Surgery, Sports Traumatology, Arthroscopy*, 5(4), 262-267.
- Hangody, L., Rathonyi, G., Duska, Z., Vasarhelyi, G., Fules, P., & Modis, L. (2004). Autologous osteochondral mosaicplasty. Surgical technique. *The Journal of Bone and Joint Surgery*, 86(Supplement 1), 65.
- Haugh, M. G., Jaasma, M. J., & O'Brien, F. J. (2009). The effect of dehydrothermal treatment on the mechanical and structural properties of collagen-GAG scaffolds. *Journal of Biomedical Materials Research Part A*, 89(2), 363-369. doi: 10.1002/jbm.a.31955
- Haugh, M. G., Murphy, C. M., McKiernan, R. C., Altenbuchner, C., & O'Brien, F. J. (2011). Crosslinking and mechanical properties significantly influence cell attachment, proliferation, and migration within collagen glycosaminoglycan scaffolds. *Tissue Engineering Part A*, 17(9-10), 1201-1208. doi: 10.1089/ten.TEA.2010.0590
- Haugh, M. G., Murphy, C. M., & O'Brien, F. J. (2009). Novel freeze-drying methods to produce a range of collagen–glycosaminoglycan scaffolds with tailored mean pore sizes. *Tissue Engineering Part C: Methods*, 16(5), 887-894. doi: 10.1089/ten.TEC.2009.0422.
- Hiramatsu, K., Sasagawa, S., Outani, H., Nakagawa, K., Yoshikawa, H., & Tsumaki, N. (2011). Generation of hyaline cartilaginous tissue from mouse adult dermal fibroblast culture by defined factors. *The Journal of clinical investigation*, 121(2), 640-657. doi: 10.1172/JCI44605
- Hoemann, C. D. (2004). Molecular and Biochemical Assays of Cartilage Components. In F. D. Ceuninck, M. Sabatini & P. Pastoureau (Eds.), *Cartilage and Osteoarthritis : Volume 2: Structure and In Vivo Analysis* (Vol. 2, pp. 127-156): Humana Press.
- Hoemann, C. D. (2004). Molecular and biochemical assays of cartilage components. In F. D. C. Massimo Sabatini, Philippe Pastoureau (Ed.), *Cartilage and osteoarthritis* (Vol. 2, pp. 127-156). Totowa, New Jersey, United States of America: Springer.

- Huang, G., Wang, S., He, X., Zhang, X., Lu, T. J., & Xu, F. (2013). Helical spring template fabrication of cell-laden microfluidic hydrogels for tissue engineering. *Biotechnology and bioengineering*, *110*(3), 980-989.
- Huang, G., Zhang, X., Xiao, Z., Zhang, Q., Zhou, J., Xu, F., & Lu, T. J. (2012). Cell-encapsulating microfluidic hydrogels with enhanced mechanical stability. *Soft Matter*, *8*(41), 10687-10694. doi: 10.1039/C2SM26126J
- Huang, S. J., & Edelman, P. G. (1995). An overview of biodegradable polymers and biodegradation of polymers *Degradable Polymers* (pp. 18-28): Springer.
- Huber, M., Trattnig, S., & Lintner, F. (2000). Anatomy, biochemistry, and physiology of articular cartilage. *Investigative radiology*, *35*(10), 573.
- Hughes, S. W. (2005). Archimedes revisited: a faster, better, cheaper method of accurately measuring the volume of small objects. *Physics education*, *40*(5), 468. doi: 10.1088/0031-9120/40/5/001
- Hunter, W. (1809). On the structure and diseases of articular cartilage. In G. S. Charles Hutton, Richard Pearson (Ed.), *The Philosophical Transactions of the Royal Society of London, from Their Commencement in 1665 to the Year 1800* (Vol. 3, pp. 690-691).
- Hunziker, J. (1990). Articular cartilage: composition, structure, response to injury, and methods of facilitating repair. *Articular cartilage and knee joint function: basic science and arthroscopy*, 19.
- Hutmacher, D. W. (2000). Scaffolds in tissue engineering bone and cartilage. *Biomaterials*, *21*(24), 2529-2543. doi: 10.1016/S0142-9612(00)00121-6
- Hyc, A., Malejczyk, J., Osiecka, A., & Moskalewski, S. (1997). Immunological response against allogeneic chondrocytes transplanted into joint surface defects in rats. *Cell Transplantation*, *6*(2), 119-124. doi: 10.1016/S0963-6897(96)00254-0
- Izadifar, Z., Chen, X., & Kulyk, W. (2012). Strategic design and fabrication of engineered scaffolds for articular cartilage repair. *Journal of Functional Biomaterials*, *3*(4), 799-838. doi: 10.3390/jfb3040799
- Jacobs, J. (1965). Patellar graft for severely depressed comminuted fractures of the lateral tibial condyle. *The Journal of Bone and Joint Surgery*, *47*(4), 842.
- Jarman-Smith, M. L., Bodamyali, T., Stevens, C., Howell, J. A., Horrocks, M., & Chaudhuri, J. B. (2004). Porcine collagen crosslinking, degradation and its capability for fibroblast adhesion and proliferation. *Journal of Materials Science: Materials in Medicine*, *15*(8), 925-932. doi: 10.1023/B:JMSM.0000036281.47596.cc
- Jeffery, A., Blunn, G., Archer, C., & Bentley, G. (1991). Three-dimensional collagen architecture in bovine articular cartilage. *Journal of Bone & Joint Surgery, British Volume*, *73*(5), 795-801.

- Jeney, F., Bazsó-Dombi, E., Oravec, K., Szabó, J., & Zs-Nagy, I. (2000). Cytochemical studies on the fibroblast-preadipocyte relationships in cultured fibroblast cell lines. *Acta Histochemica*, 102(4), 381-389.
- Johnson, T., Bahrapourian, R., Patel, A., & Mequanint, K. (2010). Fabrication of highly porous tissue-engineering scaffolds using selective spherical porogens. *Bio-Medical Materials and Engineering*, 20(2), 107-118. doi: 10.3233/BME-2010-0621.
- Johnstone, B., Yoo, J., & Stewart, M. (2008). Cell Sources for Cartilage Tissue Engineering. *European Cells and Materials*, 16(2), 40.
- Jus, S., Stachel, I., Schloegl, W., Pretzler, M., Friess, W., Meyer, M., . . . Guebitz, G. (2011). Cross-linking of collagen with laccases and tyrosinases. *Materials Science and Engineering: C*, 31(5), 1068-1077. doi: 10.1016/j.msec.2011.03.007
- Kasemkijwattana, C., Kesprayura, S., & Chanlalit, C. (2009). Autologous Chondrocytes Implantation for Traumatic Cartilage Defects of the Knee. *J Med Assoc Thai*, 92(5), 648-653.
- Kavalkovich, K. W. B., R ; Murphy, J M. ; Barry, F P. . (2000). *Effect of cell density on chondrogenic differentiation of mesenchymal stem cells*. Paper presented at the 46th Annual Meeting, Orthopaedic Research Society, Orlando, Florida. <http://www.ors.org/Transactions/46/0975.pdf>
- Kim, S., Cho, J., Hong, M., Rhie, J., & Yoon, H. (2008). Induction of chondrogenic differentiation in cultured fibroblasts isolated from the inferior turbinate. *Otolaryngology-Head and Neck Surgery*, 139(1), 143-148.
- Kimuli, M., Eardley, I., & Southgate, J. (2004). In vitro assessment of decellularized porcine dermis as a matrix for urinary tract reconstruction. *BJU international*, 94(6), 859-866. doi: 10.1111/j.1464-410X.2004.05047.x
- Kipnes, J., Carlberg, A., Loredó, G., Lawler, J., Tuan, R., & Hall, D. (2003). Effect of cartilage oligomeric matrix protein on mesenchymal chondrogenesis< i> in vitro</i>. *Osteoarthritis and Cartilage*, 11(6), 442-454. doi: 10.1016/S1063-4584(03)00055-4
- Kissa, E. (1999). *Dispersions: Characterization, Testing, and Measurement*: CRC Press.
- Kong, J., & Yu, S. (2007). Fourier transform infrared spectroscopic analysis of protein secondary structures. *Acta biochimica et biophysica Sinica*, 39(8), 549-559. doi: 10.1111/j.1745-7270.2007.00320.x
- Kyriacos A. Athanasiou, E. M. D., Jerry C. Hu, Grayson D. DuRaine, A. Hari Reddi. (2013). Perspectives on the transitional aspects of articular cartilage biology *Articular Cartilage* (Vol. 1, pp. 286). London, UK: CRC Press.
- Lane, J., Brighton, C., Ottens, H., & Lipton, M. (1977). Joint resurfacing in the rabbit using an autologous osteochondral graft. *The Journal of Bone and Joint Surgery*, 59(2), 218.

- Lee, C., Grodzinsky, A., & Spector, M. (2001). The effects of cross-linking of collagen-glycosaminoglycan scaffolds on compressive stiffness, chondrocyte-mediated contraction, proliferation and biosynthesis. *Biomaterials*, 22(23), 3145-3154. doi: 10.1016/S0142-9612(01)00067-9
- Lee, J., Edwards, H., Pereira, C., & Samii, S. (1996). Crosslinking of tissue-derived biomaterials in 1-ethyl-3-(3-dimethylaminopropyl)-carbodiimide (EDC). *Journal of Materials Science: Materials in Medicine*, 7(9), 531-541. doi: 10.1007/BF00122176
- Lefebvre, V., Huang, W., Harley, V. R., Goodfellow, P. N., & de Crombrughe, B. (1997). SOX9 is a potent activator of the chondrocyte-specific enhancer of the pro alpha1 (II) collagen gene. *Molecular and Cellular Biology*, 17(4), 2336-2346.
- Lefebvre, V., Li, P., & de Crombrughe, B. (1998). A new long form of Sox5 (L-Sox5), Sox6 and Sox9 are coexpressed in chondrogenesis and cooperatively activate the type II collagen gene. *The EMBO journal*, 17(19), 5718-5733. doi: 10.1093/emboj/17.19.5718
- Liu, Z., Xu, J., Colvin, J., & Ornitz, D. (2002). Coordination of chondrogenesis and osteogenesis by fibroblast growth factor 18. *Genes & development*, 16(7), 859. doi: 10.1101/gad.965602
- Lodish, H., Berk, A., Zipursky, S. L., Matsudaira, P., Baltimore, D., & Darnell, J. (2000). *Collagen: the fibrous proteins of the matrix* (4th ed.).
- Longobardi, L., O'Rear, L., Aakula, S., Johnstone, B., Shimer, K., Chytil, A., . . . Spagnoli, A. (2006). Effect of IGF I in the Chondrogenesis of Bone Marrow Mesenchymal Stem Cells in the Presence or Absence of TGF Signaling. *Journal of Bone and Mineral Research*, 21(4), 626-636.
- Lorenz, K., Sicker, M., Schmelzer, E., Rupf, T., Salvetter, J., Schulz-Siegmund, M., & Bader, A. (2008). Multilineage differentiation potential of human dermal skin-derived fibroblasts. *Experimental dermatology*, 17(11), 925-932.
- Lu, L., Zhu, X., Valenzuela, R. G., Currier, B. L., & Yaszemski, M. J. (2001). Biodegradable polymer scaffolds for cartilage tissue engineering. *Clinical Orthopaedics and Related Research*, 391, S251-S270.
- Mahmoudifar, N., & Doran, P. M. (2012). Chondrogenesis and cartilage tissue engineering: the longer road to technology development. *TRENDS in Biotechnology*, 30(3), 166-176. doi: 10.1016/j.tibtech.2011.09.002
- Mauck, R., Wang, C.-B., Oswald, E., Ateshian, G., & Hung, C. (2003a). The role of cell seeding density and nutrient supply for articular cartilage tissue engineering with deformational loading. *Osteoarthritis and Cartilage*, 11(12), 879-890. doi: 10.1016/j.joca.2003.08.006
- Mauck, R., Wang, C., Oswald, E., Ateshian, G., & Hung, C. (2003b). The role of cell seeding density and nutrient supply for articular cartilage tissue engineering with deformational loading. *Osteoarthritis and Cartilage*, 11(12), 879-890.

- McDevitt, C. A. (1973). Biochemistry of articular cartilage: Nature of proteoglycans and collagen of articular cartilage and their role in aging and in osteoarthritis. *Ann Rheum Dis*, 32(364).
- McPherson, J. M., & Tubo, R. Articular Cartilage Injury. In R. P. Lanza, R. Langer & J. Vacanti (Eds.), *Principles of Tissue Engineering* (2nd ed., pp. 697-709): Academic Press.
- Mendoza-Novelo, B., Mata-Mata, J. L., Vega-González, A., Cauich-Rodríguez, J. V., & Marcos-Fernández, Á. (2014). Synthesis and characterization of protected oligourethanes as crosslinkers of collagen-based scaffolds. *Journal of Materials Chemistry B*, 2(19), 2874-2882. doi: 10.1039/c3tb21832e
- Mizuno, S., & Glowacki, J. (1996). Chondroinduction of human dermal fibroblasts by demineralized bone in three-dimensional culture. *Experimental cell research*, 227(1), 89-97.
- Mizuno, S., & Glowacki, J. (1996). Three-dimensional composite of demineralized bone powder and collagen for in vitro analysis of chondroinduction of human dermal fibroblasts. *Biomaterials*, 17, 1819-1825.
- Mizuno, S., & Glowacki, J. (2005). Low oxygen tension enhances chondroinduction by demineralized bone matrix in human dermal fibroblasts in vitro. *Cells Tissues Organs*, 180(3), 151-158.
- Mizuno, S., Lycette, C., Quinto, C., & Glowacki, J. (1992). A Collagen/DBP sponge system designed for in vitro analysis of chondroinduction.
- Moore, E., Bendele, A., Thompson, D., Littau, A., Waggle, K., Reardon, B., & Ellsworth, J. (2005). Fibroblast growth factor-18 stimulates chondrogenesis and cartilage repair in a rat model of injury-induced osteoarthritis. *Osteoarthritis and Cartilage*, 13(7), 623-631. doi: 10.1016/j.joca.2005.03.003
- Moradi, A., Dalilottojari, A., Pinguan-Murphy, B., & Djordjevic, I. (2013). Fabrication and characterization of elastomeric scaffolds comprised of a citric acid-based polyester/hydroxyapatite microcomposite. *Materials & Design*, 50, 446-450. doi: 10.1016/j.matdes.2013.03.026
- Moradi, A., Pramanik, S., Ataollahi, F., Abdul-Khalil, A., Kamarul, T., & Pinguan-Murphy, B. (2014). A comparison study of different physical treatments on cartilage matrix derived porous scaffolds for tissue engineering applications. *Science and Technology of Advanced Materials*. doi: 10.1088/1468-6996/15/6/065001
- Moradi, A., Pramanik, S., Ataollahi, F., Kamarul, T., & Pinguan-Murphy, B. (2014). Archimedes revisited: computer assisted micro-volumetric modification of the liquid displacement method for porosity measurement of highly porous light materials. *Analytical Methods*, 6(12), 4396-4401. doi: 10.1039/C4AY00666F
- Moskalewski, S., Hyc, A., & Osiecka-Iwan, A. (2002). Immune response by host after allogeneic chondrocyte transplant to the cartilage. *Microscopy Research and Technique*, 58(1), 3-13. doi: 10.1002/jemt.10110

- Moutos, F. T., & Guilak, F. (2008). Composite scaffolds for cartilage tissue engineering. *Biorheology*, *45*(3), 501-512. doi: 10.3233/BIR-2008-0491
- Murphy, C. M., Haugh, M. G., & O'Brien, F. J. (2010). The effect of mean pore size on cell attachment, proliferation and migration in collagen–glycosaminoglycan scaffolds for bone tissue engineering. *Biomaterials*, *31*(3), 461-466. doi: 10.1016/j.biomaterials.2009.09.063
- National Library of Medicine. (2014a, June 23, 2014). ACAN. *Genes*. from <http://ghr.nlm.nih.gov/gene/ACAN>
- National Library of Medicine. (2014b, June 23, 2014). COL1A1. *Genes*. Retrieved June 29, 2014, June 23, 2014, from <http://ghr.nlm.nih.gov/gene/COL1A1>
- National Library of Medicine. (2014c). COL1A2. Available from National Library of Medicine Retrieved June 29, 2014, from Genetics Home Reference <http://ghr.nlm.nih.gov/gene/COL1A2>
- National Library of Medicine. (2014d, June 23, 2014). COL2A1. *Genes*. 39/06/2014, from <http://ghr.nlm.nih.gov/gene/COL2A1>
- National Library of Medicine. (2014e). PRG4. *Genes*. Retrieved 29/06/2014, 2014, from <http://ghr.nlm.nih.gov/gene/PRG4>
- Ng, L.-J., Wheatley, S., Muscat, G. E., Conway-Campbell, J., Bowles, J., Wright, E., . . . Koopman, P. (1997). SOX9 binds DNA, activates transcription, and coexpresses with type II collagen during chondrogenesis in the mouse. *Developmental biology*, *183*(1), 108-121. doi: 10.1006/dbio.1996.8487
- Nishimura, K., Solchaga, L., Caplan, A., Yoo, J., Goldberg, V., & Johnstone, B. (1999). Chondroprogenitor cells of synovial tissue. *Arthritis & Rheumatism*, *42*(12), 2631-2637.
- O'Brien, J., Wilson, I., Orton, T., & Pognan, F. (2003). Investigation of the Alamar Blue (resazurin) fluorescent dye for the assessment of mammalian cell cytotoxicity. *European Journal of Biochemistry*, *267*(17), 5421-5426.
- Österreicher, C. H., Penz-Österreicher, M., Grivennikov, S. I., Guma, M., Koltsova, E. K., Datz, C., . . . Brenner, D. A. (2011). Fibroblast-specific protein 1 identifies an inflammatory subpopulation of macrophages in the liver. *Proceedings of the National Academy of Sciences*, *108*(1), 308-313. doi: 10.1073/pnas.1017547108
- Outani, H., Okada, M., Yamashita, A., Nakagawa, K., Yoshikawa, H., & Tsumaki, N. (2013). Direct induction of chondrogenic cells from human dermal fibroblast culture by defined factors. *PloS one*, *8*(10), e77365. doi: 10.1371/journal.pone.0077365
- Page, R. L., Ambady, S., Holmes, W. F., Vilner, L., Kole, D., Kashpur, O., . . . Dominko, T. (2009). Induction of stem cell gene expression in adult human fibroblasts without transgenes. *Cloning and Stem Cells*, *11*(3), 417-426. doi: 10.1089/clo.2009.0015

- Parenteau-Bareil, R., Gauvin, R., & Berthod, F. (2010). Collagen-based biomaterials for tissue engineering applications. *Materials*, 3(3), 1863-1887. doi: 10.3390/ma3031863
- Park, H., & Miwa, K. (2003). X-ray computed tomography for micro porosity in AZ 91 D alloy. *Materials Transactions*, 44(11), 2326-2333.
- Park, S., Hung, C., & Ateshian, G. (2004). Mechanical response of bovine articular cartilage under dynamic unconfined compression loading at physiological stress levels. *Osteoarthritis and Cartilage*, 12(1), 65-73. doi: 10.1016/j.joca.2003.08.005
- Parrilli, A. F., M.; Salamanna, F.; Veronesi, F.; Giardino, R. (2010). Evaluation of the porosity of biomaterials with micro-CT. *Journal of Applied Biomaterials & Biomechanics*, 8(2), 120.
- Peinador, R. I., Calvo, J. I., ToVinh, K., Thom, V., Prádanos, P., & Hernández, A. (2011). Liquid-liquid displacement porosimetry for the characterization of virus retentive membranes. *Journal of Membrane Science*, 372(1), 366-372. doi: 10.1016/j.memsci.2011.02.022
- Pesch, K. L., & Simmert, U. (1929). Combined assays for lactose and galactose by enzymatic reactions. *Milchw Forsch*, 8, 551.
- Peterson, L., Minas, T., Brittberg, M., & Lindahl, A. (2003). Treatment of osteochondritis dissecans of the knee with autologous chondrocyte transplantation: results at two to ten years. *The Journal of Bone and Joint Surgery*, 85(Supplement 2), 17.
- Petra, M., Anastassopoulou, J., Theologis, T., & Theophanides, T. (2005). Synchrotron micro-FT-IR spectroscopic evaluation of normal paediatric human bone. *Journal of Molecular Structure*, 733(1), 101-110. doi: 10.1016/j.molstruc.2004.07.041
- Powers, C., McLeskey, S., & Wellstein, A. (2000). Fibroblast growth factors, their receptors and signaling. *Endocrine-related cancer*, 7(3), 165-197.
- Pramanik, S., Pingguan-Murphy, B., & Abu-Osman, N. A. (2012). Progress of key strategies in development of electrospun scaffolds: bone tissue. *Science and Technology of Advanced Materials*, 13(4), 043002. doi: 10.1088/1468-6996/13/4/043002
- Pridie, K. (1959). A method of resurfacing osteoarthritic knee joints. *J Bone Joint Surg Br*, 41(3), 618-619.
- R.J. Gonzalez, J. B. T. (2001). Evaluation of hepatic subcellular fractions for Alamar blue and MTT reductase activity, *Toxicology In Vitro*, pp. 257-259.
- Rampersad, S. N. (2012). Multiple Applications of Alamar Blue as an Indicator of Metabolic Function and Cellular Health in Cell Viability Bioassays. *Sensors*, 12(12), 12347-12360. doi: 10.3390/s120912347
- Ratner, B. D. (2004). *Biomaterials science: an introduction to materials in medicine*: Academic press.

- Ribeiro, A., Barbaglio, A., Oliveira, M., Santos, R., Coelho, A., Ribeiro, C., . . . Barbosa, M. (2012). Correlations Between the Biochemistry and Mechanical States of a Sea-Urchin Ligament: A Mutable Collagenous Structure. *Biointerphases*, 7(1-4), 1-15. doi: 10.1007/s13758-012-0038-6
- Riekstina, U., Muceniece, R., Cakstina, I., Muiznieks, I., & Ancans, J. (2008). Characterization of human skin-derived mesenchymal stem cell proliferation rate in different growth conditions. *Cytotechnology*, 58(3), 153-162.
- Rittié, L., & Fisher, G. (2005). Isolation and culture of skin fibroblasts. *Methods in molecular medicine*, 117, 83.
- Rodríguez-Baeza, M., Neira, C., & Aguilera, J. (2003). Thermogravimetric study of the formation of cross-linked structures in the synthesis of poly (methylsiloxane). *Journal of the Chilean Chemical Society*, 48(2), 75-77. doi: 10.4067/S0717-97072003000200013
- Rowland, C. R., Lennon, D. P., Caplan, A. I., & Guilak, F. (2013). The effects of crosslinking of scaffolds engineered from cartilage ECM on the chondrogenic differentiation of MSCs. *Biomaterials*, 34(2013), 5802-5812. doi: 10.1016/j.biomaterials.2013.04.027
- Rutherford, R. B., Moalli, M., Franceschi, R. T., Wang, D., Gu, K., & Krebsbach, P. H. (2002). Bone morphogenetic protein-transduced human fibroblasts convert to osteoblasts and form bone in vivo. *Tissue engineering*, 8(3), 441-452.
- Saalbach, A., Anderegg, U., Bruns, M., Schnabel, E., Herrmann, K., & Hausteiner, U. F. (1996). Novel fibroblast-specific monoclonal antibodies: properties and specificities. *Journal of investigative dermatology*, 106(6), 1314-1319. doi: 10.1111/1523-1747.ep12349035
- Saalbach, A., Aust, G., Hausteiner, U., Herrmann, K., & Anderegg, U. (1997). The fibroblast-specific MAb AS02: a novel tool for detection and elimination of human fibroblasts. *Cell and tissue research*, 290(3), 593-599.
- Saarakkala, S., Rieppo, L., Rieppo, J., & Jurvelin, J. (2010). Fourier transform infrared (FTIR) microspectroscopy of immature, mature and degenerated articular cartilage. In J. D. A. Mendez-Vilas (Ed.), *MICROSCOPY: SCIENCE, TECHNOLOGY, APPLICATIONS AND EDUCATION* (4 ed., Vol. 4, pp. 403-414): Formatex Research Center.
- Sanchez-Adams, J., & Athanasiou, K. A. (2012). Dermis isolated adult stem cells for cartilage tissue engineering. *Biomaterials*, 33(1), 109-119. doi: 10.1016/j.biomaterials.2011.09.038
- Schulz Torres, D., M Freyman, T., Yannas, I. V., & Spector, M. (2000). Tendon cell contraction of collagen-GAG matrices in vitro: Effect of cross-linking. *Biomaterials*, 21(15), 1607-1619. doi: 10.1016/S0142-9612(00)00051-X
- Seal, B., Otero, T., & Panitch, A. (2001). Polymeric biomaterials for tissue and organ regeneration. *Materials Science and Engineering: R: Reports*, 34(4), 147-230. doi: 10.1016/S0927-796X(01)00035-3

- Shanmugarajan, T., Kim, B.-S., Lee, H., & Im, G.-I. (2011). Growth factors and signaling pathways in the chondrogenic differentiation of mesenchymal stem cells. *Tissue Eng Regen Med*, 8, 292.
- Sharif, S., DiMemmo, L., Davidovich, M., & Sarsfield, B. Applicability of Specific Surface Area Determination on Pharmaceuticals by Inverse Gas Chromatography. *The Open-Access Journal for the Basic Principles of Diffusion Theory, Experiment and Application*.
- Shelbourne, K., Jari, S., & Gray, T. (2003). Outcome of untreated traumatic articular cartilage defects of the knee: a natural history study. *The Journal of Bone and Joint Surgery*, 85(Supplement 2), 8.
- Shirasawa, S., Sekiya, I., Sakaguchi, Y., Yagishita, K., Ichinose, S., & Muneta, T. (2006). In vitro chondrogenesis of human synovium derived mesenchymal stem cells: Optimal condition and comparison with bone marrow derived cells. *Journal of cellular biochemistry*, 97(1), 84-97.
- Sommar, P. (2010). Differentiation of human dermal fibroblasts and applications in tissue engineering.
- Strehl, R., Schumacher, K., de Vries, U., & Minuth, W. W. (2002). Proliferating cells versus differentiated cells in tissue engineering. *Tissue engineering*, 8(1), 37-42. doi: 10.1089/107632702753503036
- Strutz, F., Okada, H., Lo, C. W., Danoff, T., Carone, R. L., Tomaszewski, J. E., & Neilson, E. G. (1995). Identification and characterization of a fibroblast marker: FSP1. *The Journal of cell biology*, 130(2), 393-405. doi: 10.1083/jcb.130.2.393
- Szepes, A., Kovács, J., & Szabóné, R. P. (2005). [Use of mercury porosimetry, assisted by nitrogen adsorption in the investigation of the pore structure of tablets]. *Acta Pharmaceutica Hungarica*, 76(3), 119-125.
- Taipaleenmäki, H. (2010). *Factors Regulating Chondrogenic Differentiation*. (PhD), Annales Universitatis Turkuensis D 938, Annales Universitatis Turkuensis D 938. Retrieved from <http://www.doria.fi/handle/10024/66244>
- Thisse, B., & Thisse, C. (2005). Functions and regulations of fibroblast growth factor signaling during embryonic development. *Developmental biology*, 287(2), 390-402. doi: 10.1016/j.ydbio.2005.09.011
- Topisirovic, I., & Sonenberg, N. (2014). Distinctive tRNA Repertoires in Proliferating versus Differentiating Cells. *Cell*, 158(6), 1238-1239. doi: 10.1016/j.cell.2014.08.031
- Vaheri, A., Ruoslahti, E., Linder, E., Wartiovaara, J., Keski-Oja, J., Kuusela, P., & Saksela, O. (1976). Fibroblast surface antigen (SF): molecular properties, distribution in vitro and in vivo, and altered expression in transformed cells. *Journal of Supramolecular Structure*, 4(1), 63-70. doi: 10.1002/jss.400040107
- Vergés, E., Ayala, D., Grau, S., & Tost, D. (2008). Virtual porosimeter. *Computer-Aided Design and Applications*, 5(1-4), 557-564. doi: 10.3722/cadaps.2008.557-564

- Voytik-Harbin, S. L., Brightman, A. O., Waisner, B., Lamar, C. H., & Badylak, S. F. (1998). Application and evaluation of the alamarBlue assay for cell growth and survival of fibroblasts. *In Vitro Cellular & Developmental Biology-Animal*, 34(3), 239-246.
- Weadock, K. S., Miller, E. J., Bellincampi, L. D., Zawadsky, J. P., & Dunn, M. G. (1995). Physical crosslinking of collagen fibers: comparison of ultraviolet irradiation and dehydrothermal treatment. *Journal of Biomedical Materials Research*, 29(11), 1373-1379.
- Weadock, K. S., Miller, E. J., Keuffel, E. L., & Dunn, M. G. (1996). Effect of physical crosslinking methods on collagen-fiber durability in proteolytic solutions. *Journal of Biomedical Materials Research*, 32(2), 221-226. doi: 10.1002/(SICI)1097-4636(199610)32:2<221::AID-JBM11>3.0.CO;2-M
- Weadock, K. S., Miller, E. J., Keuffel, E. L., & Dunn, M. G. (1996). Effect of physical crosslinking methods on collagen-fiber durability in proteolytic solutions. *Journal of Biomedical Materials Research*, 32(2), 221-226. doi: 10.1002/(SICI)1097-4636(199610)32:2<221::AID-JBM11>3.0.CO;2-M
- Westermarck, S. (2000) Use of mercury porosimetry and nitrogen adsorption in characterisation of the pore structure of mannitol and microcrystalline cellulose powders, granules and tablets. Helsinki: University of Helsinki Helsinki, Finland.
- Westermarck, S., Juppo, A. M., Kervinen, L., & Yliruusi, J. (1998). Pore structure and surface area of mannitol powder, granules and tablets determined with mercury porosimetry and nitrogen adsorption. *European Journal of Pharmaceutics and Biopharmaceutics*, 46(1), 61-68. doi: 10.1016/S0939-6411(97)00169-0
- WHO/UNAIDS. (2007). Male circumcision: Global trends and determinants of prevalence, safety and acceptability.
- Wright, E., Hargrave, M. R., Christiansen, J., Cooper, L., Kun, J., Evans, T., . . . Koopman, P. (1995). The Sry-related gene Sox9 is expressed during chondrogenesis in mouse embryos. *Nature Genetics*, 9(1), 15-20. doi: 10.1038/ng0195-15
- Xu, R., Rao, H., Zhu, Y., & Chai, B. (1993). Effects of osteogenesis on dermal fibroblasts cultured in vitro. *Chinese medical journal*, 106(11), 825.
- Yang, Q., Peng, J., Guo, Q., Huang, J., Zhang, L., Yang, F., . . . Lu, S. (2008). A cartilage ECM-derived 3-D porous acellular matrix scaffold for in vivo cartilage tissue engineering with PKH26-labeled chondrogenic bone marrow-derived mesenchymal stem cells. *Biomaterials*, 29(2008), 2378-2387. doi: 10.1016/j.biomaterials.2008.01.037
- Yang, Q., Peng, J., Guo, Q., Huang, J., Zhang, L., Yao, J., . . . Wang, A. (2008). A cartilage ECM-derived 3-D porous acellular matrix scaffold for in vivo cartilage tissue engineering with PKH26-labeled chondrogenic bone marrow-derived mesenchymal stem cells. *Biomaterials*, 29(15), 2378-2387. doi: 10.1016/j.biomaterials.2008.01.037

- Yang, Z., Shi, Y., Wei, X., He, J., Yang, S., Dickson, G., . . . Li, G. (2009). Fabrication and Repair of Cartilage Defects with a Novel Acellular Cartilage Matrix Scaffold. *Tissue Engineering Part C: Methods*, 16(5), 865-876. doi: 10.1089/ten.TEC.2009.0444.
- Yang, Z., & Xiaofeng, P. (2007). Micro-CT scanning analysis for inner structure of porous media. *Heat Transfer—Asian Research*, 36(4), 208-214. doi: 10.1002/htj.20155
- Yates, K., & Glowacki, J. (2003). Gene expression changes in an in vitro model of chondroinduction: a comparison of two methods. *Wound Repair and Regeneration*, 11(5), 386-392.
- Yearbook, F. S. (2012). Statistical Yearbook of the Food And Agriculture. In S. D. (FAOSTAT) (Ed.): Food and Agriculture Organization of the United Nations.
- Yu, H. G., Chung, H., Yu, Y. S., Seo, J. M., & Heo, J. W. (2003). A new rapid and non-radioactive assay for monitoring and determining the proliferation of retinal pigment epithelial cells. *Korean Journal of Ophthalmology*, 17(1), 29-34.
- Zaleskas, J. M., Kinner, B., Freyman, T. M., Yannas, I. V., Gibson, L. J., & Spector, M. (2004). Contractile forces generated by articular chondrocytes in collagen-glycosaminoglycan matrices. *Biomaterials*, 25(7), 1299-1308. doi: 10.1016/j.biomaterials.2003.08.005
- Zhao, Q., Eberspaecher, H., Lefebvre, V., & de Crombrughe, B. (1997). Parallel expression of Sox9 and Col2a1 in cells undergoing chondrogenesis. *Developmental dynamics*, 209(4), 377-386. doi: 10.1002/(SICI)1097-0177(199708)209:4<377
- Zheng, X.-F., Lu, S.-B., Zhang, W.-G., Liu, S.-Y., Huang, J.-X., & Guo, Q.-Y. (2011). Mesenchymal stem cells on a decellularized cartilage matrix for cartilage tissue engineering. *Biotechnology and Bioprocess Engineering*, 16(3), 593-602. doi: 10.1007/s12257-010-0348-9
- Zhou, S., Yates, K., Eid, K., & Glowacki, J. (2005). Demineralized bone promotes chondrocyte or osteoblast differentiation of human marrow stromal cells cultured in collagen sponges. *Cell and tissue banking*, 6(1), 33-44.

LIST OF PUBLICATIONS

- Moradi, A., Dalilottojari, A., Pinguan-Murphy, B., & Djordjevic, I. (2013). Fabrication and characterization of elastomeric scaffolds comprised of a citric acid-based polyester/hydroxyapatite microcomposite. *Materials & Design*, 50, 446-450. doi: 10.1016/j.matdes.2013.03.026
- Moradi, A., Pramanik, S., Ataollahi, F., Kamarul, T., & Pinguan-Murphy, B. (2014). Archimedes revisited: computer assisted microvolumetric modification of liquid displacement method for porosity measurement of highly porous light materials. *Analytical Methods*. doi: 10.1039/C4AY00666F
- Moradi, A., Pramanik, S., Ataollahi, F., Abdul Khalil, A., Kamarul, T., & Pinguan-Murphy, B. (2014). A Comparison Study of Different Physical Treatments on Cartilage Matrix Derived Porous Scaffolds for Tissue Engineering Applications. *Science and Technology of Advanced Materials*. doi: 10.1039/C4AY00666F
- Ataollahi F, Pramanik S, Moradi A, Dalilottojari A, Pinguan-Murphy B, Abas W, et al. Endothelial cell responses in terms of adhesion, proliferation, and morphology to stiffness of polydimethylsiloxane elastomer substrates. *Journal of Biomedical Materials Research Part A*. 2014.
- Ataollahi F, Pinguan-Murphy B, Moradi A, Bakar Wan Abas WA, Chua KH, Abu Osman NA. New method for the isolation of endothelial cells from large vessels. *Cytotherapy*. 2014.



Short Communication

Fabrication and characterization of elastomeric scaffolds comprised of a citric acid-based polyester/hydroxyapatite microcomposite



Ali Moradi, Adel Dalilottojari, Belinda Pinguuan-Murphy, Ivan Djordjevic*

Department of Biomedical Engineering, Faculty of Engineering, University of Malaya, Kuala Lumpur 50603, Malaysia

ARTICLE INFO

Article history:

Received 1 November 2012

Accepted 9 March 2013

Available online 21 March 2013

ABSTRACT

In this paper we describe an effective technical route for the production of porous scaffolds from microcomposite material consistent of citric acid-based polyester elastomer and hydroxyapatite microparticles with potential use in tissue engineering applications. Fabricated scaffolds were characterized by field emission electron microscopy, Fourier-transform infra-red spectroscopy, thermal gravimetric analysis and mechanical tests. We demonstrate that the chemical composition, scaffold morphology, mechanical integrity and porosity of the produced microcomposite scaffolds are strongly affected by variation of the initial hydroxyapatite concentration in the mineral-polymer mixture during the fabrication process. This polyester/mineral scaffold exhibits versatility in compression modulus and strength in the range of 21.72–33.25 kPa and 49.92–101.48 kPa respectively, corresponding to the hydroxyapatite concentration in the composite (10–30 wt.%).

© 2013 Elsevier Ltd. All rights reserved.

1. Introduction

The role of a synthetic scaffold in the engineering of specific tissues is to support cellular function including the facilitation of molecular and mechanical signaling processes towards appropriate tissue regeneration [1,2]. An elastomeric polyester such as poly (1,8-octanediol-co-citrate) (POC) has recently been presented as a prominent new material for scaffold-guided tissue engineering [2–5]. The material is elastic, hydrophilic, and the POC porous scaffolds biologically degrade with minimal immunological response from the host tissue [5]. Apart from soft tissue engineering applications, POC has also been fabricated into a tough biodegradable POC–hydroxyapatite (HA) composite material for bone healing procedures [6]. The toughness, biodegradability and biological activity are strongly influenced by the concentration of HA within the composite material. This important feature of POC–HA composite is highly desirable for tissue engineering materials [6].

Orthopaedic surgeons often use degradable tissue fixation devices such as bone screws that are made of synthetic biodegradable polymers [6–10]. Qiu et al. have reported a novel approach to process microparticles of bone mineral HA and POC into bioceramic–polymer composite for bone screw fabrication [6]. Due to its reported biocompatibility and controllable degradation rates (a few months to a year), POC has potential for bone fixation applications [8]. Another important advantage is that the POC–HA

composite can be fabricated with controllable mechanical properties. In contrast to pure POC that is a soft and resilient elastic material (tensile Young's modulus ~2 MPa) [2,3], the POC–HA composite expressed controllable tensile modulus in the range of 20–300 MPa corresponding to the HA concentration in the composite (40–65 wt.%) [6]. Gross examination showed that the POC–HA implant integrated well with the surrounding cartilage and the bone morphology around the implant was similar to normal bone [6]. A significant number of research publications describe fabrication and performance of composite scaffolds produced from synthetic biodegradable polymers and HA particles [11–16]. Although POC/HA composite (with appropriate polymer/mineral composition) have shown promising results for bone fixation devices [6–10], so far no attempt has been made to produce porous tissue engineering scaffolds from the POC–HA composite.

Polymeric materials design presents an important role in biomaterials development [17]. In view of the potential uses of POC in tissue engineering applications, we report a novel POC–HA composite porous and elastic scaffold with controllable mechanical properties. HA concentrations are designed to retain the elasticity of the scaffolding material and optimal inter-connected pore size formation, with a final aim of providing a simple but elegant method to control the final properties of the scaffold [18]. Since the biological activity, osteoconductivity and osteoinductivity of HA bioceramics are well defined in clinical and laboratory practice, the work presented in this paper offers a better understanding of design parameters for production of bone tissue engineering materials.

* Corresponding author. Tel.: +60 3 7967 7616; fax: +60 3 7967 4579.
E-mail address: ivan.djordjevic@um.edu.my (I. Djordjevic).

Archimedes revisited: computer assisted micro-volumetric modification of the liquid displacement method for porosity measurement of highly porous light materials

Cite this: DOI: 10.1039/c4ay00666f

Ali Moradi,^{*a} Sumit Pramanik,^{*a} Forough Ataollahi,^{*a} Tunku Kamarul^{*b}
and Belinda Pinguan-Murphy^{*a}Received 16th March 2014
Accepted 11th April 2014

DOI: 10.1039/c4ay00666f

www.rsc.org/methods

Precise and accurate porosity measurement is essential for characterization of porous materials. Considering Archimedes' principle based liquid displacement methods of measuring porosity we have developed an excellent modified micro-volumetric method of porosity measurement. Changes in the liquid level in a glass pipette after immersing and also removing the porous sample were recorded by using a digital camera and analysed by ImageJ® software. Results of porosity measurement through a micro-volumetric method were compared with micro-CT results. Bland-Altman analysis showed a much higher precision and accuracy for our micro-volumetric method (bias = -0.023, CI:]-0.459, 0.413], SD = 1.96 σ) compared to the micro-CT method (bias = 6.075, CI:]-20.993, 33.142], SD = 1.96 σ). Our highly precise and accurate micro-volumetric method of porosity measurement is particularly applicable to small ultra-light highly porous materials.

Introduction

Porous materials find widespread applications almost in all the areas, covering engineering to medicine.¹⁻⁴ For these applications, the porosity and pore size have significant effects on different properties of porous materials. For instance, porosity is a highly determinant factor in fabrication of three-dimensional (3D) scaffolds in tissue engineering to mimic the extracellular matrix as templates onto which cells of various tissues attach, proliferate, move and function.^{4,5} Pore density is important in fabrication of synthetic materials used in various applications such as filtration, bioreactors, analytical devices, prostheses, *etc.*⁶⁻⁸ Therefore, it is essential to characterize the porosity of these materials precisely.

Due to the importance, various methods have been developed to characterize the porosity, such as BET, Archimedes' principle based and computerized tomographic imaging techniques. Archimedes' principle based liquid^{9,10} and gas¹¹⁻¹³ displacement as well as computerized tomographic imaging¹⁴ methods of porosity measurement are routinely used for porous material characterization. Eligibility of application of each technique for different porous materials depends on their physiochemical properties. Although micro-CT is assumed as a

gold standard technique for porosity measurement especially in the biomedical field, it is not applicable to non-opaque materials. The cost and time-consuming process of data acquisition especially at high resolution rendering and the need for high performance imaging machinery and users are still important concerns and hence measuring the porosity through other methods is considered. A probable invalid equation due to the absence of a truly linear region, shrinkage of some samples (especially biomaterials and elastomers), need for degassing, thermal preparation methods which may affect the sample architecture as well as the time consuming process, limited nitrogen gas adsorption with highly porous solid samples,¹⁵ restrictions with the minimum sample size (a higher amount of sample is needed for porous samples)¹⁶ and cost are some limitations of BET surface area analysers. Cost-effectiveness and feasibility have been the main reasons that Archimedes' principle based liquid displacement methods are still favourable. However, determining the porosity of non-opaque small sized highly porous light materials through these methods has always been a big concern. However Archimedes' principle based and micro-computerized tomography (micro-CT) techniques are comparatively better. In micro-CT, pore distributions from several tomographical images, generally developed by X-ray, are combined together to determine the total porosity of small 3-D scaffolds. Variations of Archimedes' principle based liquid displacement methods are still favourable due to their simplicity, inexpensiveness and ease of use for determination of the porosity of solid materials with irregular shapes.

^aDepartment of Biomedical Engineering, Faculty of Engineering Building, University of Malaya, 50603 Kuala Lumpur, Malaysia. E-mail: ralmoradi@gmail.com; prsumit@gmail.com; forough_at@yahoo.com; bpinguan@um.edu.my

^bDepartment of Orthopaedic Surgery, Faculty of Medicine Building, University of Malaya, 50603 Kuala Lumpur, Malaysia. E-mail: tkzrea@um.edu.my

A comparison study of different physical treatments on cartilage matrix derived porous scaffolds for tissue engineering applications

Ali Moradi¹, Sumit Pramanik¹, Forough Ataollahi¹, Alizan Abdul Khalil², Tunku Kamarul³ and Belinda Pinguang-Murphy¹

¹ Department of Biomedical Engineering, Faculty of Engineering Building, University of Malaya, 50603 Kuala Lumpur, Malaysia

² Department of Surgery, Faculty of Medicine Building, University of Malaya, 50603 Kuala Lumpur, Malaysia

³ Department of Orthopaedic Surgery, Faculty of Medicine Building, University of Malaya, 50603 Kuala Lumpur, Malaysia

E-mail: ralimoradi@gmail.com, prsumit@gmail.com, forough_at@yahoo.com, alizan@um.edu.my, tkzrea@um.edu.my and bpinguan@um.edu.my

Received 21 June 2014

Accepted for publication 14 October 2014

Published 12 November 2014

Abstract

Native cartilage matrix derived (CMD) scaffolds from various animal and human sources have drawn attention in cartilage tissue engineering due to the demonstrable presence of bioactive components. Different chemical and physical treatments have been employed to enhance the micro-architecture of CMD scaffolds. In this study we have assessed the typical effects of physical cross-linking methods, namely ultraviolet (UV) light, dehydrothermal (DHT) treatment, and combinations of them on bovine articular CMD porous scaffolds with three different matrix concentrations (5%, 15% and 30%) to assess the relative strengths of each treatment. Our findings suggest that UV and UV-DHT treatments on 15% CMD scaffolds can yield architecturally optimal scaffolds for cartilage tissue engineering.

Keywords: cartilage matrix, porous scaffold, cross-linking, physical treatment

1. Introduction

Attempts to repair and regenerate impaired cartilage through cartilage tissue engineering have failed to meet the ultimate needs of most patients with articular cartilage injuries. Tissue engineering multi-factor strategies are still amongst promising approaches for repair of cartilage defects. Apart from the selection of suitable cells and growth factors, use of proper scaffolds with appropriate physicochemical structure [1] will favor biocompatibility and cell adhesion/proliferation. The

scaffolds must possess suitable geometry and mechanical properties [2], high porosity and interconnectivity, stability and consistency of mechanical strength, and a proper surface micro-morphology [1]. Different three-dimensional (3D) constructs, such as complex branched helical micro-channels of micro-fluidic hydrogels, can provide good network structures [3]. The material from which the scaffold is fabricated plays a key role in chondroinduction. Various types of hydrogels, polymers, scaffolds and composites of different materials that can support cartilage matrix production have been tried [4–6]. It has been suggested that modified native extracellular matrix (ECM) may contain bioactive factors that can contribute to cell growth, migration, and differentiation. In general, the closer the material is to cartilage native matrix, the higher the probability of achieving a suitable engineered cartilage. For this reason, pure



Content from this work may be used under the terms of the [Creative Commons Attribution 3.0 licence](https://creativecommons.org/licenses/by/3.0/). Any further distribution of this work must maintain attribution to the author(s) and the title of the work, journal citation and DOI.